AD-A105 805 ARMY MISSILE COMMAND REDSTONE ARSENAL AL GROUND EQU--ETC F/G 11/4
WHOLE-FIELD EXPERIMENTAL STRESS ANALYSIS USING LASER SPECKLE IN--ETC(U)
FEB 81 T L VANDIVER
UNCLASSIFIED DRSMI/RL-81-10-TR SBIE-AD-E950 170 NL

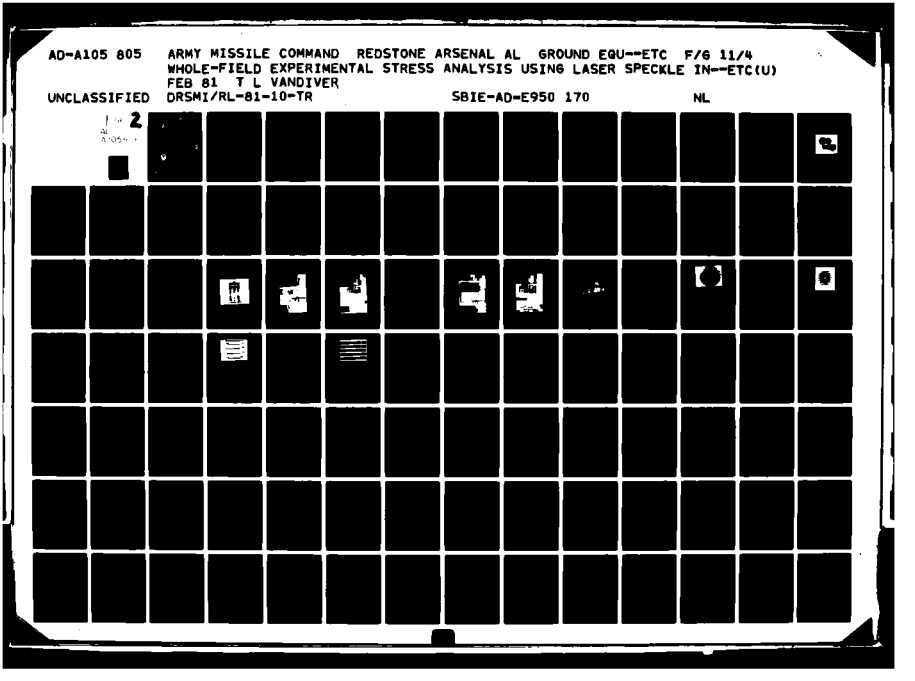

AD-E950170

(12) LEVEL III

AD A105805

TECHNICAL REPORT RL-81-10

WHOLE-FIELD EXPERIMENTAL STRESS ANALYSIS USING LASER SPECKLE INTERFEROMETRY

Terry L. Vandiver
Ground Equipment and Missile Structures Directorate
US Army Missile Laboratory

14 February 1981

U.S. ARMY MISSILE COMMAND
Redstone Arsenal, Alabama 35898

Approved for public release; distribution unlimited.

81 10 14

DISPOSITION INSTRUCTIONS

DESTROY THIS REPORT WHEN IT IS NO LONGER NEEDED. DO NOT RETURN IT TO THE ORIGINATOR.

DISCLAIMER

THE FINDINGS IN THIS REPORT ARE NOT TO BE CONSTRUED AS AN OFFICIAL DEPARTMENT OF THE ARMY POSITION UNLESS SO DESIGNATED BY OTHER AUTHORIZED DOCUMENTS.

TRADE NAMES

USE OF TRADE NAMES OR MANUFACTURERS IN THIS REPORT DOES NOT CONSTITUTE AN OFFICIAL INDORSEMENT OR APPROVAL OF THE USE OF SUCH COMMERCIAL HARDWARE OR SOFTWARE.

UNCLASSIFIED

SECURITY CLASSIFICATION OF THIS PAGE (When Data Entered)

REPORT DOCUMENTATION PAGE		READ INSTRUCTIONS BEFORE COMPLETING FORM
1. REPORT NUMBER TR-RL-81-10	2. GOVT ACCESSION NO. AD-A105 805	3. RECIPIENT'S CATALOG NUMBER
4. TITLE (and Subtitle) Whole-field Experimental Stress Analysis Using Laser Speckle Interferometry		5. TYPE OF REPORT & PERIOD COVERED Technical Report 6. PERFORMING ORG. REPORT NUMBER
7. AUTHOR(s) Terry L. Vandiver		8. CONTRACT OR GRANT NUMBER(s)
9. PERFORMING ORGANIZATION NAME AND ADDRESS Commander, US Army Missile Command ATTN: DRSMI-RLA Redstone Arsenal, Alabama 35898		10. PROGRAM ELEMENT, PROJECT, TASK AREA & WORK UNIT NUMBERS
11. CONTROLLING OFFICE NAME AND ADDRESS Commander, US Army Missile Command ATTN: DRSMI-RPT Redstone Arsenal, Alabama 35898		12. REPORT DATE 14 February 1981 13. NUMBER OF PAGES 140
14. MONITORING AGENCY NAME & ADDRESS(if different from Controlling Office)		15. SECURITY CLASS. (of this report) Unclassified 15a. DECLASSIFICATION/DOWNGRADING SCHEDULE

16. DISTRIBUTION STATEMENT (of this Report)

Approved for public release; distribution unlimited.

17. DISTRIBUTION STATEMENT (of the abstract entered in Block 20, if different from Report)

18. SUPPLEMENTARY NOTES

19. KEY WORDS (Continue on reverse side if necessary and identify by block number)

Laser Speckle Interferometry	Shear Testing
Nondestructive Testing	Laminates
Optics	Elasticity Constants
Composite Structures	Flaw Detection

20. ABSTRACT (Continue on reverse side if necessary and identify by block number)

The objective of this study was to develop a whole-field experimental stress analysis method for composite structures. A data-gathering system, using the optical technique of laser speckle interferometry, was used to capture deformation of bodies under load on a film record. The speckle interferograms were analyzed by a computer-aided scanning system. A mathematical and geometrical interpretation of interferometric data is presented. The interferograms were analyzed at strategic image points on the test specimens to obtain displacement data which was used to calculate strains, shearing strains, and

DD FORM 1 JAN 73 1473 EDITION OF 1 NOV 65 IS OBSOLETE

UNCLASSIFIED

SECURITY CLASSIFICATION OF THIS PAGE (When Data Entered)

Item 20 (Concluded)

correlated with shearing stresses. Anisotropic elastic constants such as Young's modulus, shear modulus, and Poisson's ratio were calculated. A full-field aperture analysis was used as a tool to qualitatively observe the free edge effects of shear specimens. The techniques presented in this report are significant because full-field or discrete information can be obtained from any point rather than averaging data from a small region.

ACKNOWLEDGMENTS

The author expresses appreciation to Mr. J. A. Schaeffel, Jr., for his guidance of aperture reconstruction; and Ms. A. F. Dempsey, Mr. R. B. McGowan, Ms. M. Williams, and Mr. T. Yost for their assistance with the laboratory work and data reduction.

TABLE OF CONTENTS

LIST OF FIGURES

LIST OF FIGURES (Concluded)

LIST OF TABLES

LIST OF SYMBOLS

Symbol	Definition
A_X	Cross Sectional Area
D	Spacing Between Fringes
E_1, E_2, E_3	Young's Moduli of Elasticity
F_1, F_2	Applied Axial Load
G_{12}, G_{13}, G_{23}	Lamina Shear Moduli
G_{XY}	Shear Modulus
K	Interferogram Magnification Ratio
S	Film Scale Factor
U_Θ	In-plane Displacement at Given Angles
Y	Screen Location
Z	Aperture-Viewing Plane Distance
a_{ij}	Elastic Potential Constants
b	Shear Specimen Thickness
f	Distance from Interferogram to Analyzer Screen
m	Fringe Order
γ_{XY}	Shear Strain
ε_X, ε_Y, ε_Z	Components of Strain
λ	Wavelength of Laser Light
ν_{ij}	Poisson Coefficients
σ_X, σ_Y, σ_Z	Normal Stress Components
τ_{XY}, τ_{XZ}, τ_{YZ}	Shear Stress Components

I. INTRODUCTION

Increasing demand for new materials has prompted the use of composites for such applications as rocket motor cases, helicopter blades, aircraft tail sections, and ground support equipment. Laminated composite structures have merit because of the high strength-to-weight ratio and low cost of manufacture. With the increasing use of composites for structural applications, there is a need for new methods to characterize and evaluate composite materials for engineering design and structural analyses. Because of the nonhomogeneity of laminated composite structures, different techniques of analysis must be used. The ultimate strength of a material in shear and the shear modulus are difficult material properties to measure experimentally. The difficulties are encountered in attempting to create regions of pure shear in a test specimen.

Several different test fixtures are currently being used to measure in-plane shear: the two-rail; three-rail; ±45° specimen; and 10° off-axis specimen system [1]. The three-rail shear test fixture was selected for this effort. Ideally, a state of pure shear exists near the center of the specimens with loading on two parallel edges, while the remaining two edges are stress free.

The primary objective of this study was to develop a whole-field experimental stress analysis method to investigate composite materials. The technique selected was the optical process of laser speckle interferometry. Some conventional methods of measuring surface strain and displacements utilize strain gages, dial gages, and various other mechanical and electrical sensing devices. Therefore, a full field view of the strain or displacement distribution requires a large number of measurements at different locations and is very time consuming. Laser speckle interferometry is a technique which provides a sensitive, noncontact method of measuring the in-plane components of displacement from the whole-field point of view in an efficient manner.

In the analytical considerations portion of this report, Section III, a mathematical and geometrical formulation is presented showing how displacement data can be obtained using laser speckle interferometry. The displacement data were in turn used to calculate strains, shearing strains, which were correlated with shearing stresses. This correlation allowed the calculation of anisotropic elastic constants relating stress to strain. The resulting equations were used to calculate a portion of the 21 elastic constants of the anisotropic material at different load levels and locations on the shear specimen. The remaining elasticity constants were obtained from data of interferograms of 0° and 90° fiber-oriented tensile specimens.

The type of composite material selected and the preparation of the test specimens are discussed in Section II. The optical and mechanical setups and procedures used to prepare and analyze interferograms are described in Section IV. Results of the testing and analyzed data are given in Section V.

II. MATERIAL CONSIDERATIONS

The type composite material used in this research task was Scotchply XP-250, a high-strength moldable epoxy E-glass prepreg designed for fast production cure cycles. XP-250 is a general-purpose grade for structural

applications. Its primary advantage over some other prepreg is faster curing at temperatures as low as 250°F [2]. Scotchply XP-250 was selected for this research project because Tennessee Technological University performed some post-crazing stress analyses of the material while under contract to the US Army Missile Laboratory.

Square unidirectional 0-degree panels were manufactured by the 3M Company, Industrial Specialists Division at St. Paul, Minnesota. The panel dimensions as received were 33.0 cm X 33.0 cm X 0.18 cm. Each panel was 8 plys thick with 0.23-mm average ply thickness. Resin burnout tests performed revealed the panels, as received, were 33 percent resin content by weight. Figure 1 shows the purity of the glass remains after a typical resin burnout.

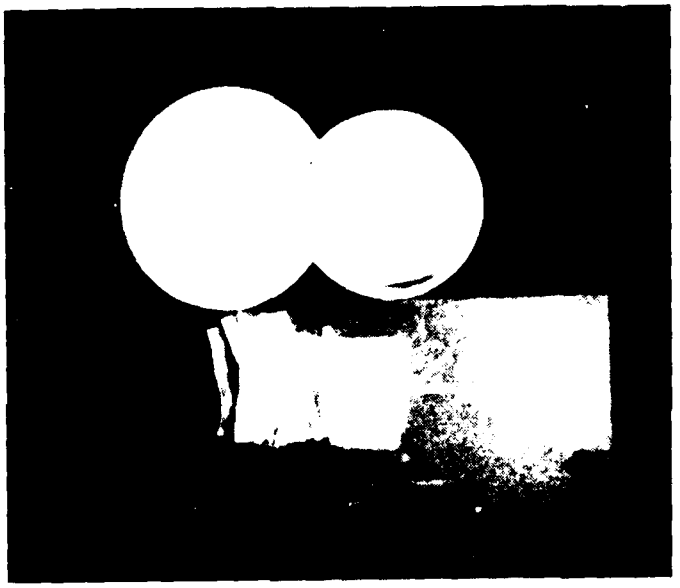

Figure 1. XP-250 resin burnout test.

Shear test panels were manufactured inhouse to the finished form shown in Figure 2. The specimens were saw-cut 2.5 mm oversize on the top and bottom edges, and the final dimensions were obtained by milling and sanding. Brown tracers throughout the material indicated the fiber orientation in relation to a vertical axis. Strain gages were affixed to the shear specimens at 45° to the fiber orientation. The gages were SR4, 120 ohm, 6.35 mm long, by BLH Electronics, Inc. The same gages were used parallel to the fibers on the $[0]_s$ tensile specimens and perpendicular to the fibers on the $[90]_s$ test specimens. The tension test coupons were manufactured by Sperry Rand Company, Huntsville Division, in the final form shown in Figure 3. The figure shows a typical $[90]_s$ test coupon where the $[0]_s$ specimen is the same length but only 1.27 cm wide [3]. The endtabs were made from [0/90], symmetrical, 14-ply-thick material. The plys adjacent to the adhesion interface were parallel to the specimen orientation. Eastman 910 adhesive was used to affix the endtabs to the specimens.

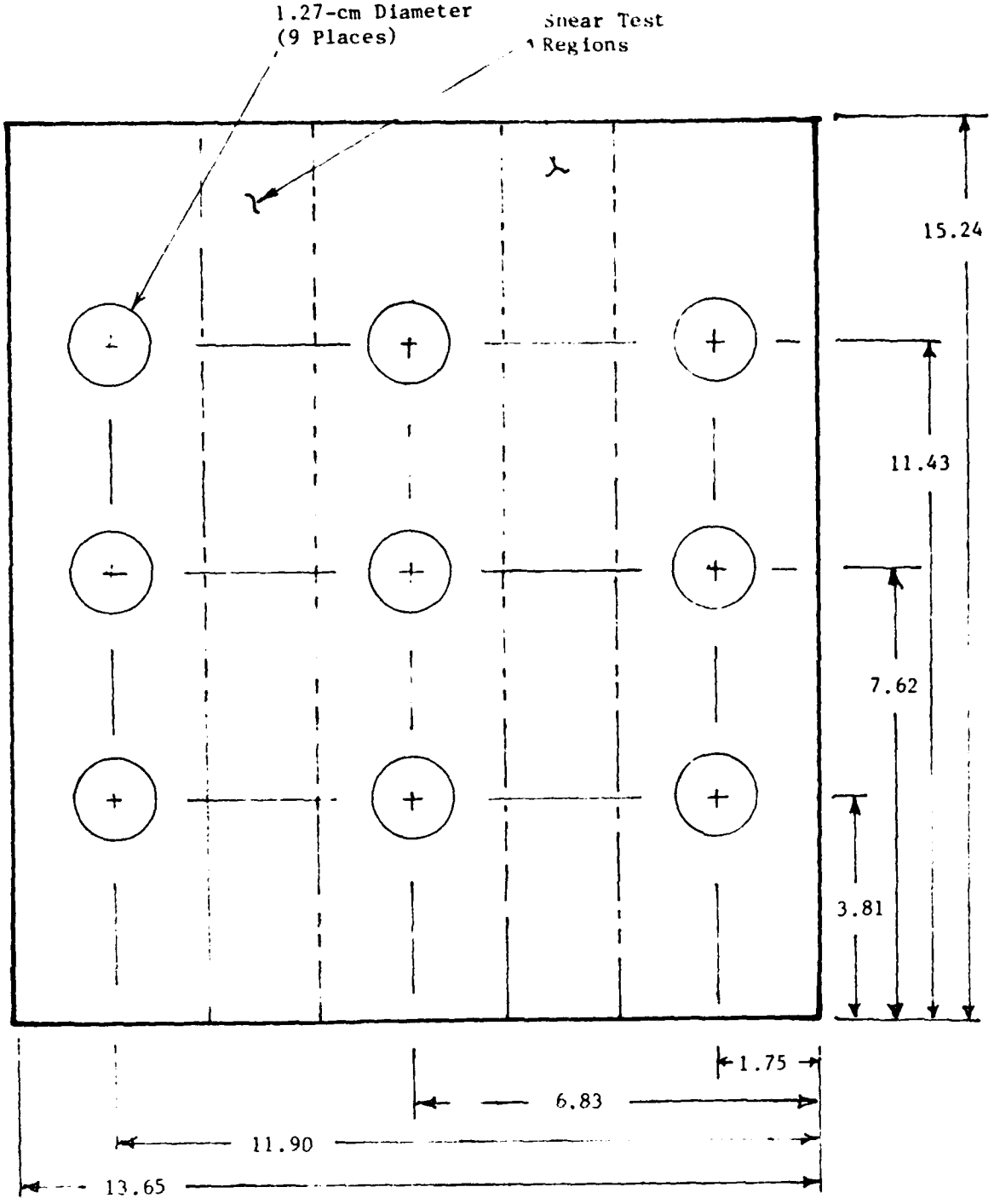

Figure 2. XP-250 shear test specimen (cm).

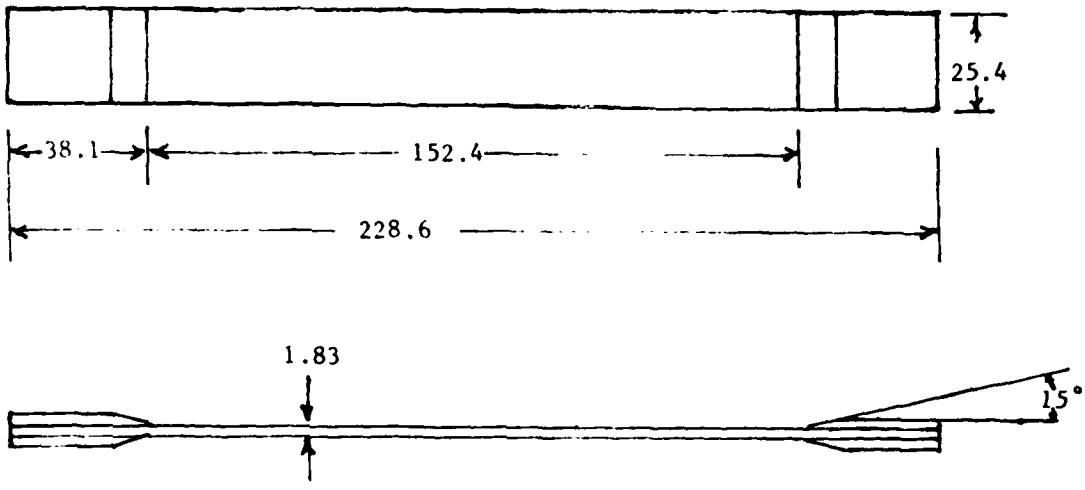

Figure 3. XP-250 90° tensile specimen (mm).

All the specimens received a light coat of flat white paint on one side to provide a good illuminable surface required for laser speckle interferometry.

III. ANALYTICAL CONSIDERATIONS

A. Displacement Determination

A computer-aided laser scanning technique [4], as described in Section IV of this report, was utilized to analyze the interferograms. The interferograms were housed in an X-Y translation table equipped with stepping motors and controlled by a computer program. Figure 4 shows the basic scanning setup of the translation table used to project interference fringes onto a diffusion screen. The fringe spacing and angle of orientation at each coordinate were entered into the computer, which in turn calculated the displacement component in the Θ direction from

$$U_\Theta = \frac{m\lambda fs}{D} \tag{1}$$

where

U_Θ = In-plane displacement at a point between loaded and unloaded model

m = Fringe order

D = Spacing between fringes

λ = Wavelength used in data analysis

f = Distance from interferogram to analyzer screen

s = Film scale factor

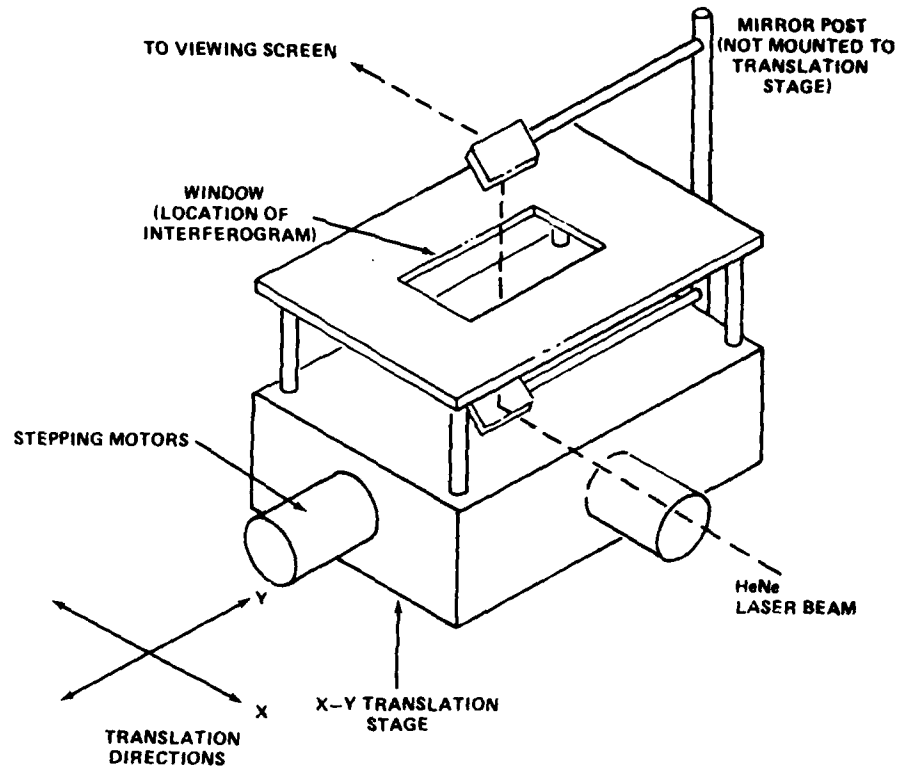

Figure 4. X-Y translation stage and laser beam path.

The displacement is inversely proportional to the fringe spacing and the direction is perpendicular to the fringes, as shown in Figure 5. The vertical, U_V, and the horizontal, U_H, components of in-plane displacement were obtained from

$$U_V = \frac{m\lambda fs}{D} \cos\Theta \tag{2}$$

$$U_H = \frac{m\lambda fs}{D} \sin\Theta \tag{3}$$

The wavelength of the HeNe laser used in the data analysis is 6328 Å. The film scale factor, S, is found by dividing the true length of the illuminated test specimen by the image length on the interferogram. The computer program used in the analysis appears in Appendix A.

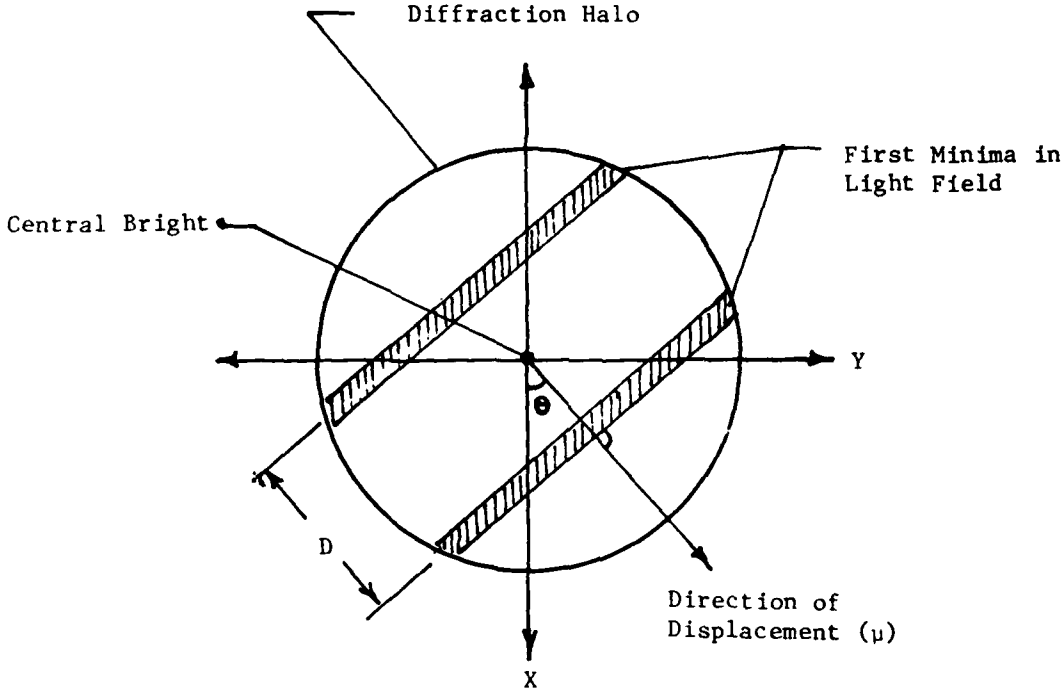

Figure 5. Diffraction halo geometry.

B. Anisotropic Elasticity Constants Theory

In the general case of a homogeneous anisotropic body with no elements of elastic symmetry, the generalized Hooke's Law can be expressed in Cartesian coordinates X, Y, Z and have the form

$$\left.\begin{aligned}
\varepsilon_X &= a_{11}\sigma_X + a_{12}\sigma_Y + a_{13}\sigma_Z + a_{14}\tau_{YZ} + a_{15}\tau_{XZ} + a_{16}\tau_{XY} \\
\varepsilon_Y &= a_{21}\sigma_X + a_{22}\sigma_Y + \ldots\ldots + a_{26}\tau_{XY} \\
\varepsilon_Z &= a_{31}\sigma_X + a_{32}\sigma_Y + \ldots\ldots + a_{36}\tau_{XY} \\
\gamma_{YZ} &= a_{41}\sigma_X + a_{42}\sigma_Y + \ldots\ldots + a_{46}\tau_{XY} \\
\gamma_{XZ} &= a_{51}\sigma_X + a_{52}\sigma_Y + \ldots\ldots + a_{56}\tau_{XY} \\
\gamma_{XY} &= a_{61}\sigma_X + a_{62}\sigma_Y + a_{63}\sigma_Z + a_{64}\tau_{YZ} + a_{65}\tau_{XZ} + a_{66}\tau_{XY}
\end{aligned}\right\} \quad (4)$$

The 36 coefficients, a_{ij}, contained in Equation (4) are called the elastic constants by S. G. Lekhnitskii [5]; however, when assuming three planes of elastic symmetry, the generalized Hooke's law becomes

$$\left.\begin{aligned}
&(a)\quad \varepsilon_X = a_{11}\sigma_X + a_{12}\sigma_Y + a_{13}\sigma_Z \\
&(b)\quad \varepsilon_Y = a_{12}\sigma_X + a_{22}\sigma_Y + a_{23}\sigma_Z \\
&(c)\quad \varepsilon_Z = a_{13}\sigma_X + a_{23}\sigma_Y + a_{33}\sigma_Z \\
&(d)\quad \gamma_{YZ} = a_{44}\tau_{YZ} \\
&(e)\quad \gamma_{XZ} = a_{55}\tau_{XZ} \\
&(f)\quad \gamma_{XY} = a_{66}\tau_{XY}
\end{aligned}\right\} \qquad (5)$$

Thus the elastic potential takes the form

$$\left.\begin{matrix}
a_{11} & a_{12} & a_{13} & 0 & 0 & 0 \\
 & a_{22} & a_{23} & 0 & 0 & 0 \\
 & & a_{33} & 0 & 0 & 0 \\
 & & & a_{44} & 0 & 0 \\
 & & & & a_{55} & 0 \\
 & & & & & a_{66}
\end{matrix}\right\} \qquad (6)$$

The constants a_{16}, a_{26}, a_{36}, and a_{45} are equal to zero, and nine independent elastic constants remain. All the coefficients of mutual influence vanish in a coordinate system the direction of whose axes coincide with the principal directions. The remaining elastic constants are called the principal constants and can be expressed in terms of "technical constants." [5] Taking for the principal "technical constants" the notations E_1, E_2, E_3 (Young's Moduli), G_{23}, G_{13}, G_{12} (Shear Moduli), and ν_{12}, ν_{21}, ν_{13}, ν_{31}, ν_{23}, ν_{32} (Poisson Coefficients), Equations (5) can be written in the form

$$\left.\begin{aligned}
&(a)\quad \varepsilon_X = \frac{1}{E_1}\sigma_X - \frac{\nu_{21}}{E_2}\sigma_Y - \frac{\nu_{31}}{E_3}\sigma_Z \\
&(b)\quad \varepsilon_Y = \frac{-\nu_{12}}{E_1}\sigma_X + \frac{1}{E_2}\sigma_Y - \frac{\nu_{32}}{E_3}\sigma_Z \\
&(c)\quad \varepsilon_Z = \frac{-\nu_{31}}{E_1}\sigma_X - \frac{\nu_{23}}{E_2}\sigma_Y + \frac{1}{E_3}\sigma_Z
\end{aligned}\right\} \qquad (7)$$

$$\left.\begin{aligned} \text{(d)}\quad \gamma_{YZ} &= \frac{1}{G_{23}}\tau_{YZ} \\ \text{(e)}\quad \gamma_{XZ} &= \frac{1}{G_{13}}\tau_{XZ} \\ \text{(f)}\quad \gamma_{XY} &= \frac{1}{G_{12}}\tau_{XY} \end{aligned}\right\} \qquad (7)$$

where

$$\left.\begin{aligned} E_1\nu_{21} &= E_2\nu_{12} \\ E_2\nu_{32} &= E_3\nu_{23} \\ E_3\nu_{13} &= E_1\nu_{31} \end{aligned}\right\} \qquad (8)$$

C. Determination of Anisotropic Elastic Constants

Young's moduli of elasticity were calculated in the following manner. Figure 6 shows an element of $[0]_s$ composite material. A $[0]_s$ fiber orientation tensile test coupon was loaded in the X-direction to obtain data required to calculate E_1. Allowing σ_Y and σ_Z to equal zero and solving Equation (7a) for E_1 yields

$$E_1 = \frac{\sigma_X}{\varepsilon_X} \qquad (9)$$

and

$$\sigma_X = \frac{F_X}{A_X} \qquad (10)$$

where

E_1 ≡ Young's modulus of elasticity

σ_X ≡ Stress in the X-direction

ε_X ≡ Strain in the X-direction

F_X ≡ Load applied in the X-direction

A_X ≡ Cross sectional area of test specimen

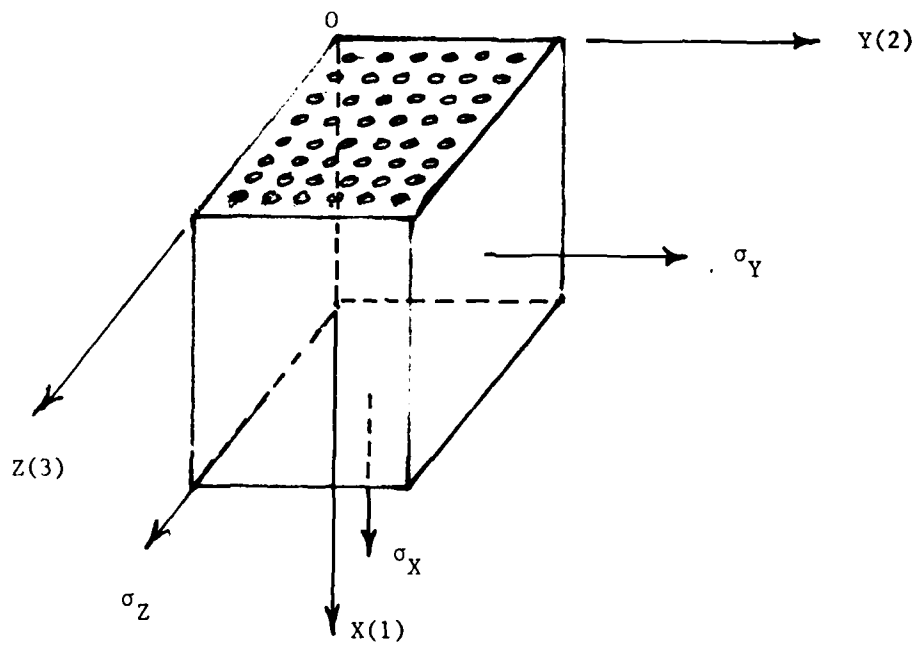

Figure 6. Element of $[0]_s$ composite material.

Likewise allowing σ_X and σ_Z to equal zero and solving Equation (7b) for E_2 yields

$$E_2 = \frac{\sigma_Y}{\epsilon_Y} \tag{11}$$

It was assumed that $E_2 = E_3$ due to the direction of the fiber layup, as shown by planes XOY and XOZ in Figures 7a and 7b. The strains used in the above equation were obtained using conventional strain gages, as well as with laser speckle interferometry.

Figure 8 shows a typical interferogram transparency with the scan region encircled. The dots represent discrete data points taken from the interferogram. Three vertical scans were made on each $[0]_s$ and $[90]_s$ test specimen. Each vertical scan contained approximately twenty (20) data points. The fringe spacing and angle of orientation at each point were entered into the computer which, in turn, calculated the displacements and resolved the direction into horizontal (Y) and vertical (X) components. Having obtained the displacements, the strain field was calculated using the following procedure. Figure 9 shows the detailed coordinate grid used to scan the interferograms.

The vertical strain between points A and D plus the horizontal strain between points A and B will be used as examples. By knowing the displacement at points A and D the deformation per unit length in the vertical direction becomes

$$\epsilon_X = \frac{\partial U_X}{\partial X} = \frac{\Delta U_X}{\Delta X} \tag{12}$$

and

$$\frac{\Delta U_X}{\Delta X} = \frac{U_X\big|_D - U_X\big|_A}{\overline{X_{AD}}} \tag{13}$$

where

ϵ_X ≡ Strain in the X-direction

ΔU_X ≡ Displacement change in the X-direction

ΔX ≡ Distance between scan points in the X-direction

$U_X\big|_D$ ≡ Vertical displacement at point D

$U_X\big|_A$ ≡ Vertical displacement at point A

$\overline{X_{AD}}$ ≡ Scaled distance between points A and D on the interferogram

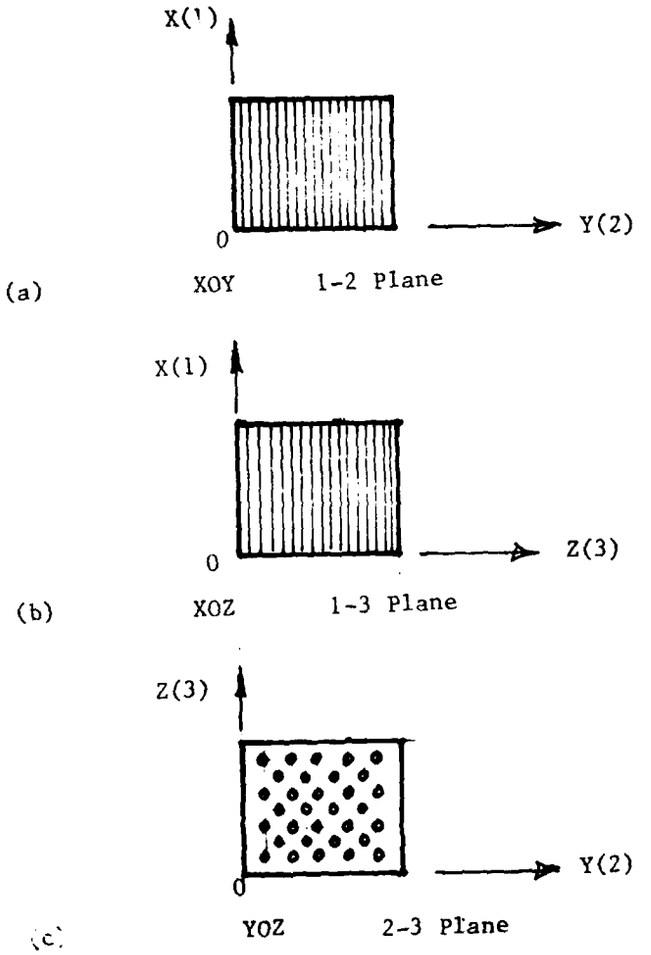

Figure 7. Plane geometry of $[0]_s$ composite material.

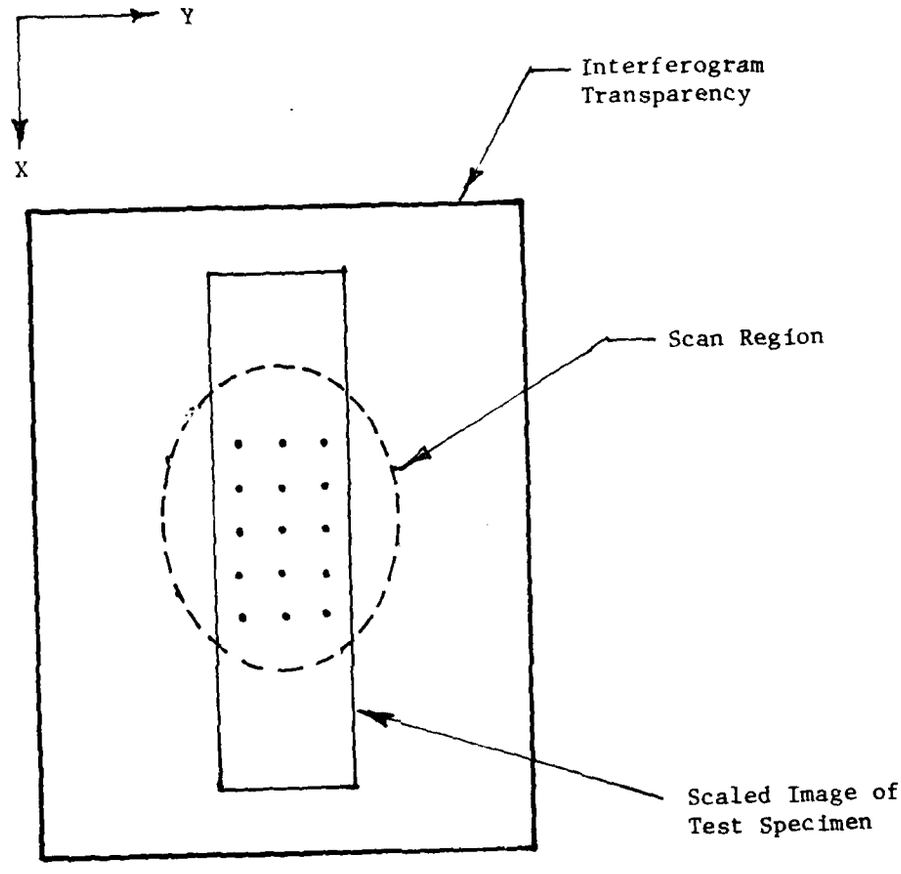

Figure 8. Interferogram showing the scan region of $[0]_s$ and $[90]_s$ test specimens.

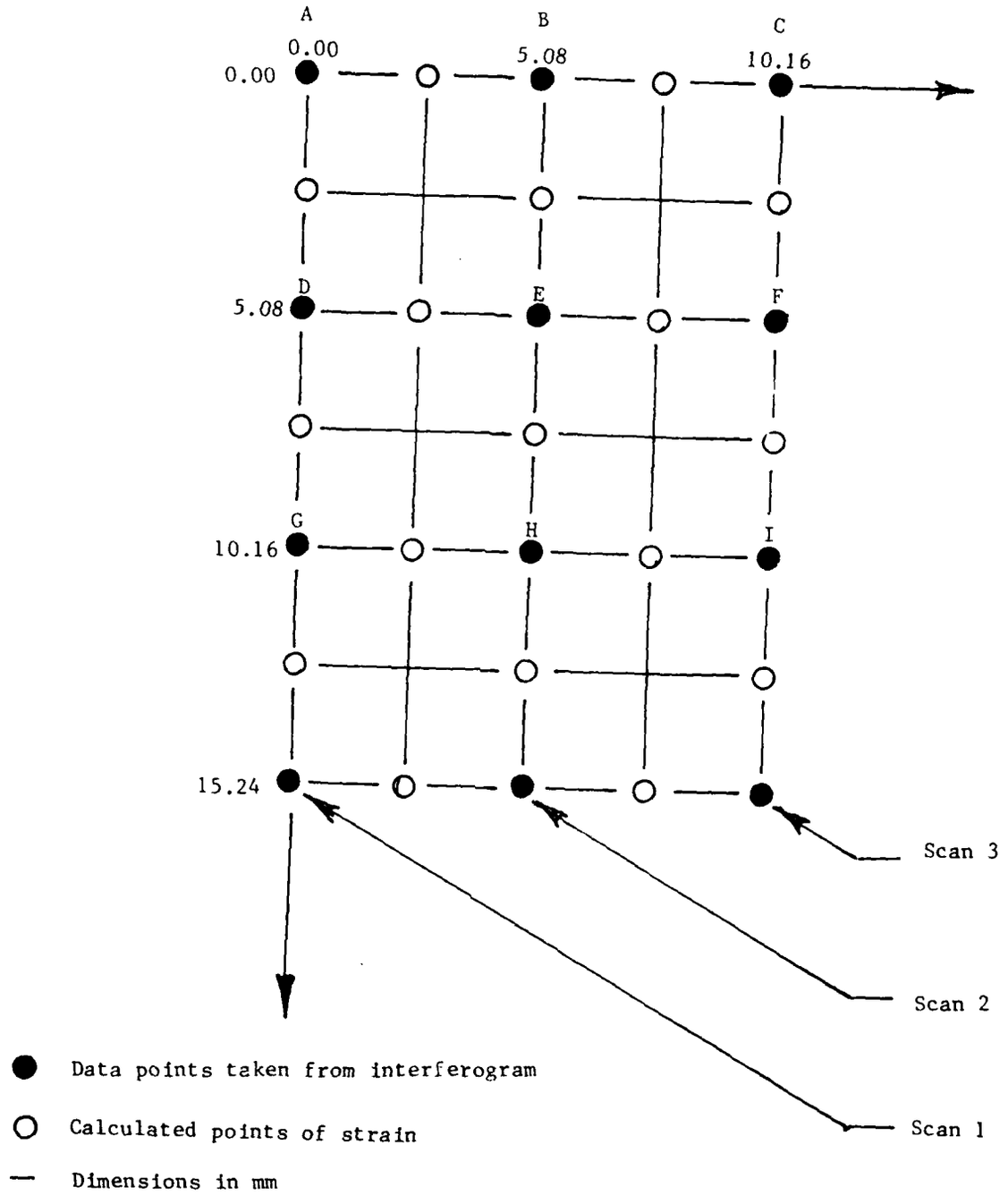

Figure 9. Coordinate grid for scan data (90-degree test specimen).

Likewise solving for the horizontal strain between points A and B becomes

$$\epsilon_Y = \frac{\partial U_Y}{\partial Y} = \frac{\Delta U_Y}{\Delta Y} \tag{14}$$

and

$$\frac{\Delta U_Y}{\Delta Y} = \frac{U_Y\big|_B - U_Y\big|_A}{\overline{Y_{AB}}} \tag{15}$$

The shear moduli of the composite material were calculated in the following way. Solving Equation (7f) for G_{12} yields

$$G_{12} = \frac{\tau_{XY}}{\gamma_{XY}} \tag{16}$$

and due to incremental loading

$$\tau_{XY} = \frac{F_2 - F_1}{2bh} \tag{17}$$

where

G_{12} ≡ Lamina shear modulus

τ_{XY} ≡ Shearing stress

γ_{XY} ≡ Shearing strain

F ≡ Applied load

b ≡ Specimen thickness

h ≡ Specimen shear length

It was assumed that $G_{12} = G_{13}$ due to the direction of the fiber layup, as shown by planes XOY and XOZ in Figures 7a and 7b. The shearing stress, τ_{XY}, was calculated in the conventional manner; however, the shearing strain, γ_{XY}, was calculated from displacement data obtained through laser speckle interferometry.

Figure 10 shows the 3-rail test fixture and the computer scan locations on the shear panels. A set of nine (9) data points was taken extremely close to the free edge as well as in the center of the specimen. The free edge shear stress should approach zero and the maximum shear stress should occur in the region of the center scan. Figure 11 shows the coordinate grid system for

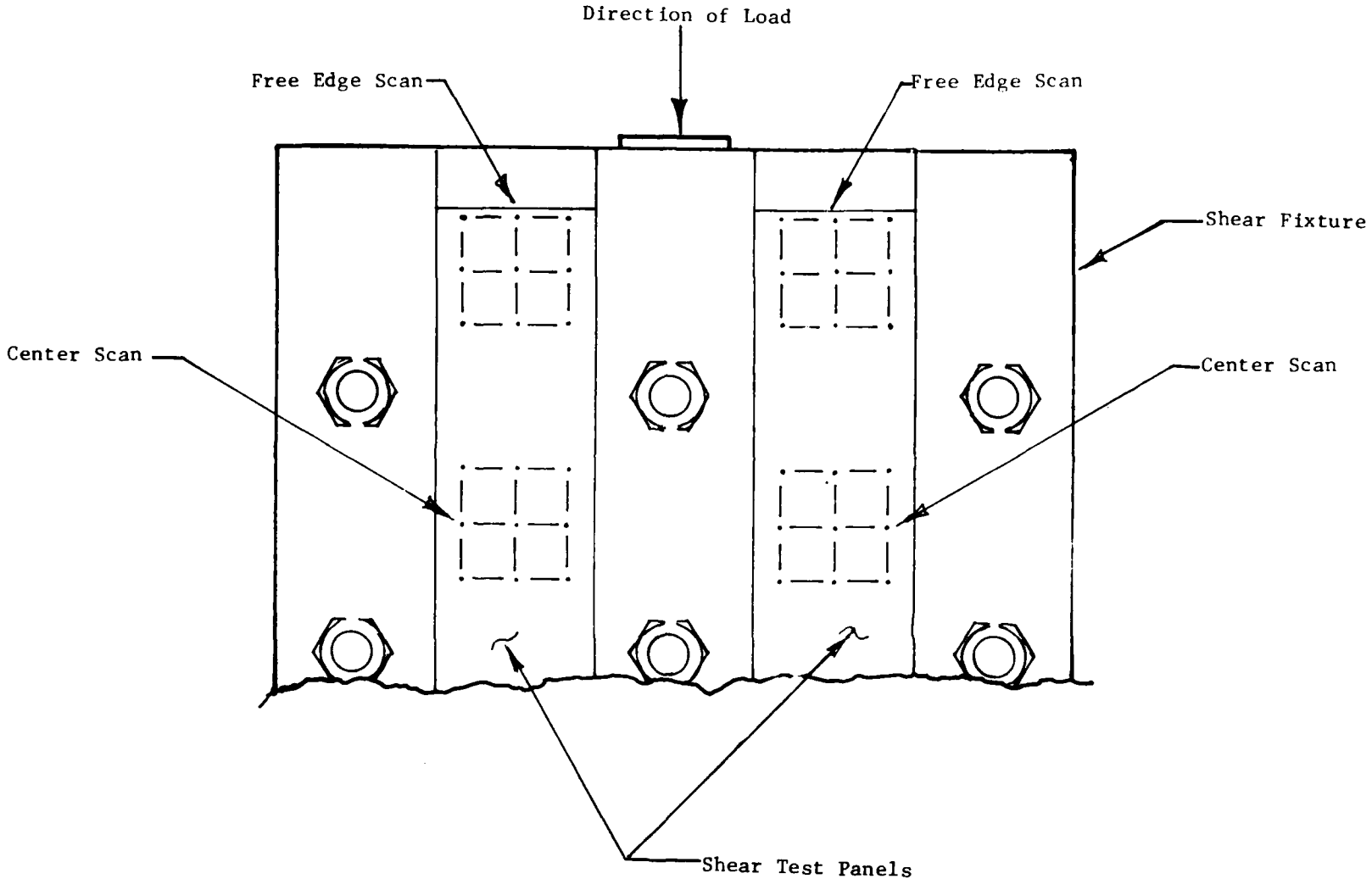

Figure 10. Computer scan locations for shear test panels.

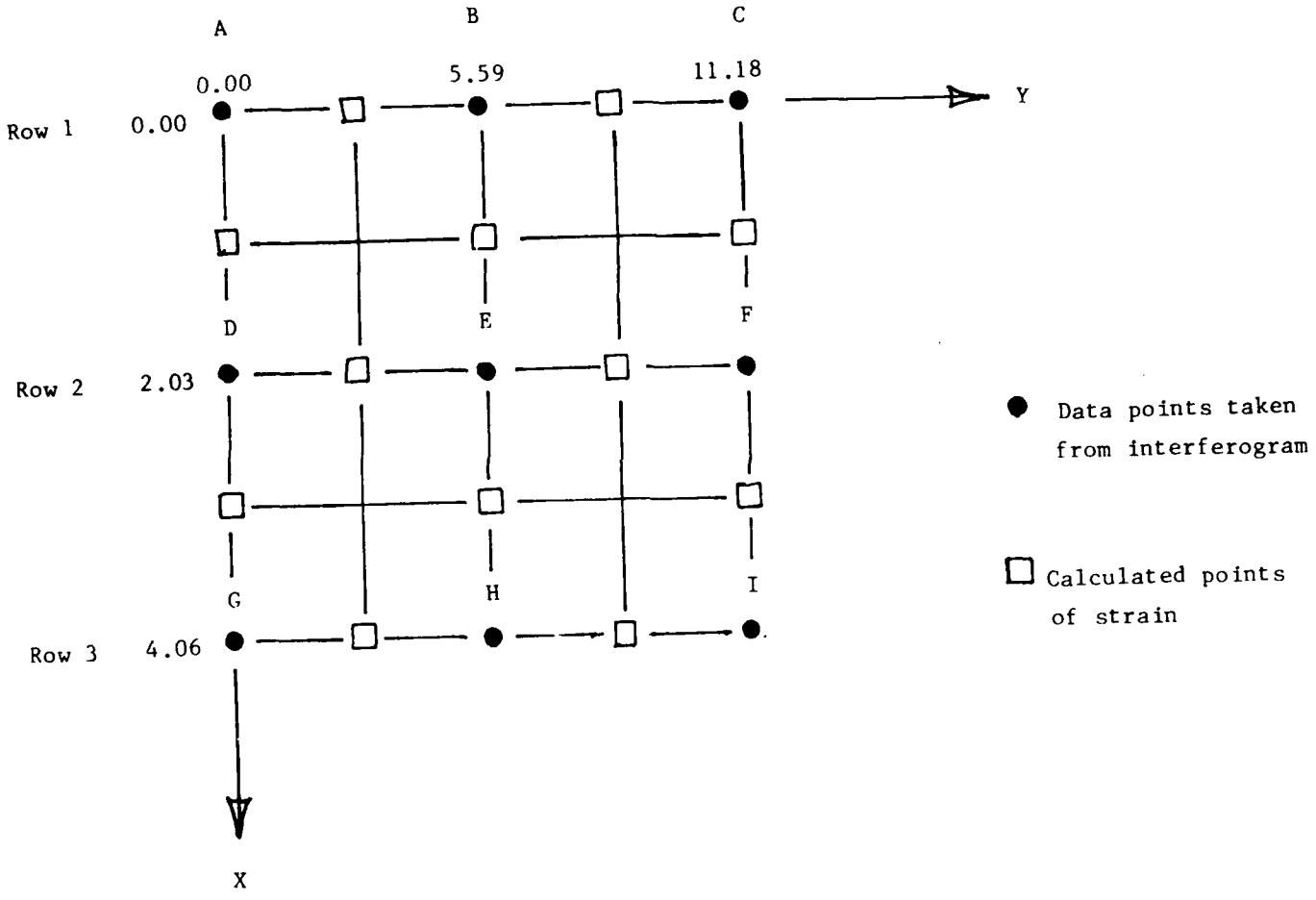

Figure 11. Coordinate grid system for shear scan data. (dimensions in mm)

the shear scan data. The coordinate system shown is for a left-hand specimen where the right-hand specimen would be mirrored about the center rail, with the origin always at the outside rail. Using the mirrored technique allows left-hand data to be directly correlated with the right-hand data on the same datum. The shearing strain γ_{ij} was calculated in the following way

$$\gamma_{XY} = \frac{\partial U_X}{\partial Y} + \frac{\partial U_Y}{\partial X} \tag{18}$$

and for small changes

$$\gamma_{XY} = \frac{\Delta U_X}{\Delta Y} + \frac{\Delta U_Y}{\Delta X} \tag{19}$$

where the changes in vertical and horizontal displacements, ΔU_X and ΔU_Y, are found in the same manner as described in Equations (13) and (15), but with respect to different axes.

The shear modulus, G_{23}, was calculated from

$$G_{23} = \frac{E_R}{2(1 + \nu_R)} \tag{20}$$

where E_R and ν_R are the modulus of elasticity and Poisson's ratio for the epoxy resin system.

The Poisson's coefficients were determined from the displacement data taken from laser speckle interferometry. Tensile specimens with $[0]_s$ fiber orientation were used to find ν_{12} and ν_{13}

$$\nu_{12} = \frac{\varepsilon_Y}{\varepsilon_X} = \nu_{13} \tag{21}$$

where ε_Y is the transverse strain and ε_X is the longitudinal strain. The coordinate convention shown in Figure 9 was used in the analysis. Tensile specimens with $[90]_s$ fiber orientation were used to find ν_{21} and ν_{31}

$$\nu_{21} = \frac{\varepsilon_X}{\varepsilon_Y} = \nu_{31} \tag{22}$$

where ν_{ij} is the Poisson's coefficient in the specified directions. The Poisson's ratio for the epoxy resin system of 0.360 was used for the values of ν_{23} and ν_{32} due to the geometry of the element, as shown in Figure 6.

IV. OPTICAL TEST SETUPS AND PROCEDURES

A. Laser Speckle Setup for Shear and Tensile Tests

The experimental test arrangement used to prepare the laser speckle interferogram is shown in Figure 12. A 44,482-Newton-capacity Instron tensile test machine was used to apply incremental loading to the tensile and shear specimens at a rate of 1.3 mm/min. A Spectra Physics model 166 argon laser adjusted at 0.45 W was used as the coherent light source to illuminate the test specimens. A double-exposure photography technique was used to make the interferograms using Kodak Minicard II film SO424, 102 mm × 127 mm. This type film is especially green-light sensitive. The interferograms were developed using conventional photography techniques.

Figure 13 shows the three-rail shear test fixture used in determining the in-plane shear properties. The three-rail test fixture is currently being considered by ASTM as a standard test fixture. The shear panel is clamped between the two outside stationary rails on the edges while the third rail clamps the panel at center. The center rail is loaded by the test machine, loading the specimen in shear parallel to the fibers. The three-rail fixture is unique because the specimen is held in place by clamping friction rather than by bearing on the bolts. The rails have emery cloth bonded to the inside surfaces to aid in the adhesion. The test plate holes are 12.7 mm in diameter, as compared with 9.5-mm-diameter bolts. Due to the great differences in these diameters considerable misalignment is possible in the assembly of the specimen in the test fixture, perhaps with the middle rail tilted from vertical. This would destroy the equality of the test sections on each side of the center rail in addition to creating an oblique loading condition on the center rail. To eliminate this problem, cylindrical spacers the same diameters as the shear test sections were used to align the rails during the squaring and bolt-up procedures. Figure 14 shows the optics side of the experimental mechanics setup. The argon laser was located under the vibration-free table with the beam channeled through a beam-steering device onto a front surface mirror, and finally through a Spectra Physics 332 spatial filter with a 4.7-micron diameter. Figure 15 shows the basic instrumentation setup for the shear testing. The strain gage information was displayed on a type 549 storage oscilloscope with a type Q plug-in strain gage preamplifier. The strain gage information of the scope was fed into a Moseley model ZD-ZA X-Y recorder so that a permanent copy could be obtained.

Two people were required to make a complete set of interferograms. One person was required on the optics side of the test setup, while the other was stationed on the instrumentation side of the test arrangement. The observer on the instrumentation side started and stopped the tensile test machine at the incremental loadings, in addition to controlling the remote shutter by the glow-lighted panel shown in the lower left of Figure 15. A glow light was used above the strip chart recorder so that the observer could see the load increments. The complete process is done in the dark with the exception of two glow lights on the instrumentation side of the test setup. The leakage of any white light on the film plate will destroy the interferometric data. The person on the optics side of the setup changed film packs at each load increment. The test specimens were imaged in this stepwise fashion due to the high sensitivity of laser speckle.

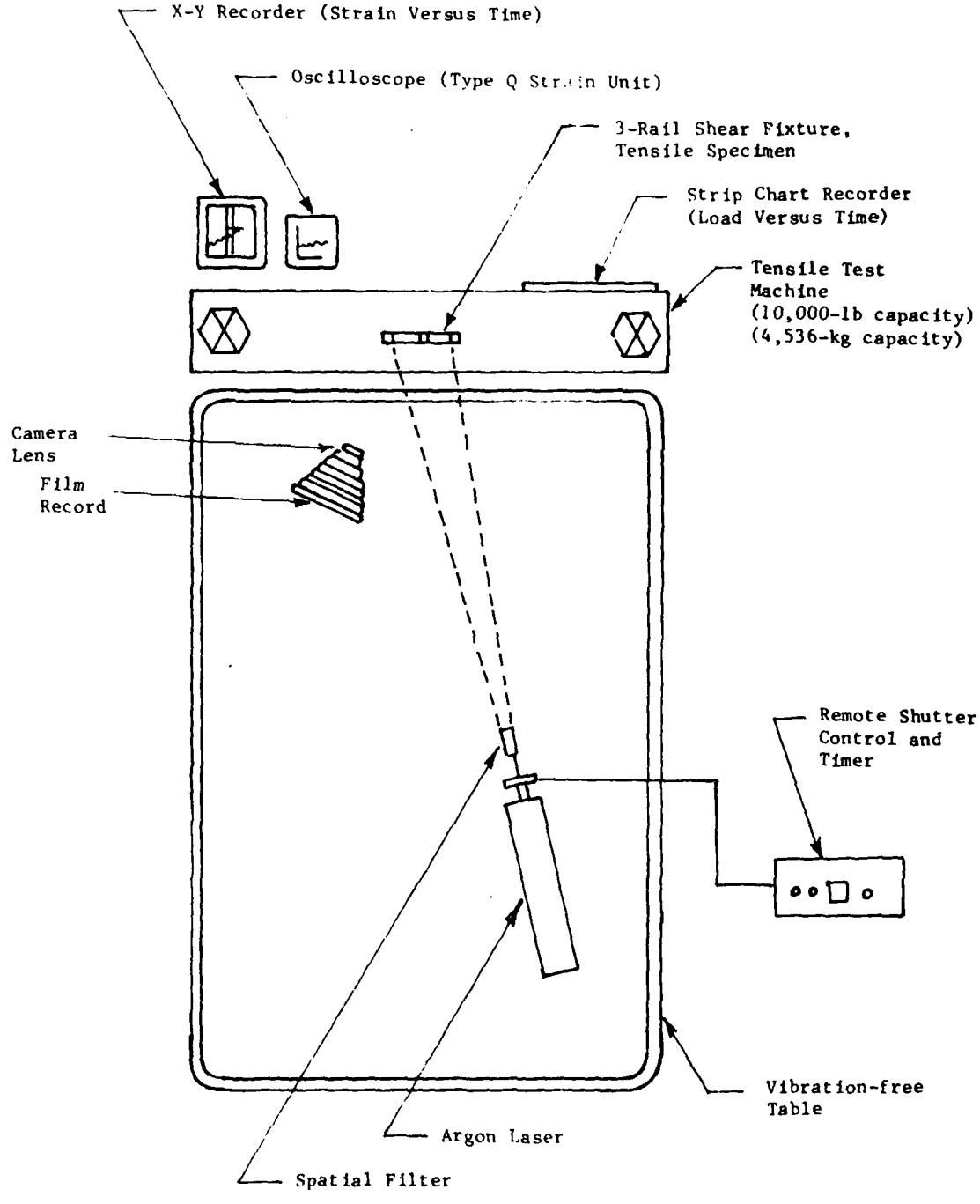

Figure 12. Experimental test arrangement.

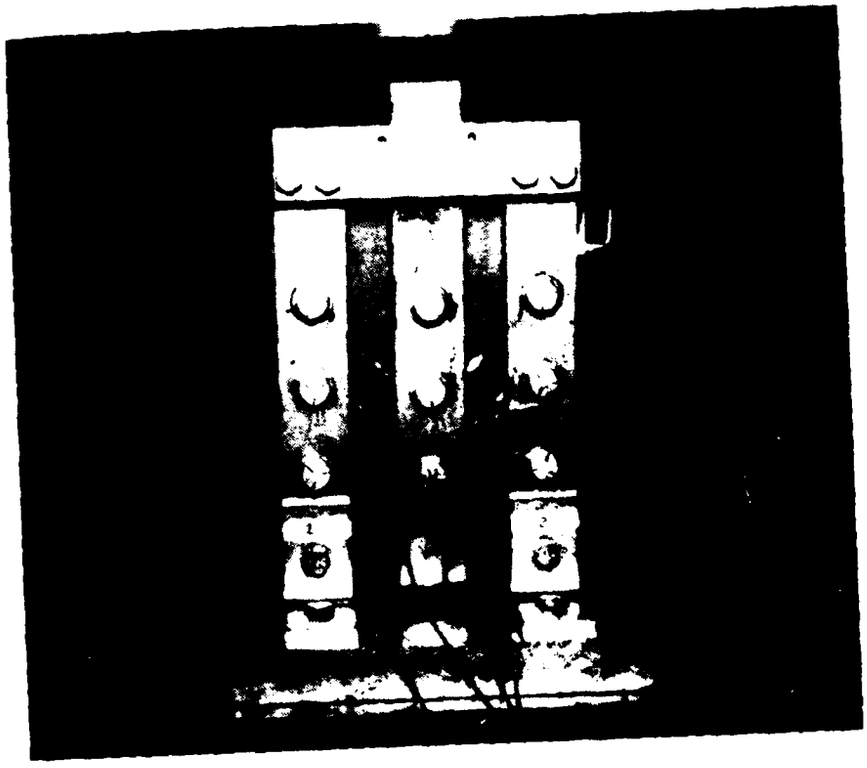

Figure 13. Three-rail shear test fixture.

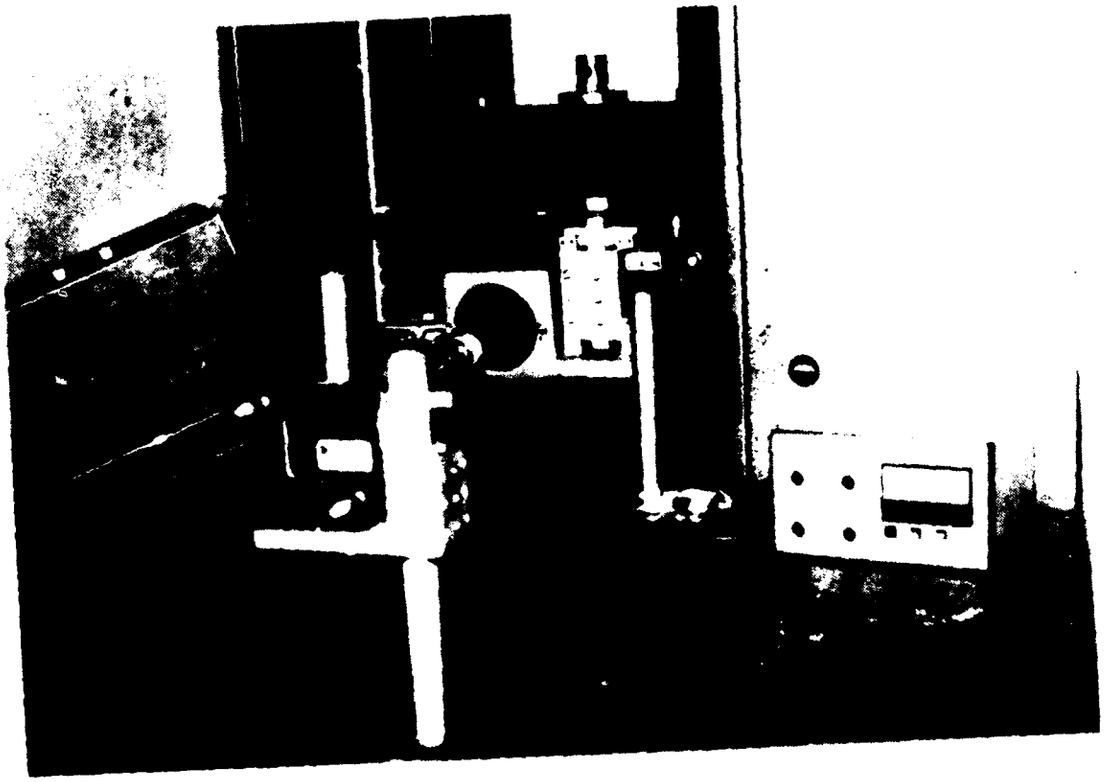

Figure 14. Optical setup for shear test.

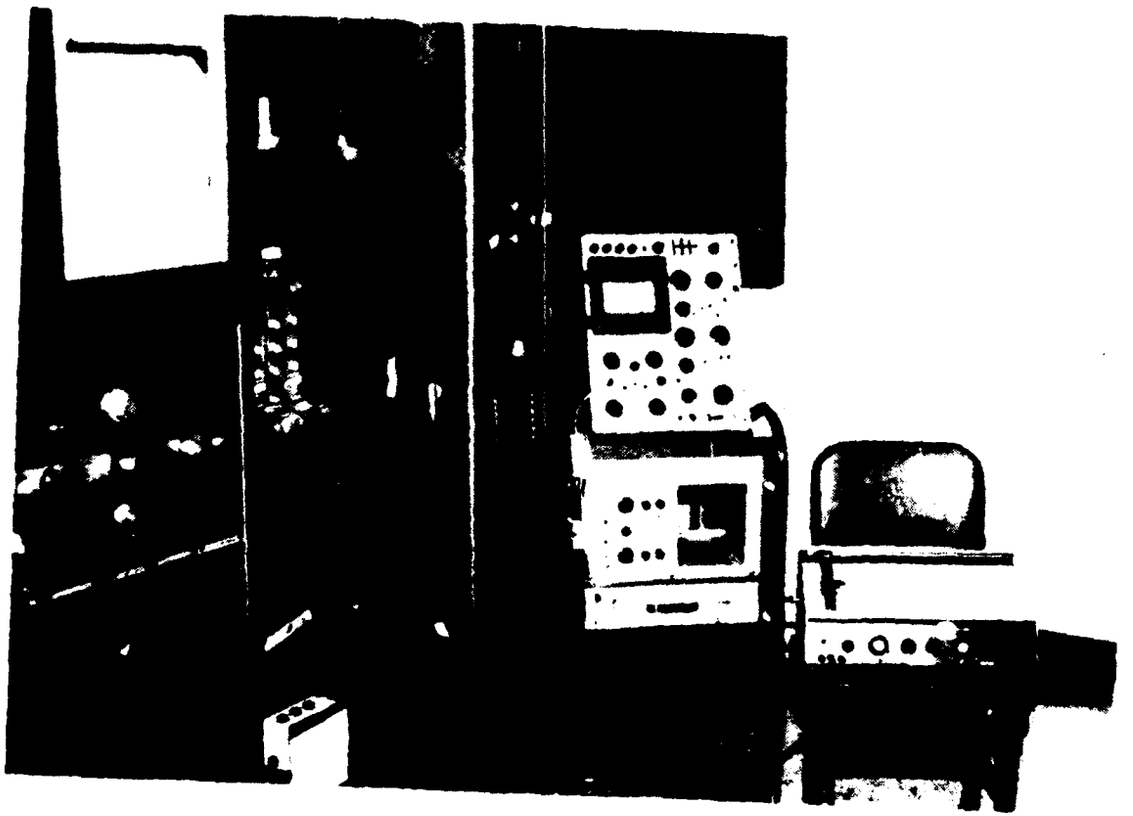

Figure 15. Instrumentation setup for shear test.

Figure 16 shows the optics required to prepare interferograms of the zero- and ninety-degree orientation tensile specimens. An iris was used to allow only enough filtered laser light to strike the specimen to fill the image transparency. Figure 17 shows the instrumentation side of the experimental test arrangement. The oscilloscope and X-Y recorder were used to collect strain data to correlate with those obtained through laser speckle.

B. Setup for Aperture Analysis of Interferograms

A system for analyzing interferograms developed by Schaeffel [6] was used to analyze selected areas on the shear specimens. Figure 18 is a photograph of the aperture analysis system from the collimated light at the right to the permanent film record at the left. Figure 19 is a sketch of the system. An interferogram is placed in the parallel light field produced by the collimater which generates an infinite number of Young's fringe diffraction halos. At this point an aperture can be placed in a location of the diffraction field to map selectively a small region of each diffraction halo into the viewing plane for photographing a permanent record. Then displacements can be determined from the interpretation of the fringe patterns from the following equation:

$$r = \frac{K\lambda Z_2}{Y}(m + \tfrac{1}{2}) \tag{23}$$

where

$r \equiv$ Displacement

$K \equiv$ Interferogram magnification ratio

$Z_2 \equiv$ Aperture-viewing plane distance

$Y \equiv$ Screen location

$m \equiv$ Fringe order

$\lambda \equiv$ Wavelength of laser light

The complete development of Equation (23) can be found in Schaeffel [6]. A Spectra Physics Model 125 He-Ne laser was used as the light source with the beam expanded through a Spectra Physics model 332 spatial filter and collimated with a 50.8-mm-diameter Spectra Physics model 336 collimater. The computer scan locations shown in Figure 10 were observed at the free edge and center locations of the shear specimens using aperture reconstruction. A typical reconstructed fringe pattern of the right-hand center scan of a shear specimen is shown in Figure 20. Enough of the diffraction field is mapped to demonstrate the displacement field. The center column of fringes is the displacement mapping of the shear specimen. The direction of the displacements is in a direction orthogonal to the fringes. The shearing action is easily detectable from the orientation and curvature of the center column of fringes. The fringe patterns on each side of the center rail are parallel and show no curvature; thus the displacement is vertical. Any point on the film record can be used to find the point displacement and strains, as well as to provide

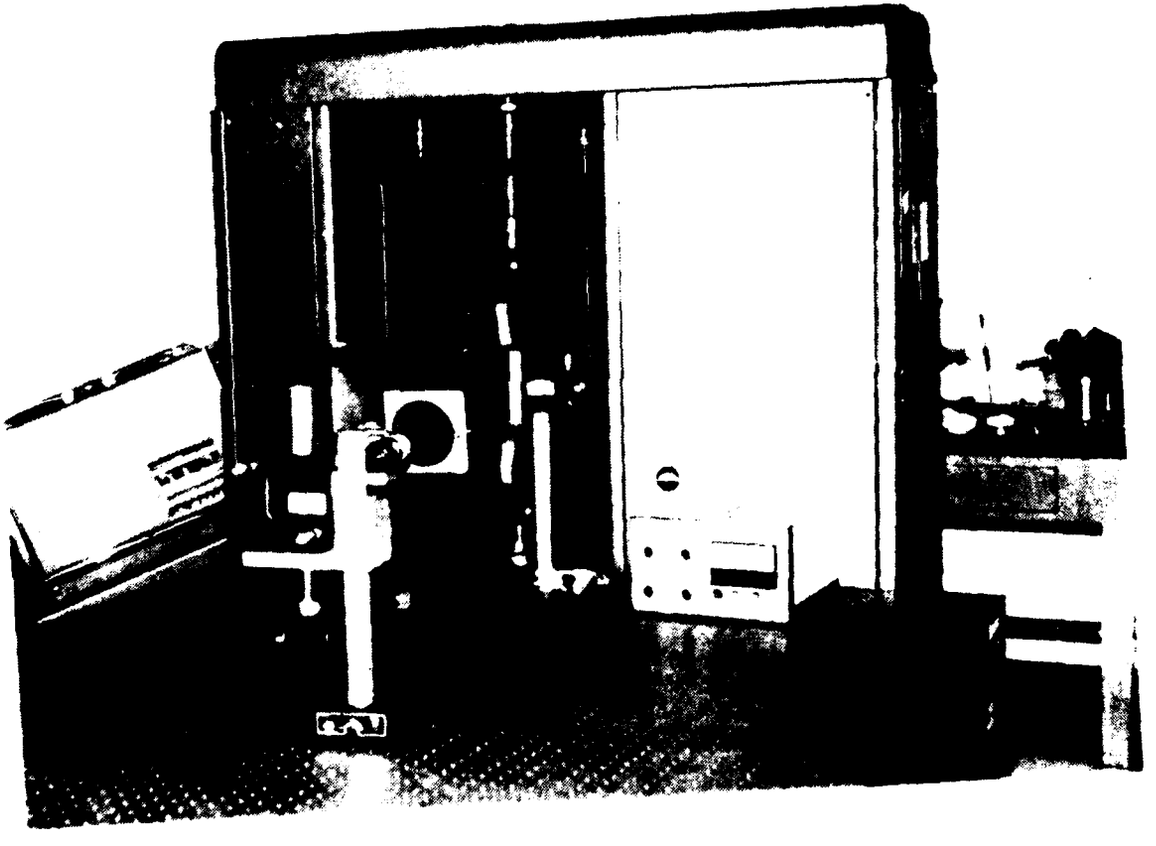

Figure 16. Optics setup for tensile test.

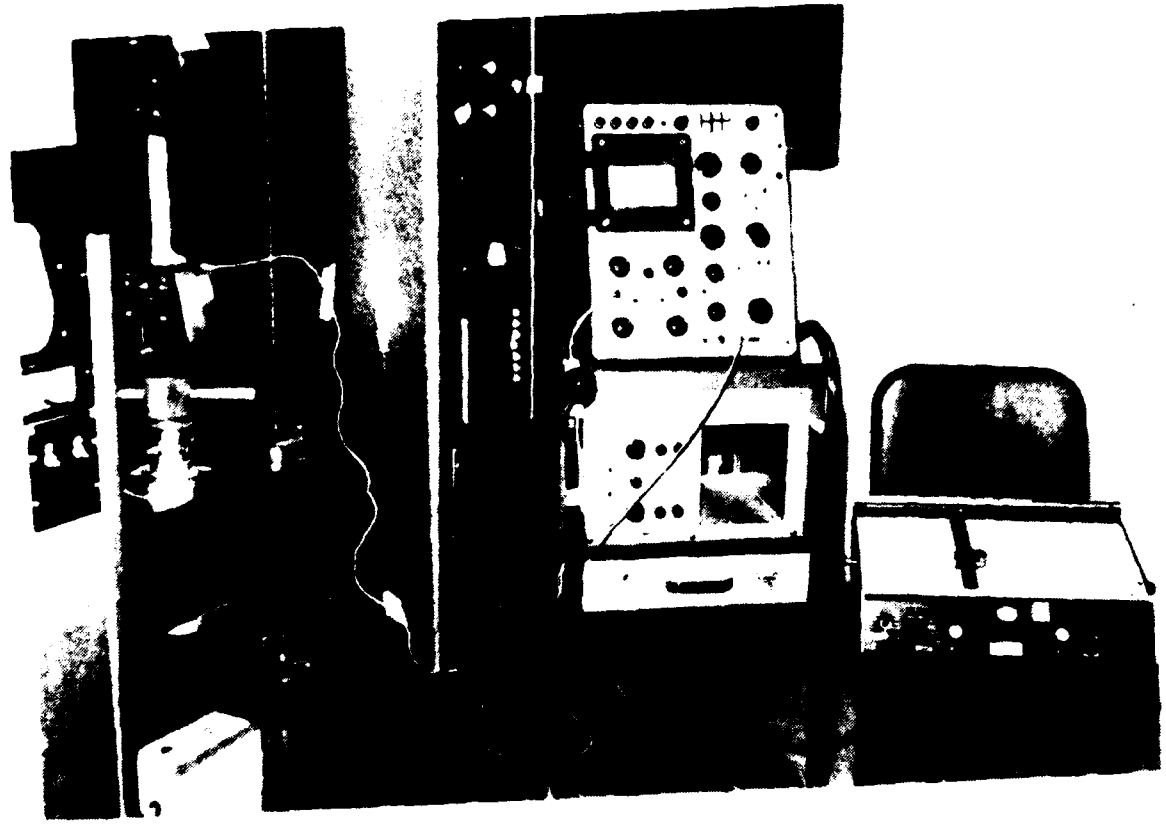

Figure 17. Instrumentation setup for tensile test.

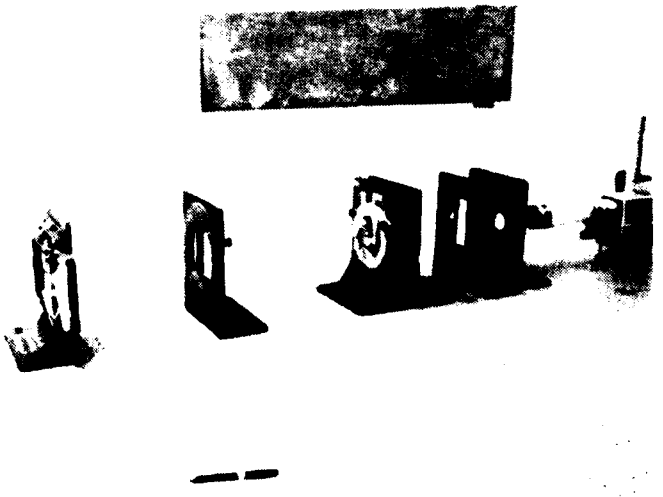

Figure 18. Aperture analysis system.

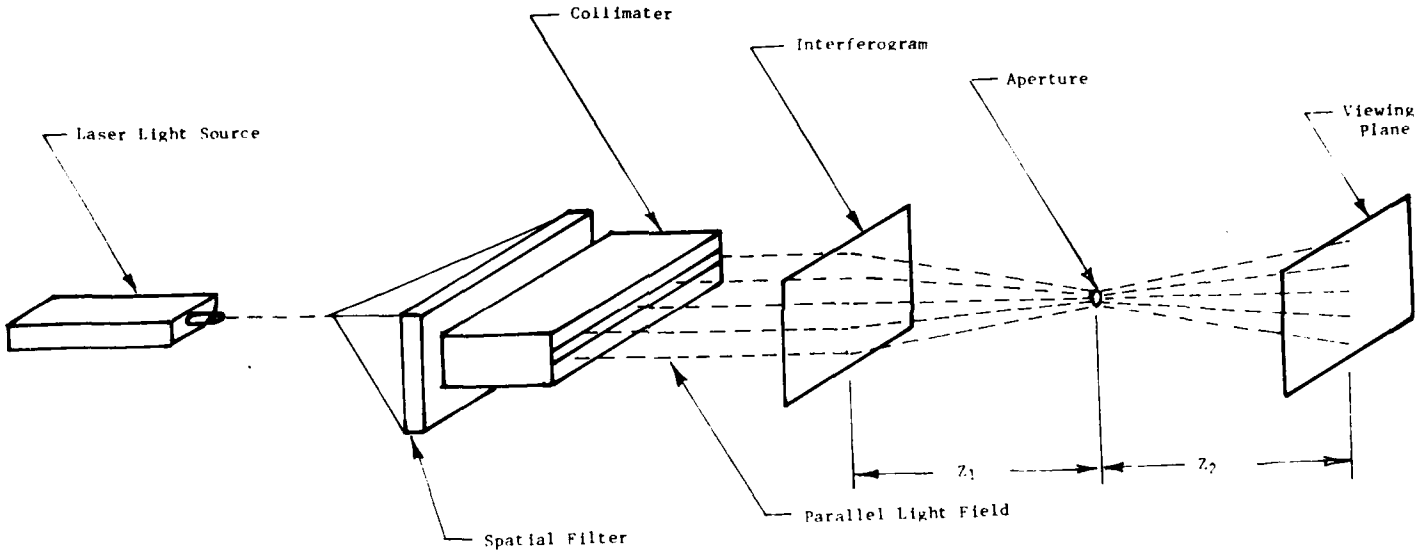

Figure 19. Aperture reconstruction of laser speckle interferograms.

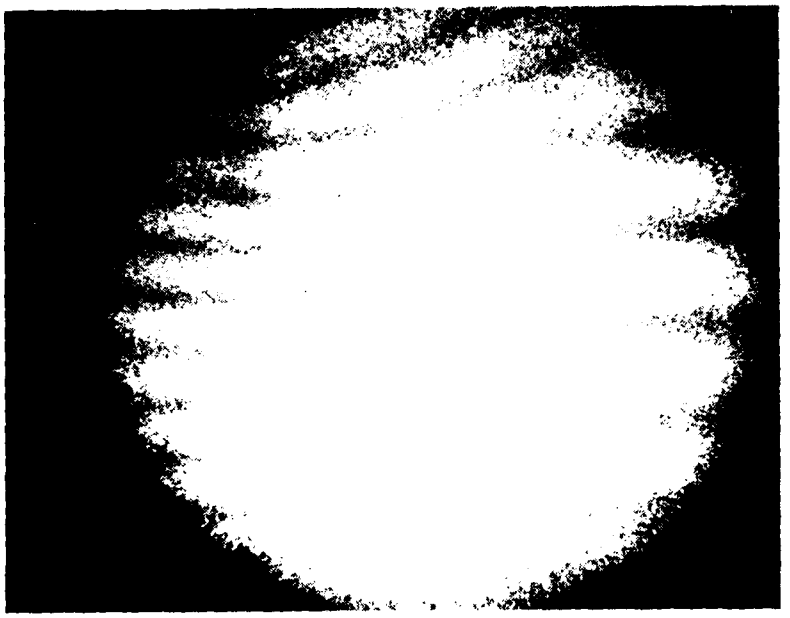

Figure 20. Reconstructed interferogram of XP-250 shear panel.

the viewer with a full field displacement mapping. The full field mapping is an excellent tool for nondestructive testing of specimens in shear because it can be used to observe boundary conditions where strain gaging is not feasible. The particular aperture reconstructed interferogram shown in Figure 20 was loaded from 7740 Newtons to 9296 Newtons with a delta of 1556 Newtons. Appendix C contains a series of aperture reconstructed interferograms representing different load levels as the shear specimens were taken to failure.

C. Computer Aided Scanning System

The data for the shear and tensile specimens were collected by an electromechanical single beam speckle interferometric analyzer system as shown in Figure 21. The computer aided reduction system was developed primarily for applications in speckle interferometric data analysis [4]. The basic system consists of two parts which include an optical display of interference data and the computer hardware used in the numerical analysis. The interferograms were placed in a viewing window of the X-Y translation table and illuminated by a laser beam which produced an interference fringe pattern at a point, as shown in Figure 22. The diffraction halo was centered and viewed on a diffuser screen which included a 25.4-cm 360-degree protractor. The protractor was used to measure the displacement angle of the interference fringes. The displacement of the region illuminated by the laser beam is inversely proportional to the fringe spacing as given by Equation (1). The direction of the displacement is along an axis perpendicular to the fringe orientation.

Since a very small area of the interferogram is illuminated, the data yields the displacement at a point. Therefore, to obtain a complete description of the surface, mappings of the regions as shown in Figures 9 and 11 were used

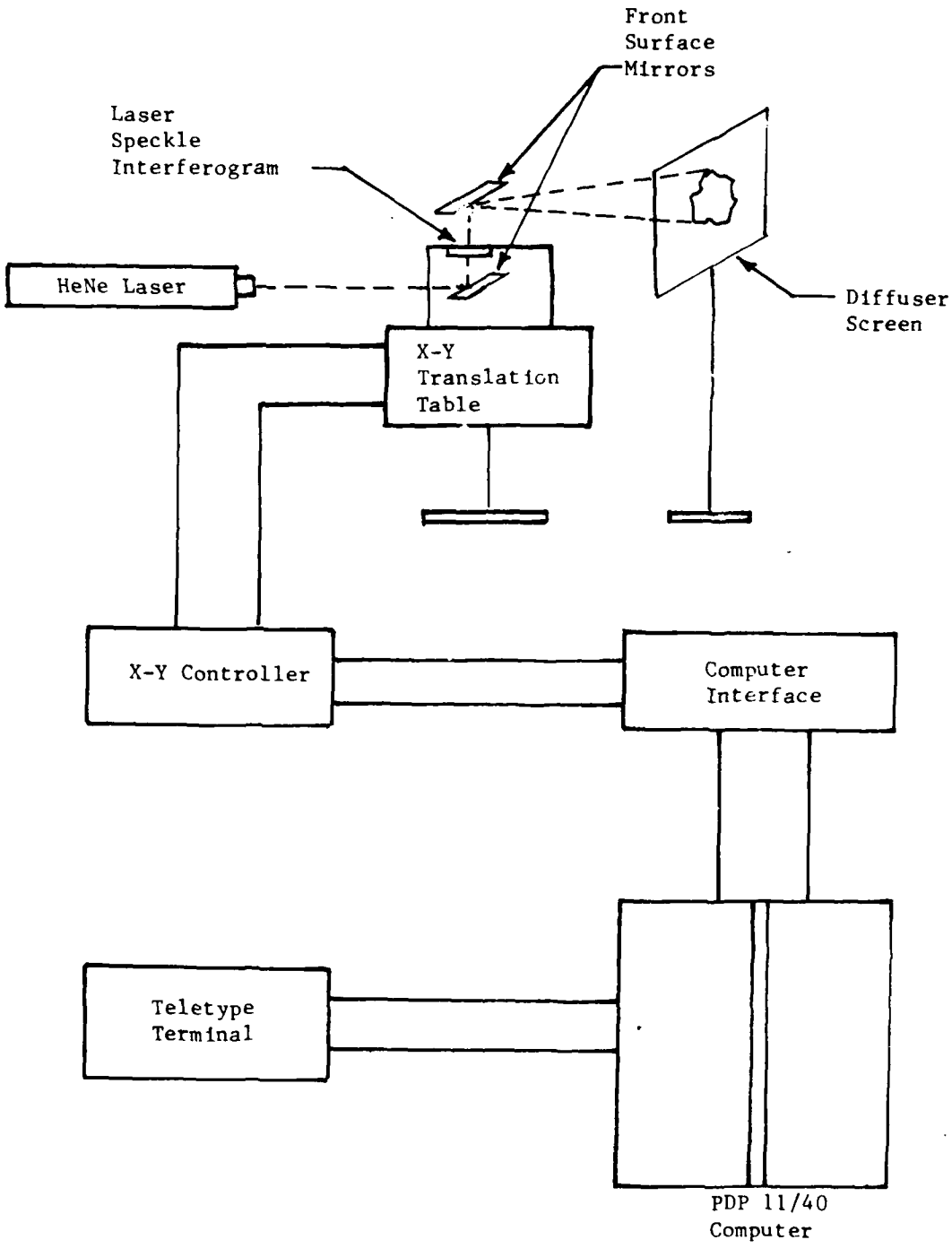

Figure 21. Electromechanical single-beam speckle interferometric analyzer system.

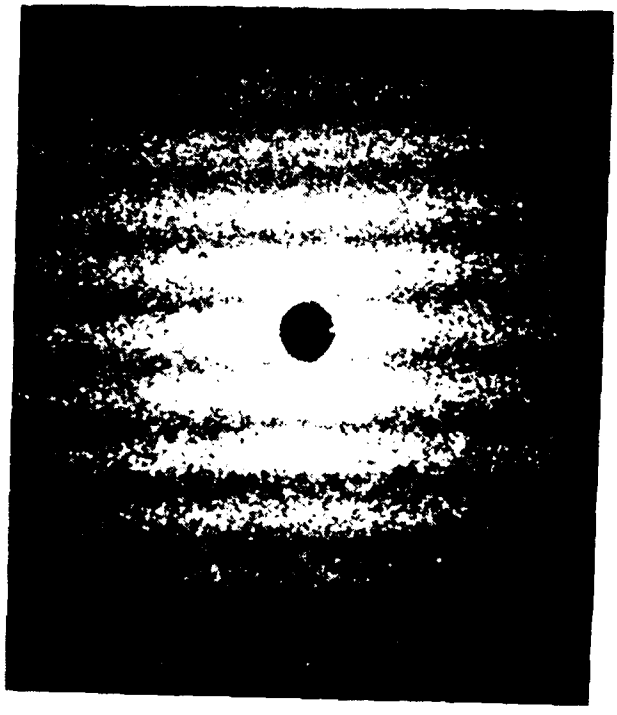

Figure 22. Typical speckle photography fringe pattern.

for the tensile and shear specimens. The mapping configurations were obtained by the X-Y translation table as shown in Figure 4. The laser beam passes through a point on the interferogram and the film plate is then translated relative to the stationary laser beam. The X-Y stage has the capacity to translate 152 mm in each direction in 0.025-mm increments, with a 0.0025-mm repositioning accuracy. Location of the desired point on the interferogram was controlled by the translation stage stepping motors which were in turn controlled by the computer. The computer program used to control the scan pattern and calculate the displacements appears in Appendix A.

V. RESULTS AND DISCUSSION

The test specimen nomenclature for the tensile specimens was set up as shown in Figure 23. Tables 1 and 2 show the physical dimensions of the $[0]_s$ and $[90]_s$ tensile test specimens. The end tab region averaged 8.2 mm. The ply properties for the $[0]_s$ tension tests are summarized in Table 3. The average values for Young's modulus of elasticity and ultimate strengths of 39.3 G Pa and 830.5 M Pa, respectively, agree well with the values of 39.3 G Pa and 896.3 M Pa published by the 3M Company [2]. The average ultimate strength of the specimens was 7.3 percent lower than that obtained by the 3M Company. The lower strength could be due to the mode of failure. As shown in Figure 24, the "shaving brush" failure is exhibited by specimens 2, 3, 4, and 5, while

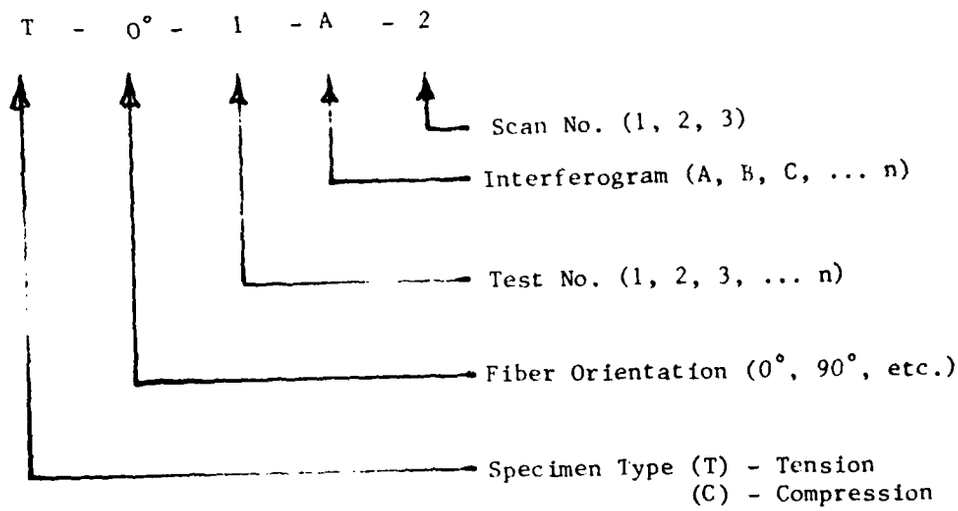

Figure 23. Coupon test specimen nomenclature.

Table 1. Physical Dimensions of $[0]_s$ Tensile Specimens

Specimen	Width (mm)	Thickness (mm)	Gage Length (mm)
T-0°-1-A	12.7	1.87	151.9
T-0°-2-J	12.9	1.85	152.7
T-0°-3-B	12.2	1.83	152.4
T-0°-4-N	12.7	1.95	151.9
T-0°-5-E	12.7	1.84	152.4
Mean	12.6	1.87	152.3

Table 2. Physical Dimensions of $[90]_s$ Tensile Specimens

Specimen	Width (mm)	Thickness (mm)	Gage Length (mm)
T-90°-1-A	24.9	1.69	152.7
T-90°-4-E	25.1	1.61	151.9
T-90°-5-F	25.4	1.68	152.4
T-90°-6-A	25.4	1.72	151.9
T-90°-7-G	25.1	1.83	151.9
Mean	25.2	1.71	152.2

Table 3. Ply Properties From $[0]_s$ Tension Tests

Properties / Specimen	Ultimate Stress X_1^T (M Pa)	Ultimate Strain ε (μcm/cm)	Young's Modulus E_{11} (G Pa)	Poisson's Ratio $\nu_{12} = \nu_{13}$
T-0°-1	814.3	21,500	39.4	0.265
T-0°-2	755.6	21,250	38.8	0.300
T-0°-3	878.6	22,200	41.0	0.303
T-0°-4	810.0	22,995	36.4	0.294
T-0°-5	894.0	22,550	41.1	0.306
Mean Value	830.5	22,099	39.3	0.294
		Standard Deviation	1.9	0.017
		Coefficient of Variation	4.83	5.8

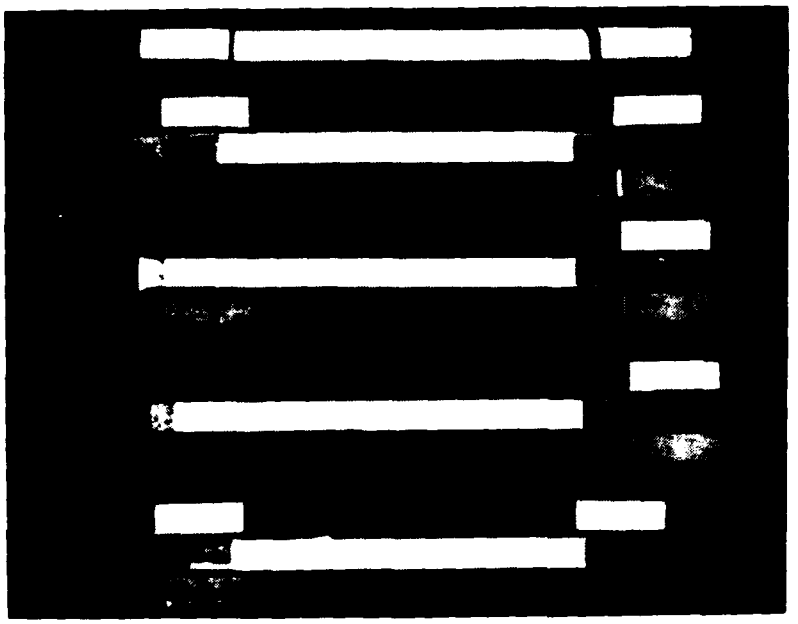

Figure 24. The failed $[0]_s$ tensile specimens.
(Top-to-bottom: Specimens 1 through 5)

specimen 1 exhibited a splintering effect and failed near the end tab, but was not considered an end tab failure. An audible noise occurred on each $[0]_s$ tensile specimen which was accompanied with a small drop in the load and strain readings near one-third of the ultimate load. It was not determined whether the noise was from slippage of end tabs or alignment of the loading structure on the tensile test machine (Instron). It is recommended that movie film be made on future testing of this nature to aid in determination of the source of noise. Poisson's ratio determined from laser speckle interferometry of the $[0]_s$ specimens was 0.294, with a standard deviation of 0.017 and a coefficient of variation of 5.8. The value varies by 1.6 percent with that obtained by Smith and Huang. The displacements obtained from the $[0]_s$ specimens through laser speckle interferometry are plotted in Figures A-1 through A-7 and appear in Appendix A. The stress-strain curves for the $[0]_s$ specimens are shown in Figures A-8 through A-12.

Five tension tests were conducted on unidirectional specimens loaded at 90 degrees to the fiber direction. The ply properties are summarized in Table 4. The average values for Young's modulus of elasticity of 13.08 G Pa agrees well with the value of 12.0 G Pa value obtained by Smith and Huang [7]. The ultimate strength of 29.1 M Pa was much lower than 52 M Pa obtained by Smith and Huang [7]. The elastic region, however, was in excellent agreement. End tab failure was the cause of the low ultimate strength as can be observed in Figure 25. The specimens broke either at the end tabs or slightly inside the end tabs. Specimen 4 is the only one that had a failure away from the end

Table 4. Ply Properties from $[90]_s$ Tension Tests

Properties / Specimens	Ultimate Stress X_2^T (M Pa)	Ultimate Strain ε (μcm/cm)	Young's Modulus E_{22} (G Pa)	Poisson's Ratio $\nu_{21} = \nu_{31}$ Test Value	Poisson's Ratio ν_{21} Calculated Value
T-90°-1	39.1	3800	11.4	0.085	0.085
T-90°-4	23.7	1700	14.7	0.082	0.109
T-90°-5	21.2	1605	13.9	0.088	0.104
T-90°-6	30.0	2425	12.8	0.076	0.096
T-90°-7	31.3	2570	12.6	0.080	0.094
Mean Value	29.1	2420	13.08	0.082	0.098
Standard Deviation			1.3	0.004	0.009
Coefficient of Variation			9.94	4.88	9.49

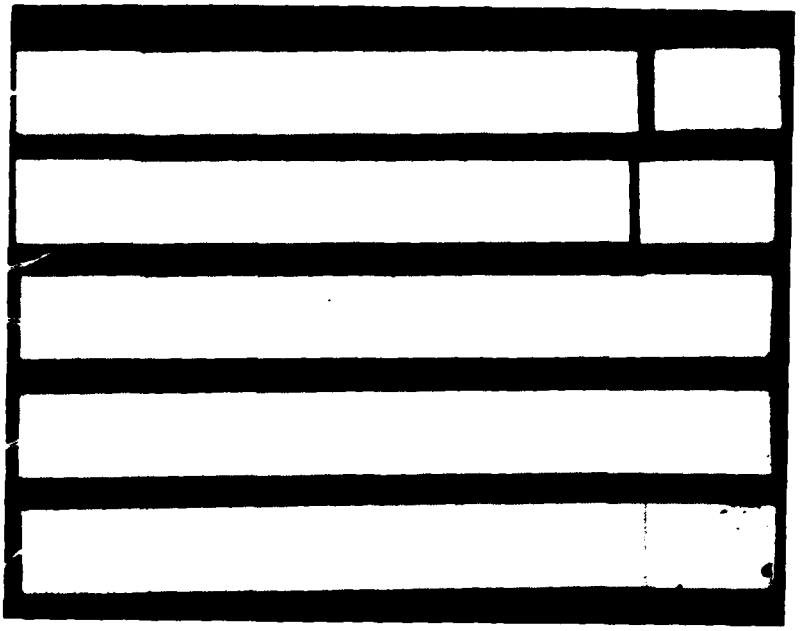

Figure 25. The failed $[90]_s$ tensile specimens.
(Top-to-bottom: Specimens 1, 4, 5, 6, 7)

tab. The displacement versus scan position is plotted in Figures A-13 through A-19, and the stress versus strain is plotted in Figures A-20 through A-24 and appear in Appendix A.

The nomenclature code for the shear test specimens is shown in Figure 26. The free edge and center scan displacement data obtained through laser speckle interferometry for shear specimen 7 is shown in Tables B-1, B-2, and B-3. Each table presents the displacements resolved into horizontal and vertical directions at different load levels and at specified coordinates. The minus signs on the displacements designate the direction and are not to be interpreted as negative values. The displacements were used to calculate strains and shear strains. The shear strains versus scan position are plotted for the different load levels of specimen 7 in Figures B-1, B-2, and B-3. The displacement data from the left-hand side of shear specimen 8 are presented in Tables B-4, B-5, and B-6. The data are presented for free edge as well as center scan for the coordinate positions shown in Figures 10 and 11. The shear strains versus scan positions are plotted in Figures B-4, B-5, and B-6. The right-hand displacement data for specimen 8 is presented in Tables B-7, B-8, and B-9, while the shear strains versus scan position data are presented in Figures B-7, B-8, and B-9.

Laser speckle interferometry allowed data to be analyzed at any point of interest in the stress field. This technique allowed indepth observation of such areas as the free edge of the shear specimen. The work performed in this project showed that there were displacements in both the horizontal and vertical directions which yield some strain in both directions as well as shearing strain. As expected, the shearing strain increased as the data were taken farther away

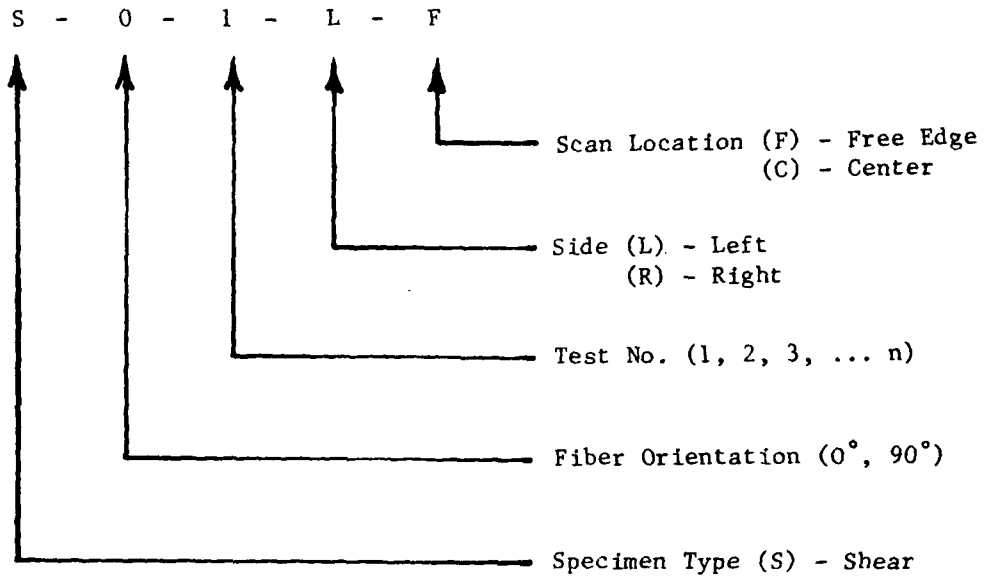

Figure 26. Shear test specimen nomenclature.

from the free edge, but was not linear; however, the shearing strains became more constant at locations closer to the center rail. The shear moduli decreased as the total load increased, which yields an increasing shear strain coupled with increased loading, thus confirming the nonlinear characteristics of the material. The shear modulus, G_{XY}, at different locations on the specimen and load increments, is presented in Table 5. A plot of the shear moduli taken at the same scan point but at different load ranges is presented in Figure B-10.

VI. SUMMARY AND CONCLUSIONS

A whole-field experimental stress analysis method was developed to investigate the behavior of composite laminates. The method employed was the photomechanical technique of laser speckle interferometry. Interferograms were prepared of $[0]_s$ and $[90]_s$ tensile specimens deformed under load. The interferograms were analyzed with a computer-aided optics system to obtain displacement fields. The resulting displacement data were used to calculate strains which were correlated with stresses. The stress correlation allowed anisotropic elastic constants such as the moduli of elasticity, Poisson's ratio, and shear modulus to be calculated. The results were in good agreement with data in the literature and the auxiliary strain gage system. The analytical and geometric techniques of obtaining anisotropic elastic constants from the full field displacements through laser speckle interferometry were presented in detail.

Zero-degree unidirectional shear specimens were analyzed using the three-rail shear test fixture. Displacement data were taken at the free edge of the shear specimens where it is inconvenient to apply strain gages. Data were also

Table 5. Shear Moduli at Increasing Load Ranges

Shear Specimen S-0°-8-L
Shear Modulus G_{XY} (GPa)

	Load Range: (2359-4116) Newtons		
	Y = 0.00 cm	Y = 0.56 cm	Y = 1.12 cm
X = 0.0 cm	1.86	2.87	4.67
X = 0.2 cm	1.58	2.16	3.04
	Load Range: (7654-9345) Newtons		
	Y = 0.00 cm	Y = 0.56 cm	Y = 1.12 cm
X = 0.0 cm	3.89	1.76	1.75
X = 0.2 cm	3.46	1.35	1.84
	Load Range: (12,905-14,685) Newtons		
	Y = 0.00 cm	Y = 0.56 cm	Y = 1.12 cm
X = 0.0 cm	3.13	1.32	1.21
X = 0.2 cm	2.89	1.75	1.56

analyzed in the center section of the specimen where the maximum amount of strain should occur. The displacement data from different load ranges were used to calculate strains, shearing strains, which were correlated with shearing stresses. The shear modulus was calculated from laser speckle data and agreed well with work performed with strain gages. It is recommended that the techniques be improved to produce interferograms with less exposure time, perhaps a pulsed laser light source, to avoid the delay associated with incremental loading.

The techniques of laser speckle interferometry and aperture analysis were both found effective in obtaining the displacement and strain fields. The techniques can be used quantitatively by technical investigators to obtain discrete data, as well as qualitatively by less technical personnel on a nondestructive evaluation basis. The foremost advantage of using laser speckle interferometry as a whole-field experimental stress analysis method is that the investigator obtains full-field information rather than average data from small regions. It is recommended that this technique be expanded to include analysis of a wide range of composite materials with different geometrical configurations.

REFERENCES

1. Chamis, C. C., and J. H. Sinclair, "10° Off-Axis Tensile Test for Intralaminar Shear Characterization of Fiber Composites," NASA TN D-8215, April 1976.

2. 3M Company, "Scotchply Reinforced Plastic Type XP-250," Technical Data Sheet No. 4, December 1968.

3. Standard Test Method for Tensile Properties of Oriented Fiber Composites, ASTM American National Standard ANSI/ASTM D 3039-76.

4. Schaeffel, J. A., B. R. Mullinix, W. F. Ranson, and W. F. Swinson, "Computer Aided Nondestructive Flaw Detection System for Composite Materials," US Army Missile Command, Redstone Arsenal, Alabama, Technical Report No. T-78-5, 26 September 1977.

5. Lekhnitskii, S. G., Theory of Elasticity of an Anisotropic Elastic Body, Holden-Day Series in Mathematical Physics, 1963.

6. Schaeffel, J. A., "Aperture Analysis of Laser Speckle Interferograms," US Army Missile Command, Redstone Arsenal, Alabama, Technical Report No. RL-80-11, 26 August 1980.

7. Smith, D. G., and J. Huang, "Post-Crazing Stress Analysis of Glass-Epoxy Laminates," Tennessee Technological University, US Army Missile Command Contract DAAK40-78-C-0165, May 1979.

APPENDIX A

TENSILE SPECIMEN DATA

APPENDIX A

LIST OF FIGURES

APPENDIX A

LIST OF FIGURES (Concluded)

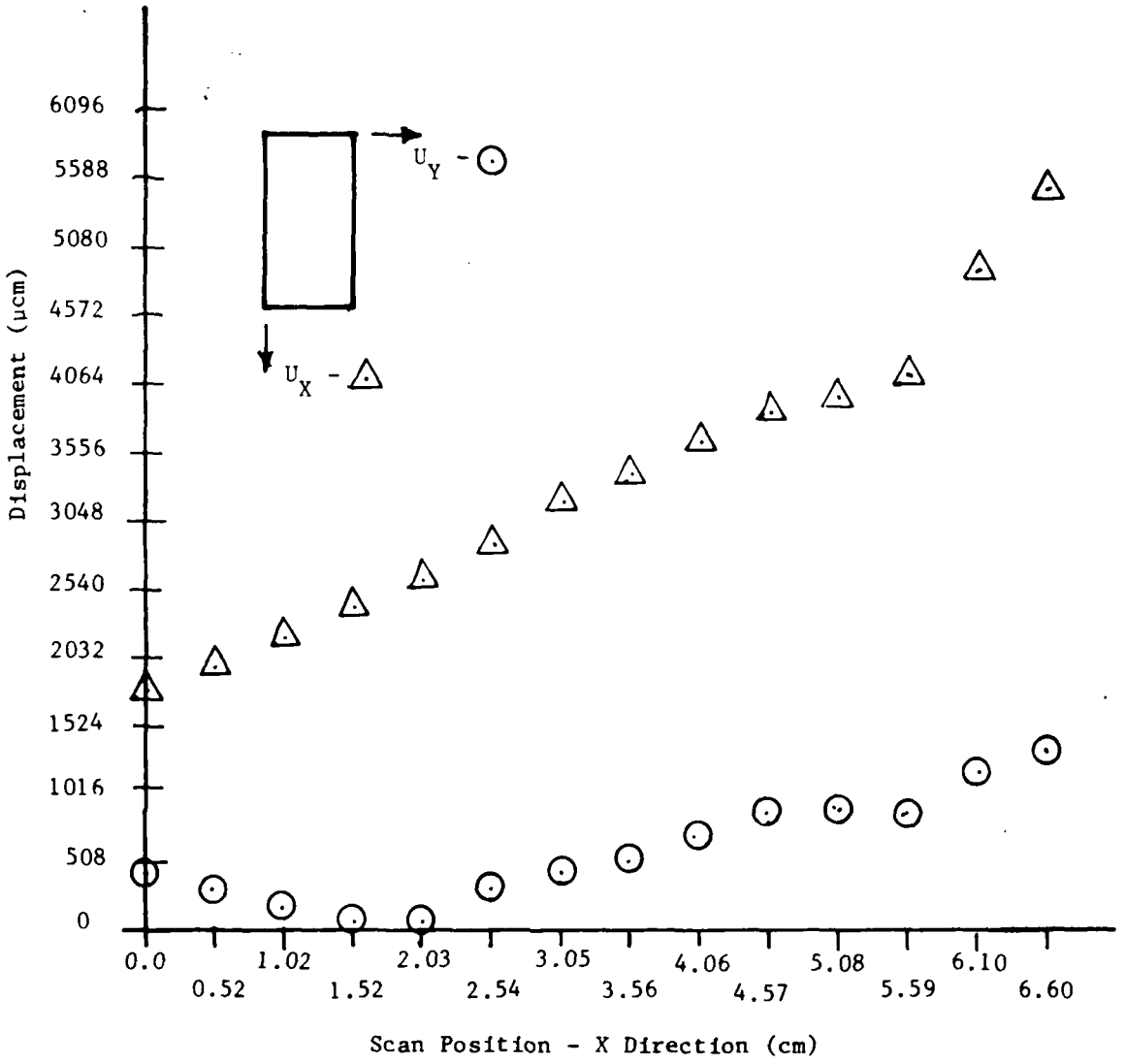

Figure A-1. Displacement versus scan position (T-0°-1-A-2).

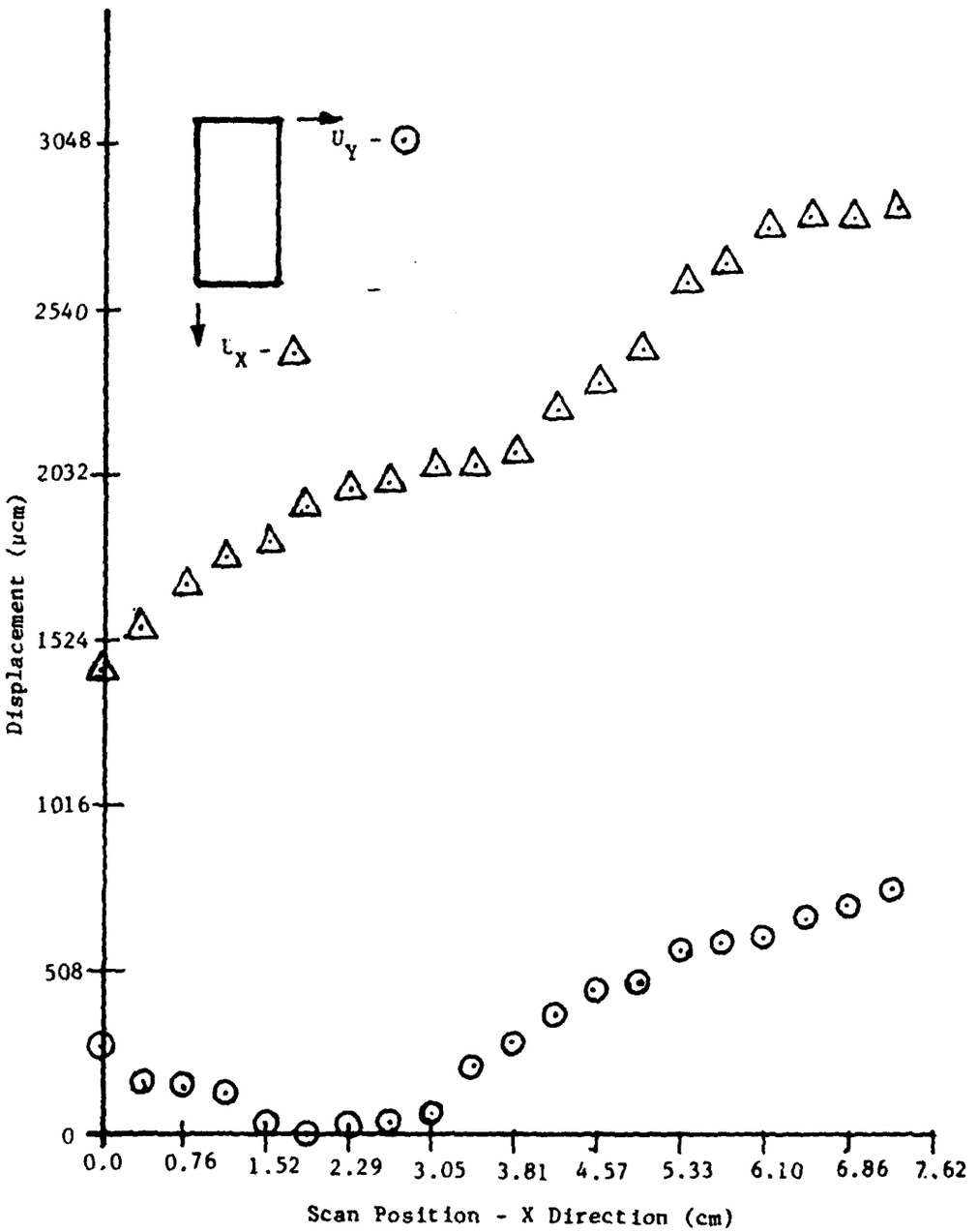

Figure A-2. Displacement versus scan position (T-0°-2-K-1).

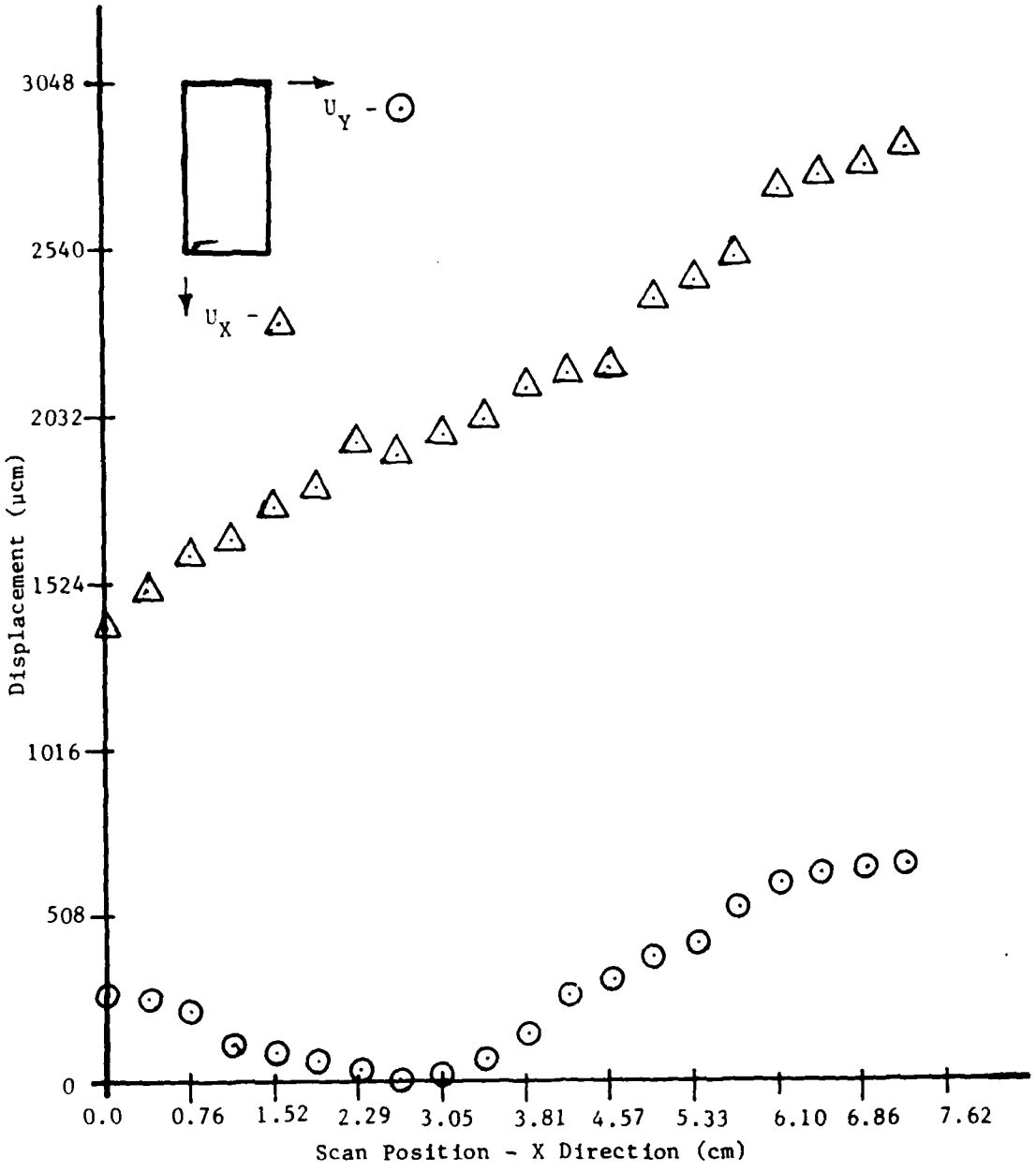

Figure A-3. Displacement versus scan position (T-0°-2-K-2).

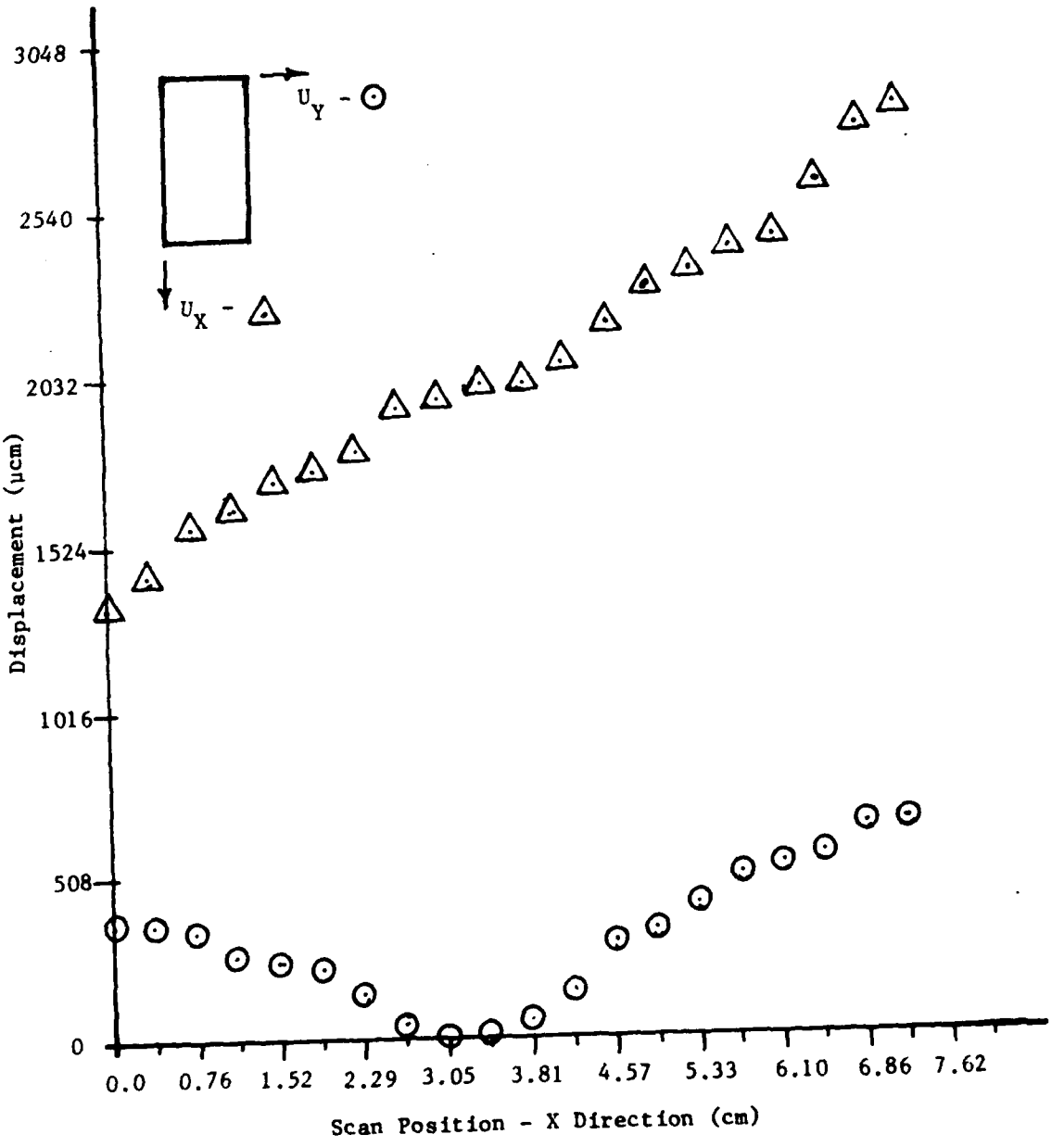

Figure A-4. Displacement versus scan position (T-0°-2-K-3).

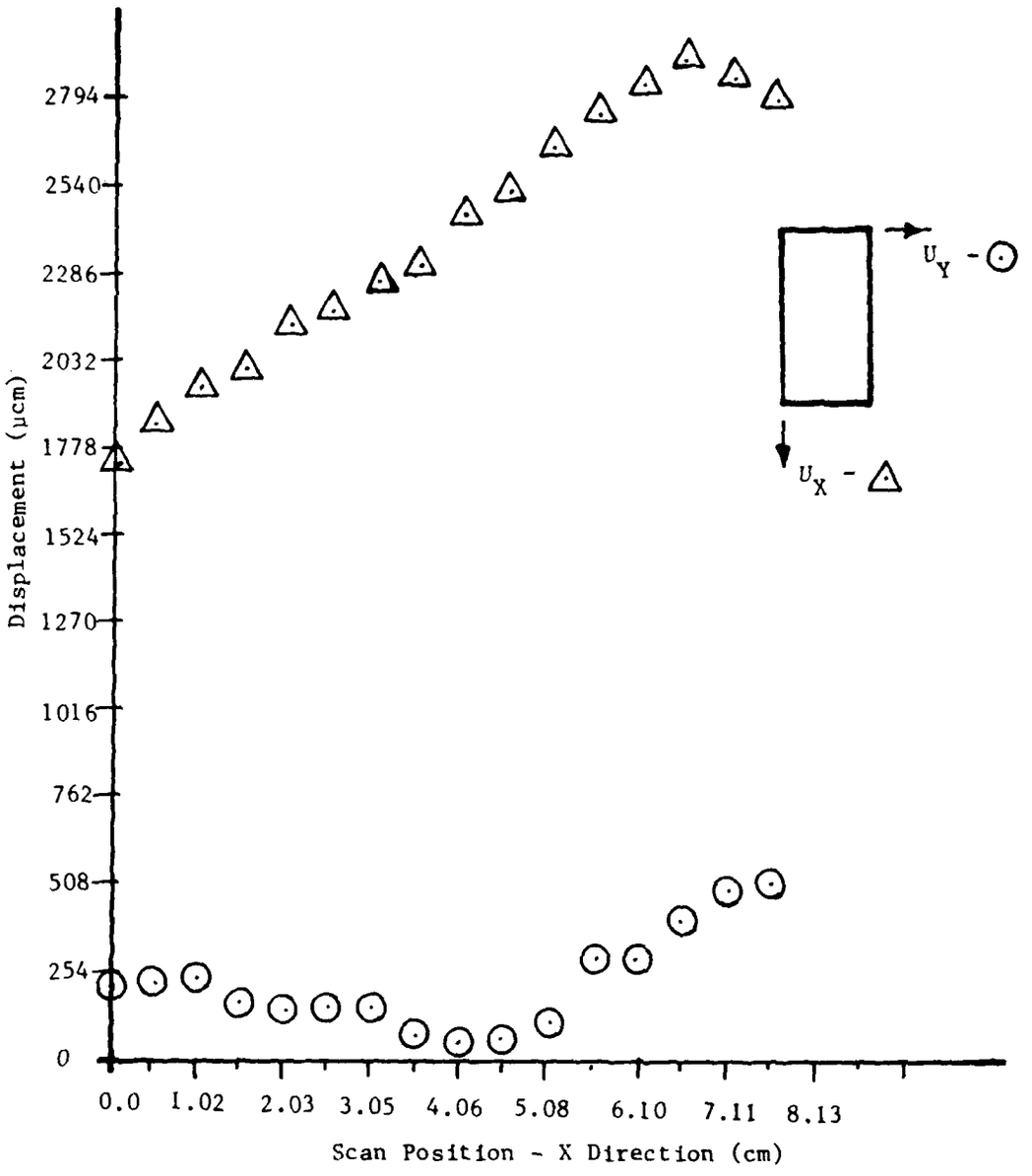

Figure A-5. Displacement versus scan position (T-0°-3-B-2).

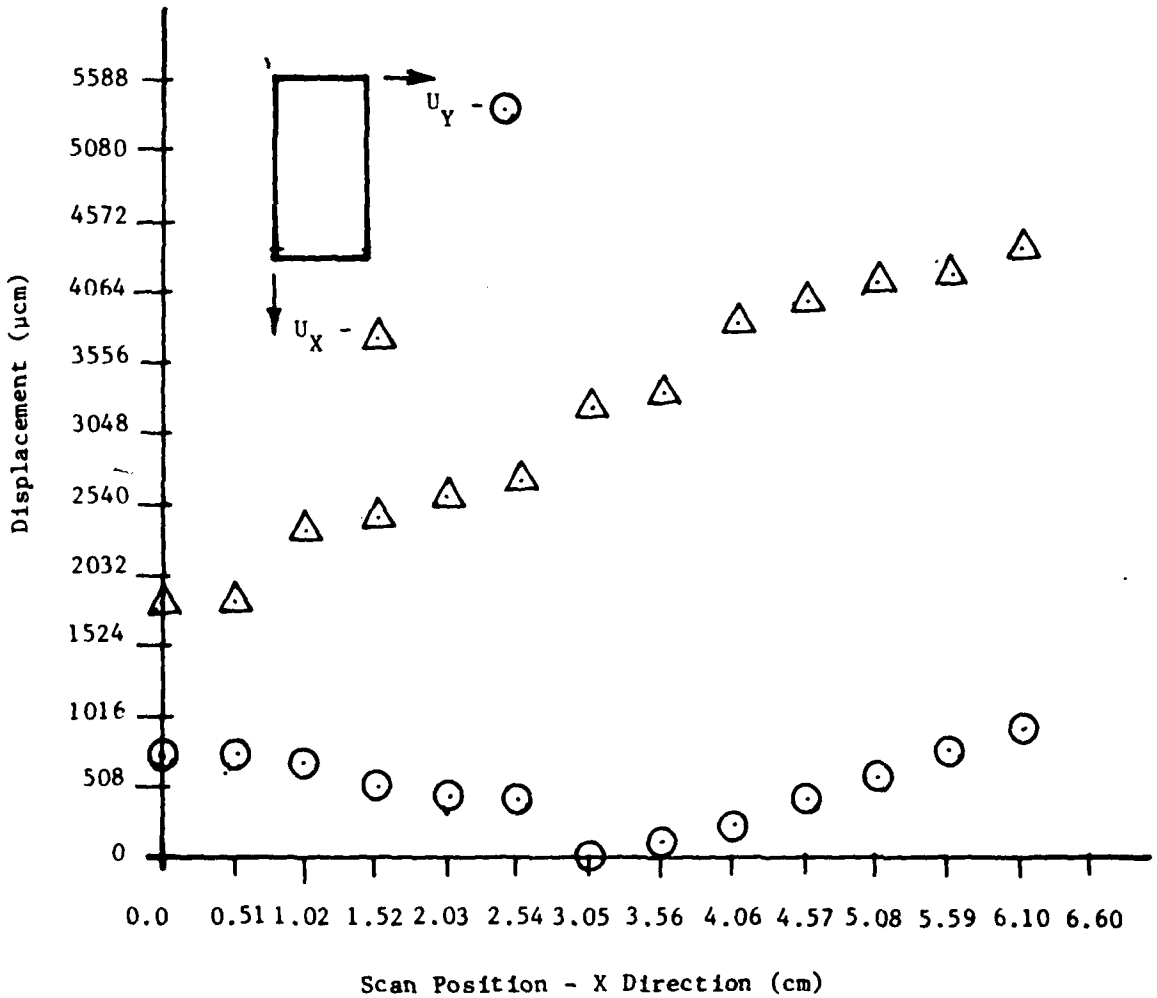

Figure A-6. Displacement versus scan position (T-0°-4-N-2).

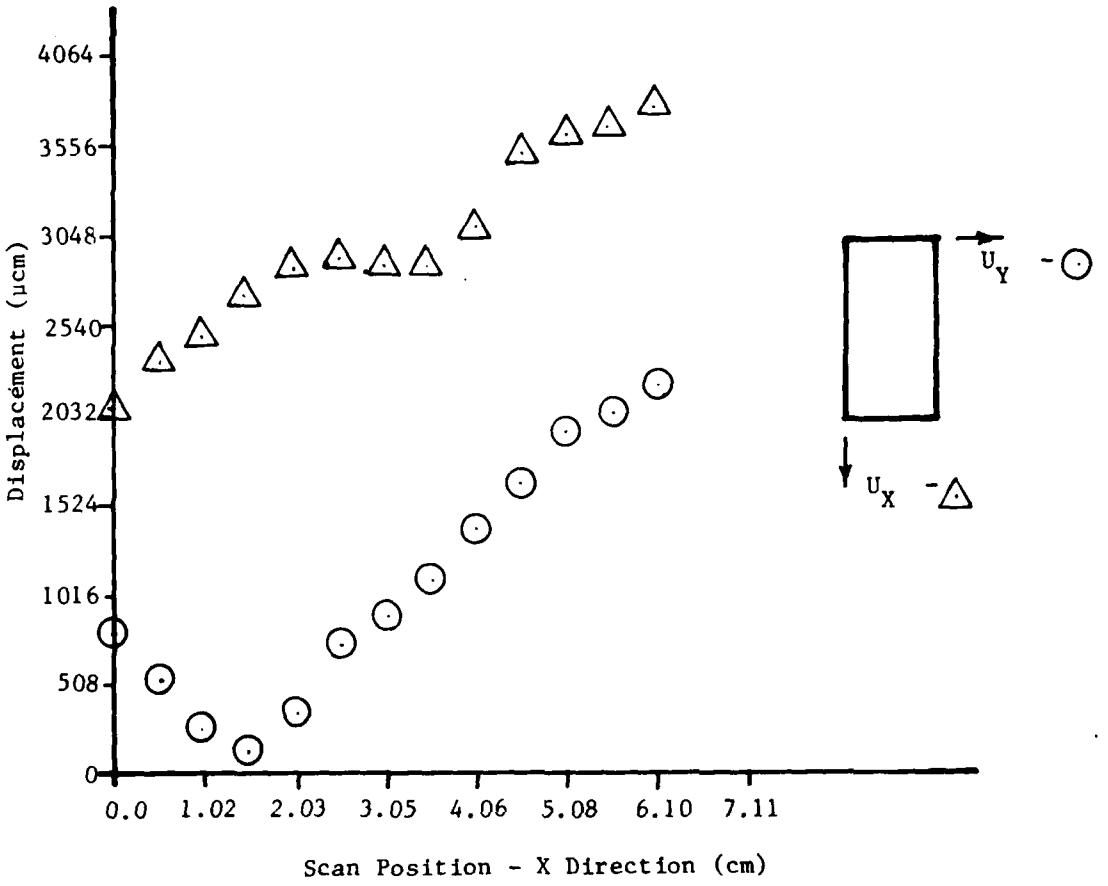

Figure A-7. Displacement versus scan position (T-0°-5-F-2).

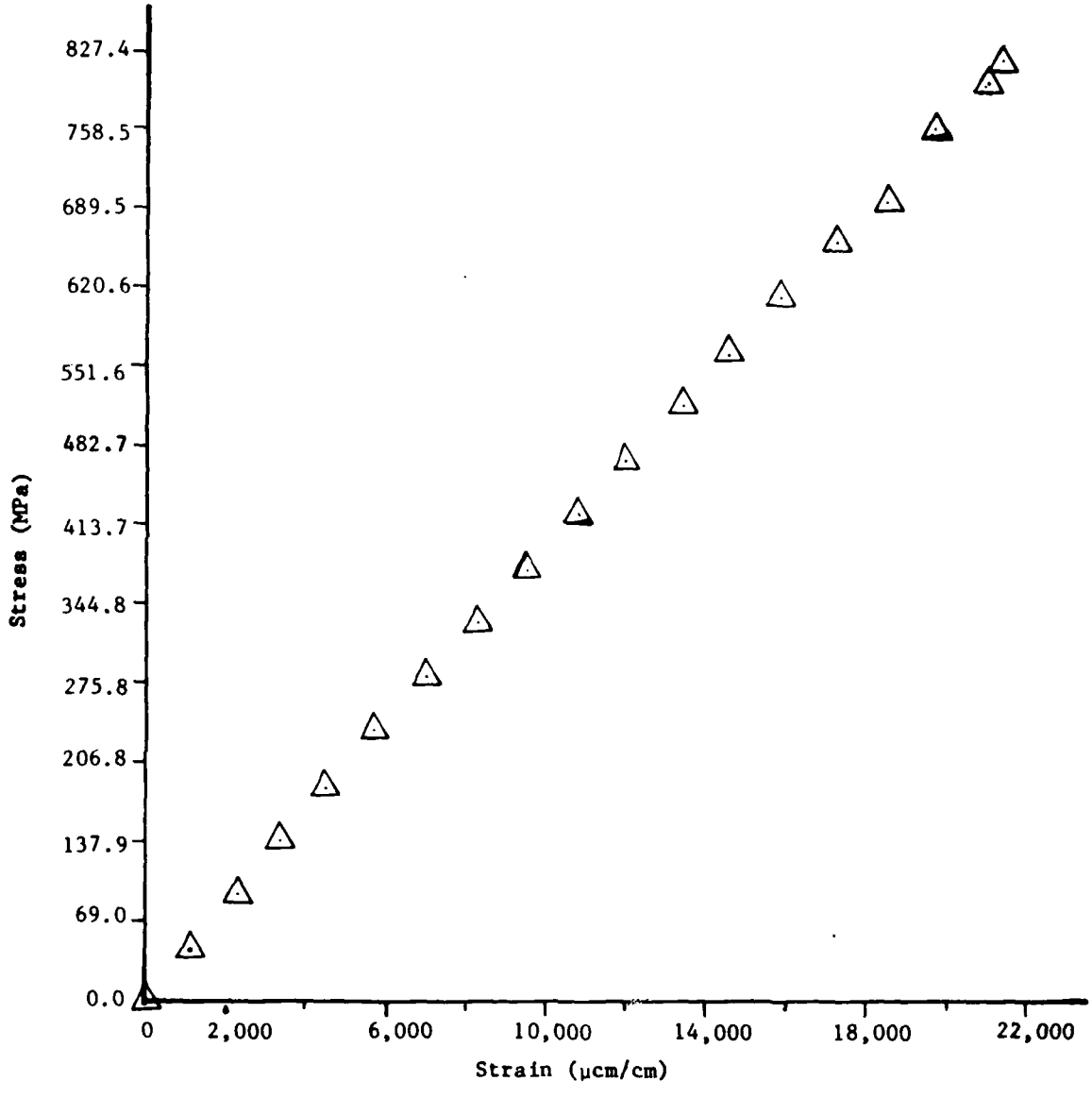

Figure A-8. Stress versus strain (T-0°-1).

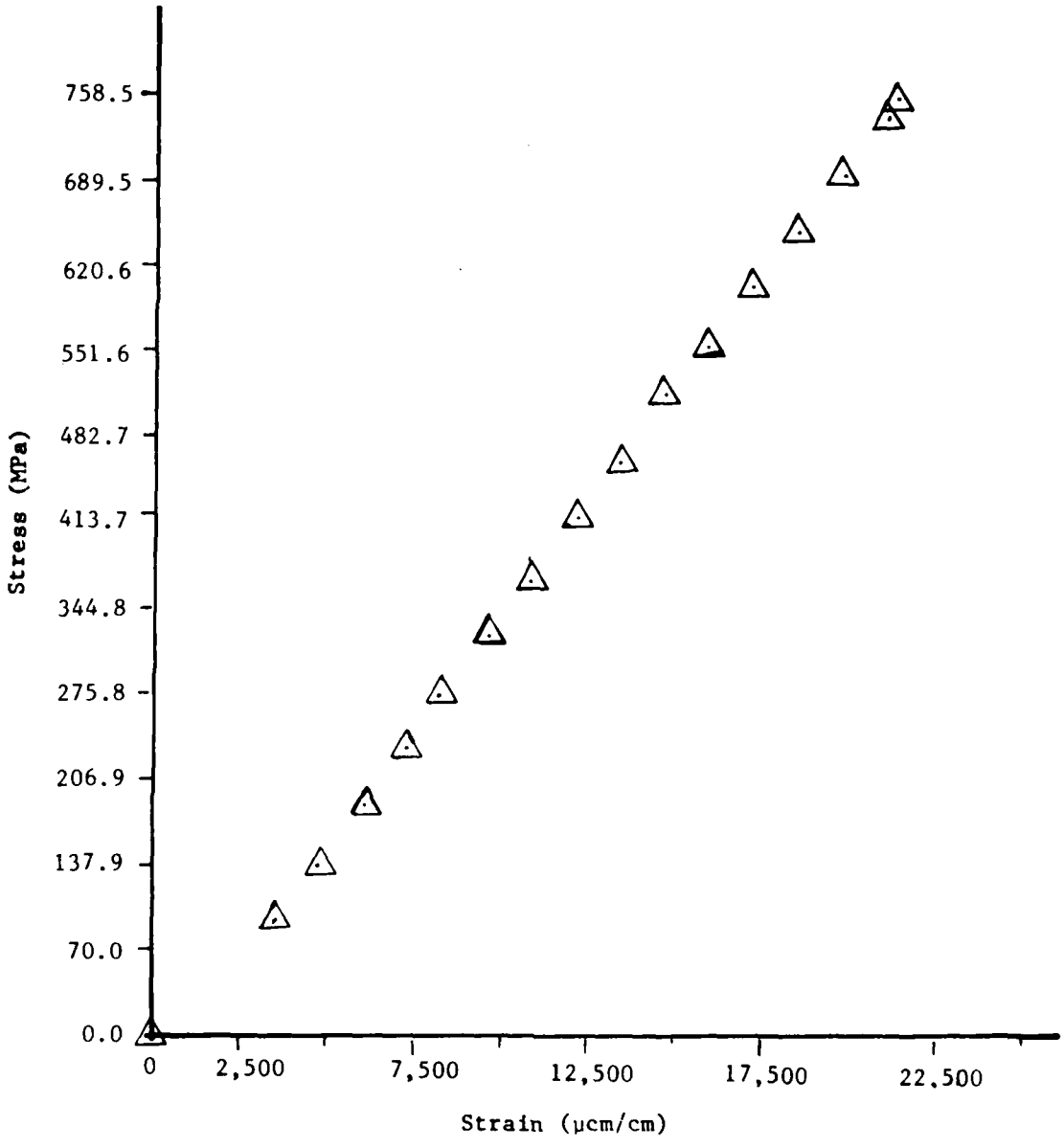

Figure A-9. Stress versus strain (T-0°-2).

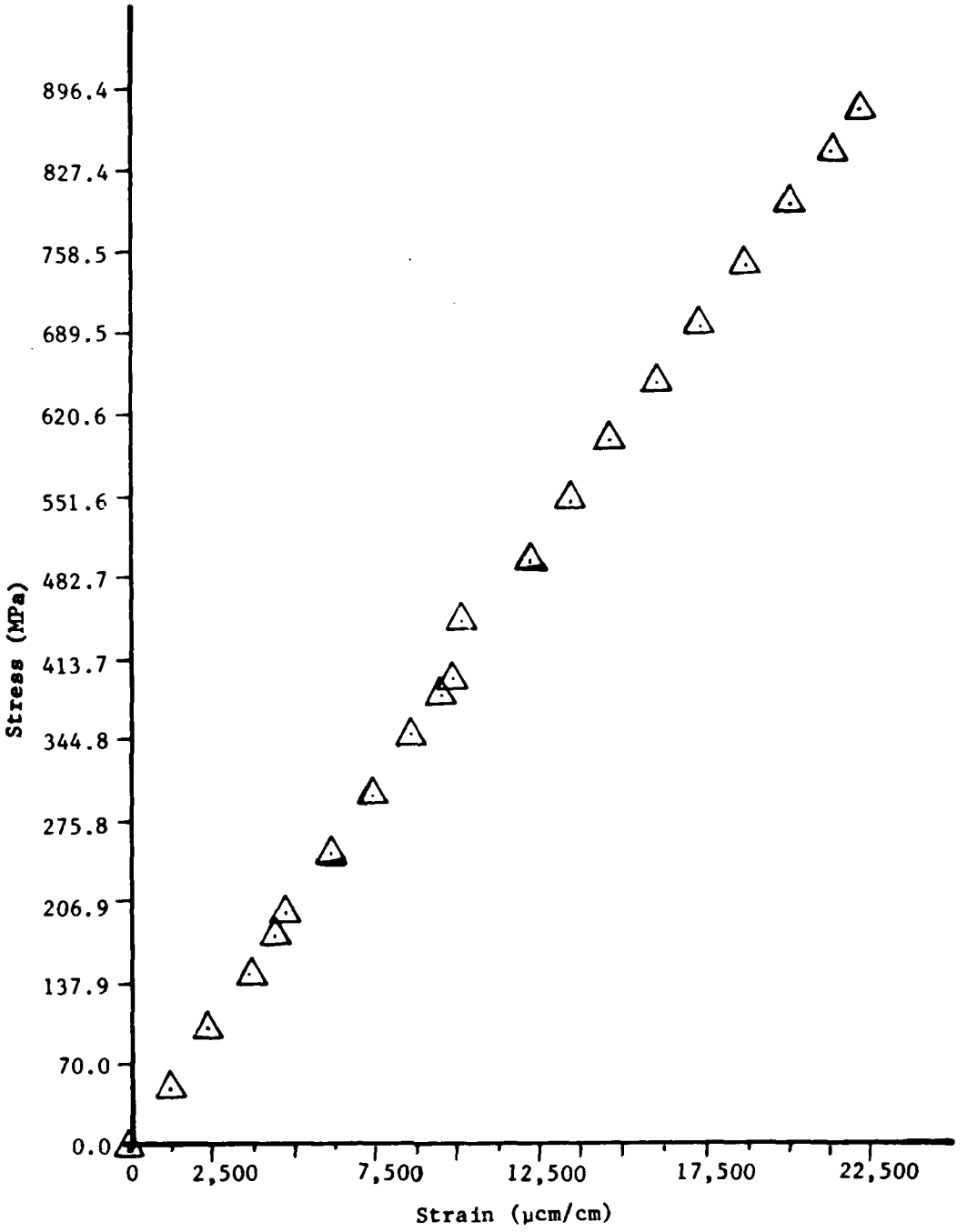

Figure A-10. Stress versus Strain (T-0°-3).

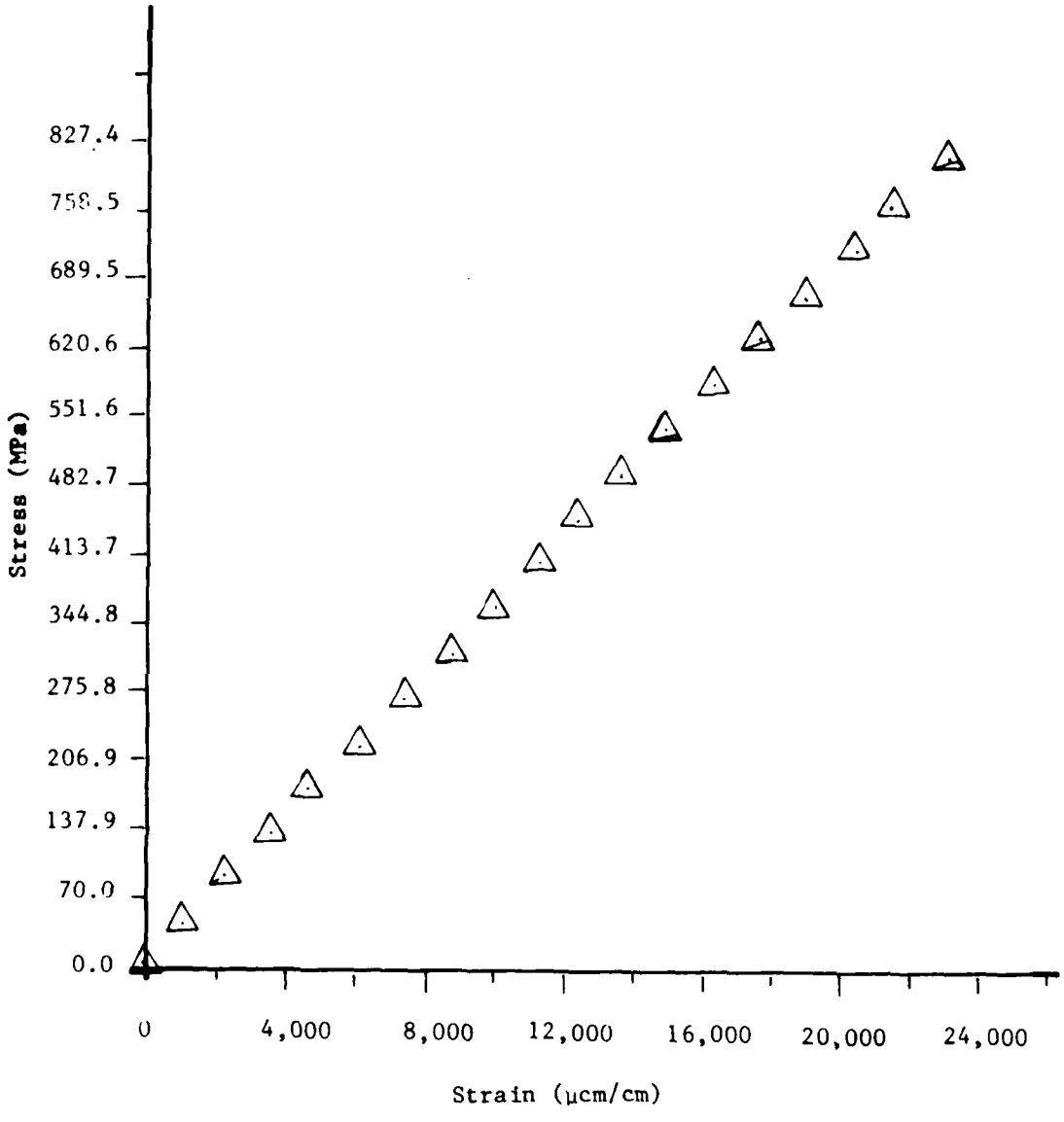

Figure A-11. Stress versus strain (T-0°-4).

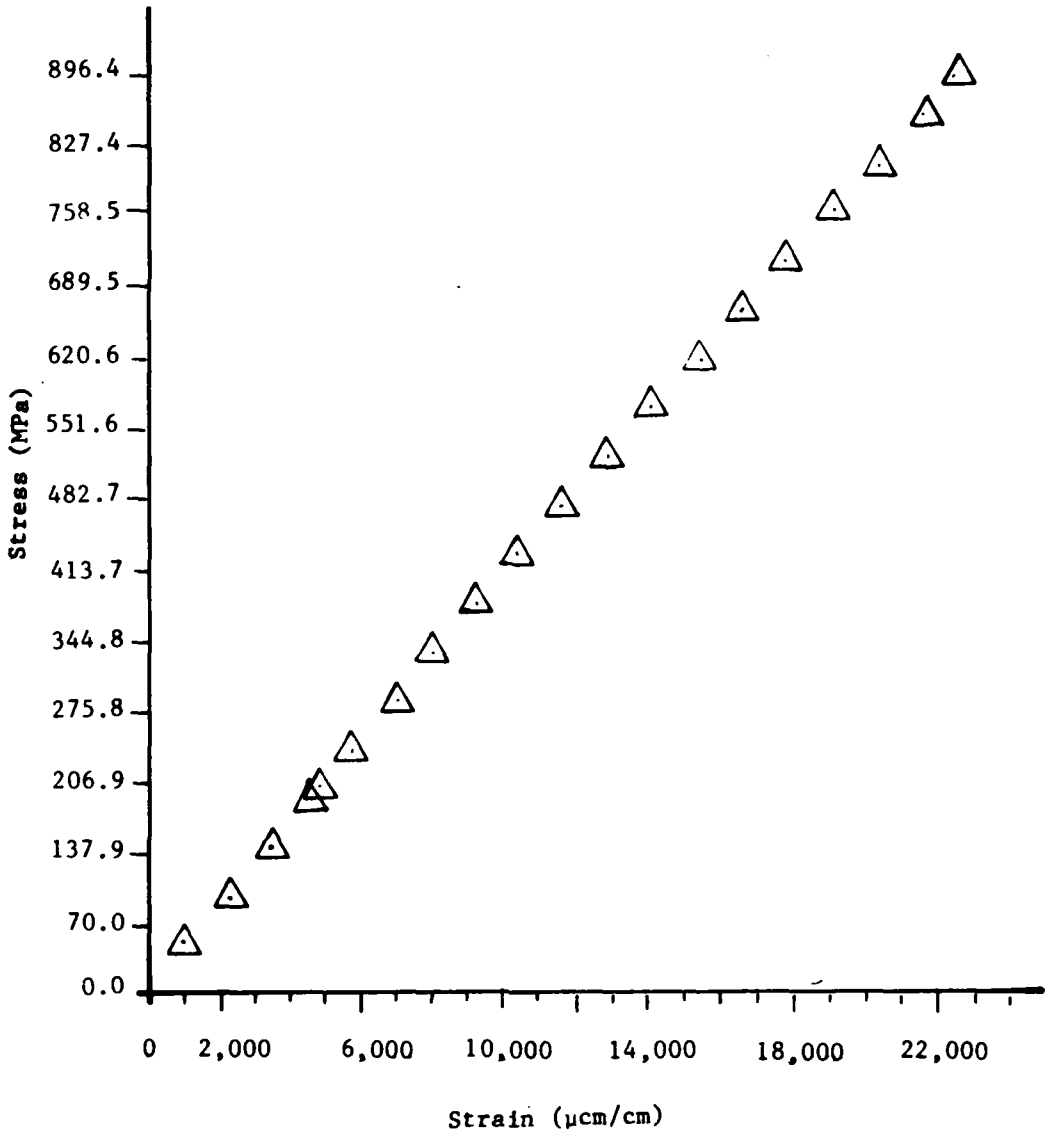

Figure A-12. Stress versus strain (T-0°-5).

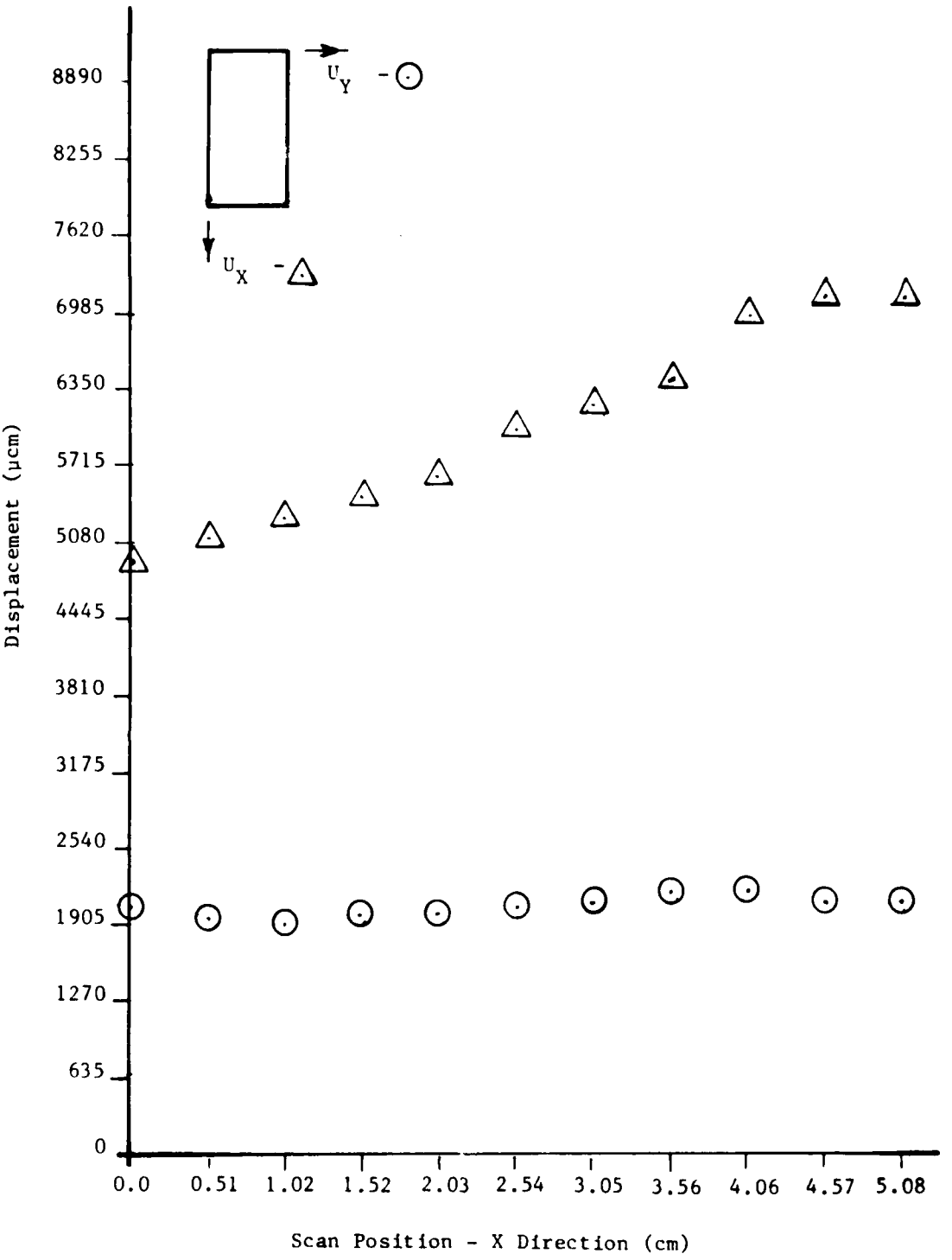

Figure A-13. Displacement versus scan position (T-90°-1-A-1).

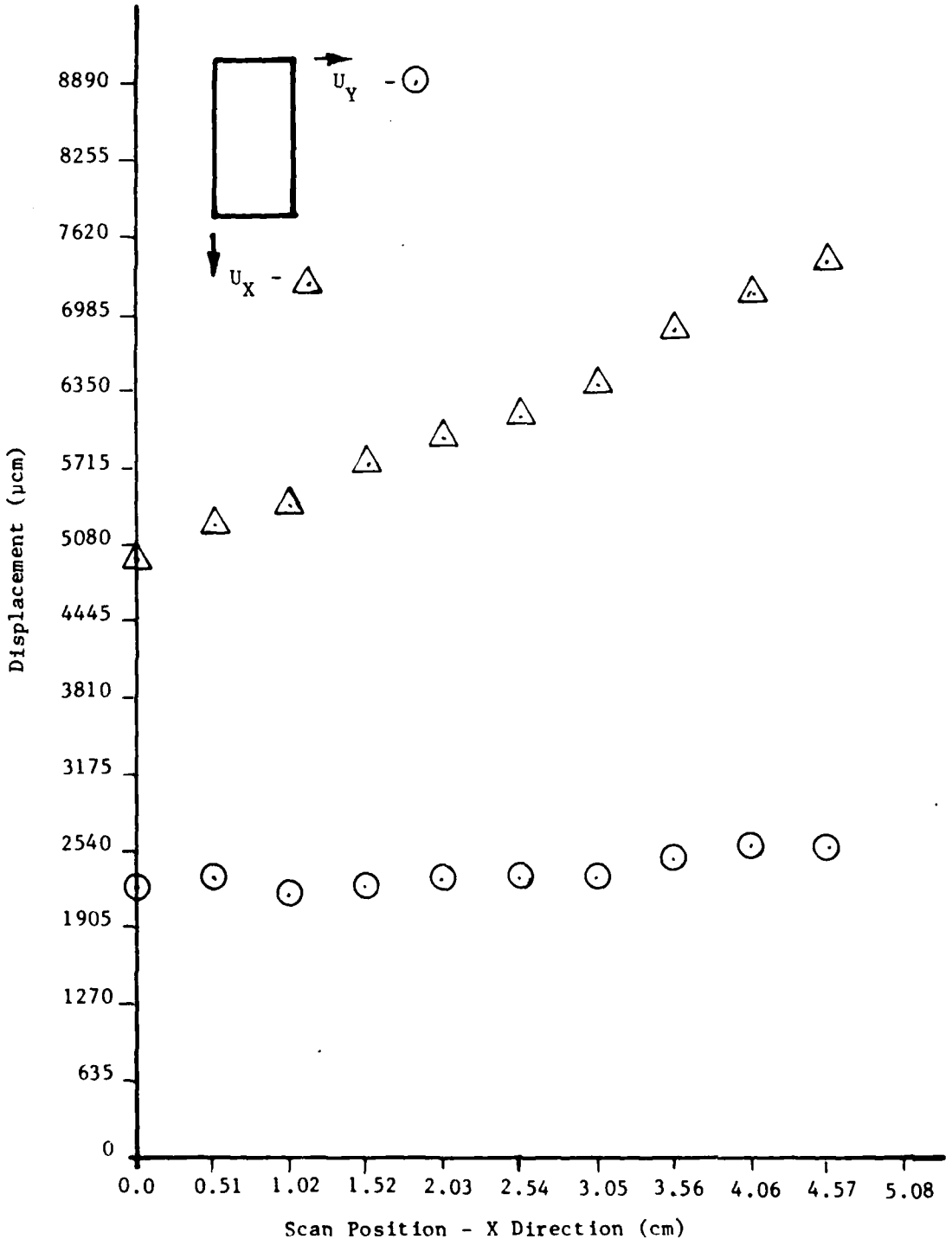

Figure A-14. Displacement versus scan position (T-90°-1-A-2).

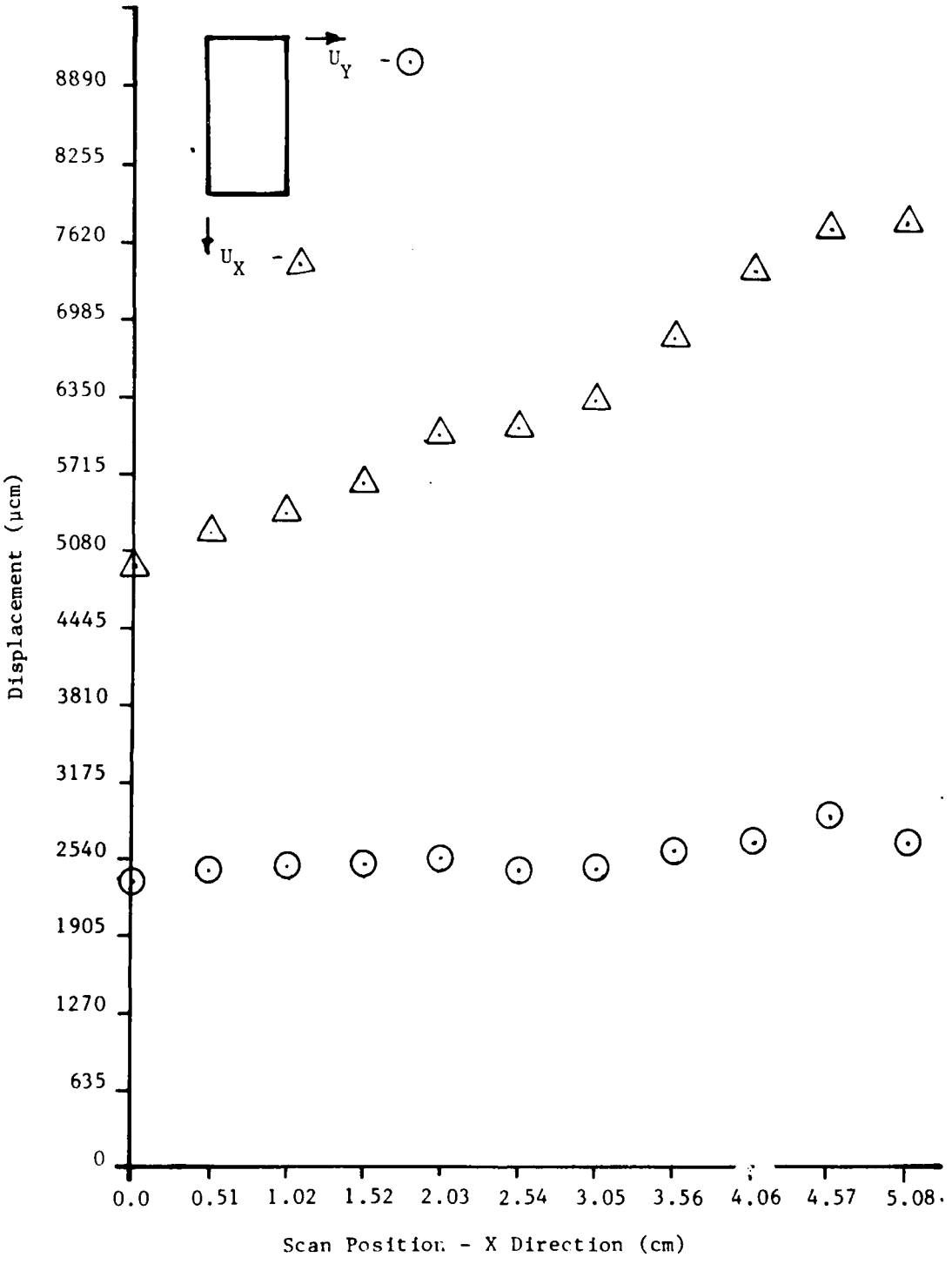

Figure A-15. Displacement versus scan position (T-90°-A-3).

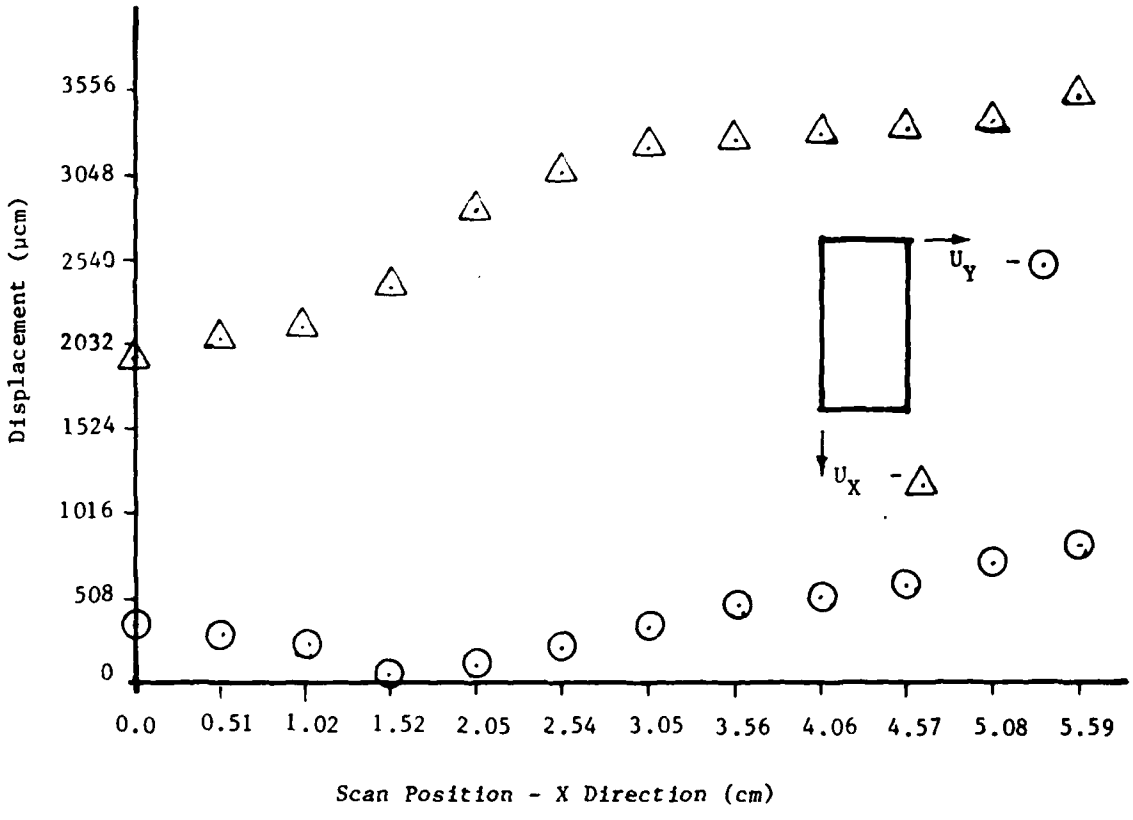

Figure A-16. Displacement versus scan position (T-90°-4-E-2).

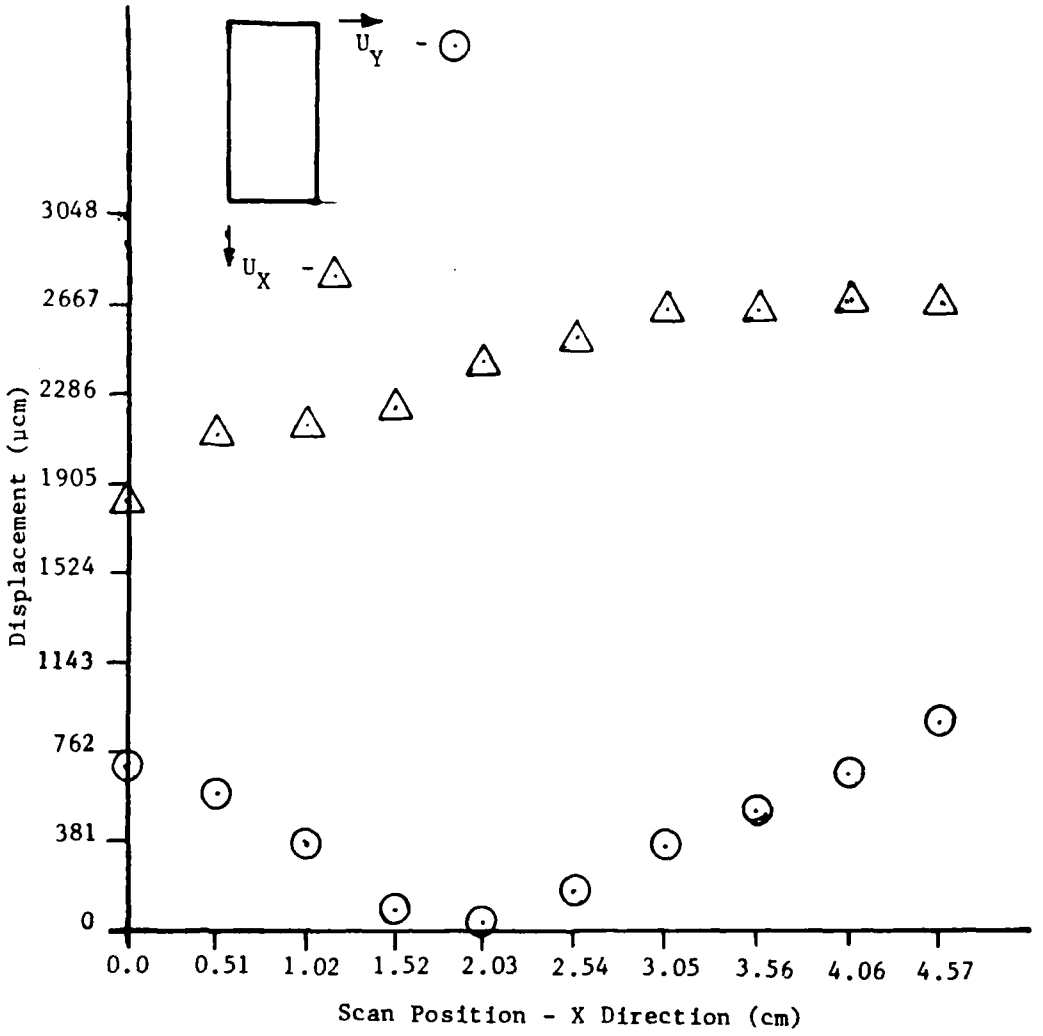

Figure A-17. Displacement versus scan position (T-90°-5-F-2).

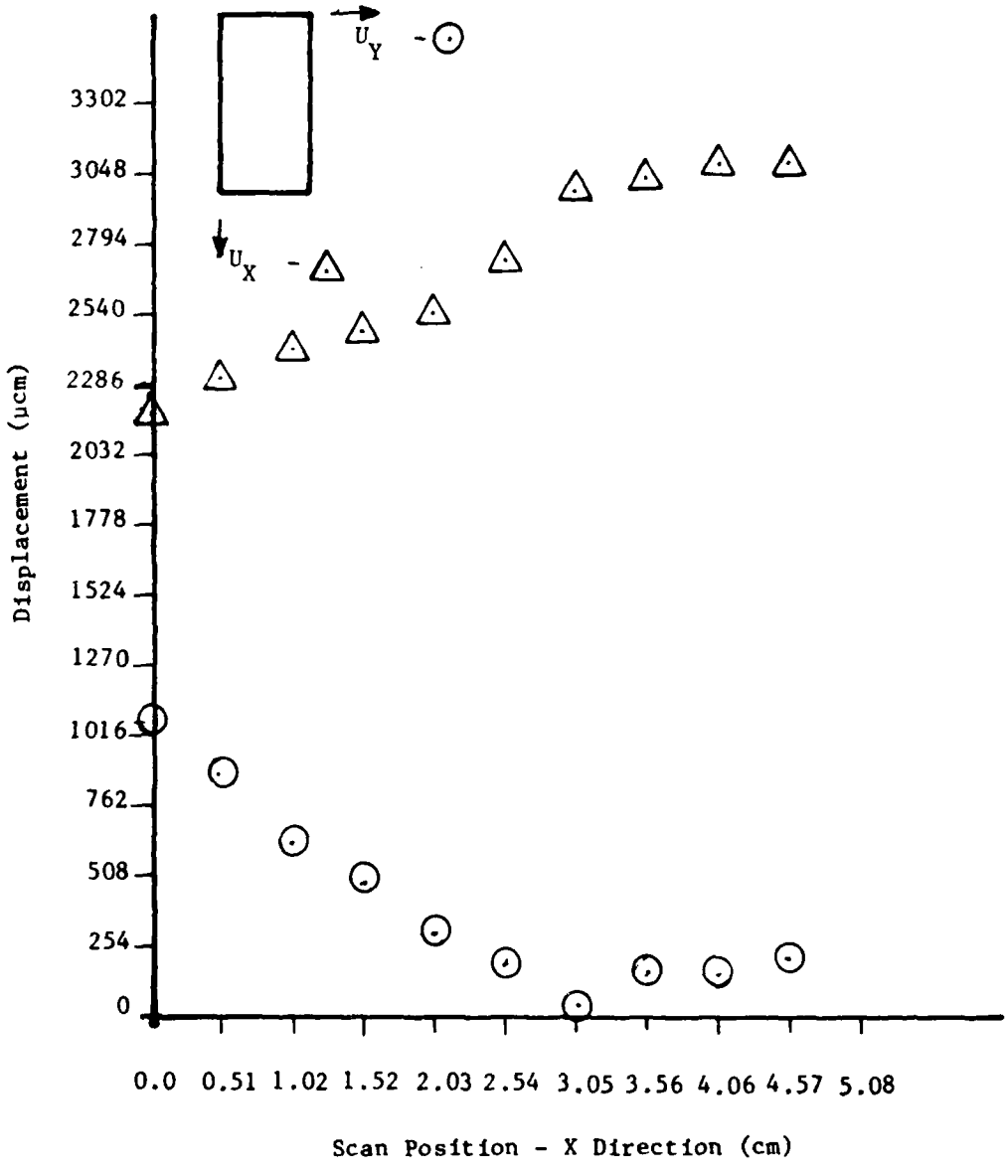

Figure A-18. Displacement versus scan position (T-90°-6-A-2).

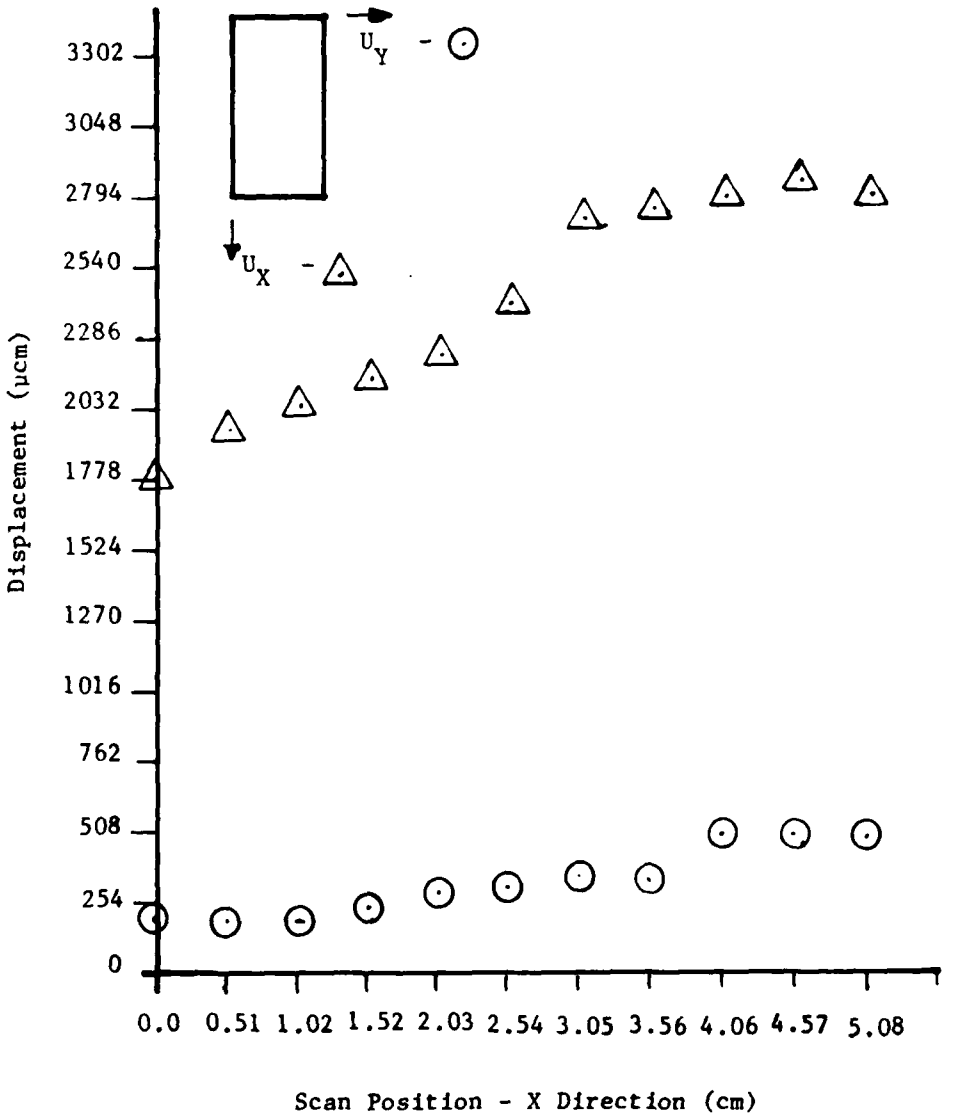

Figure A-19. Displacement versus scan position (T-90°-7-G-2).

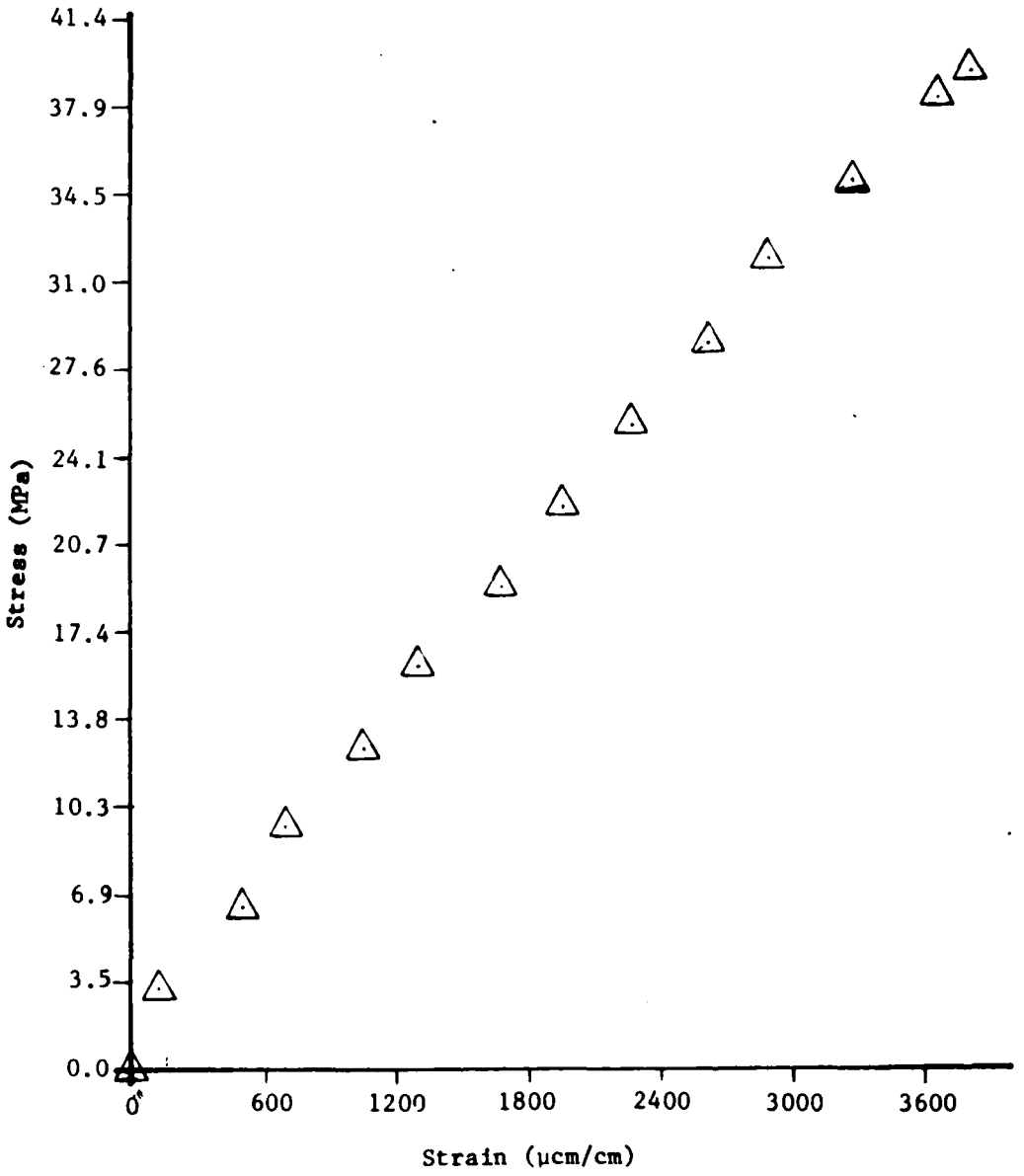

Figure A-20. Stress versus strain (T-90°-1).

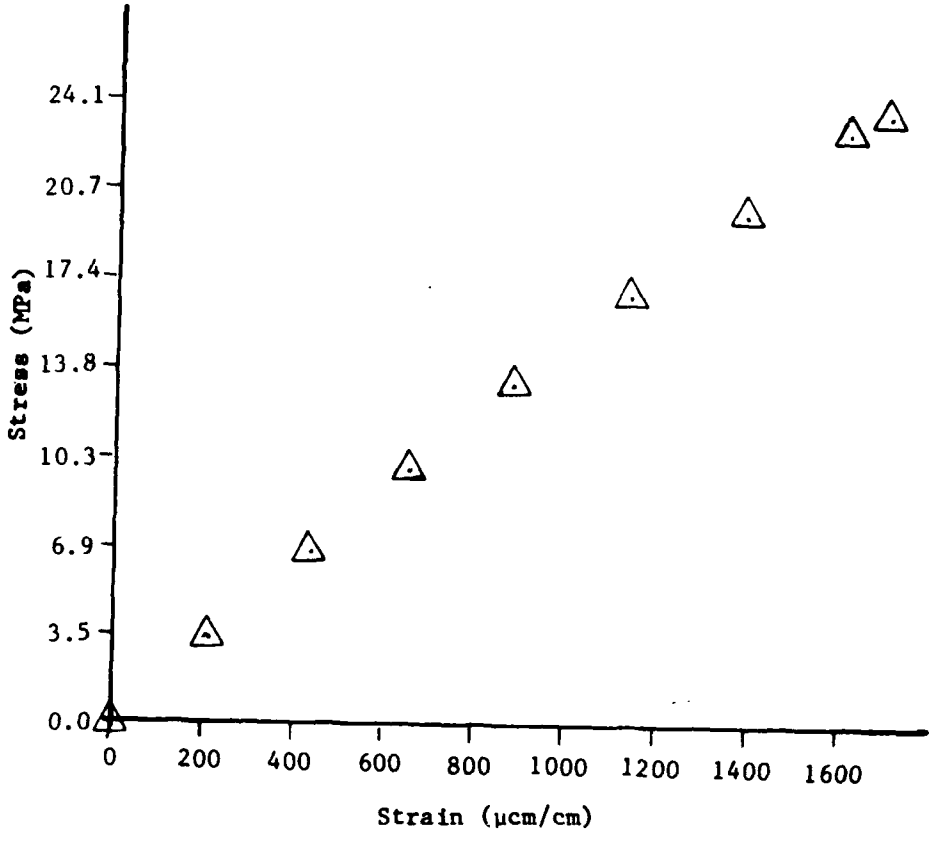

Figure A-21. Stress versus strain (T-90°-4)

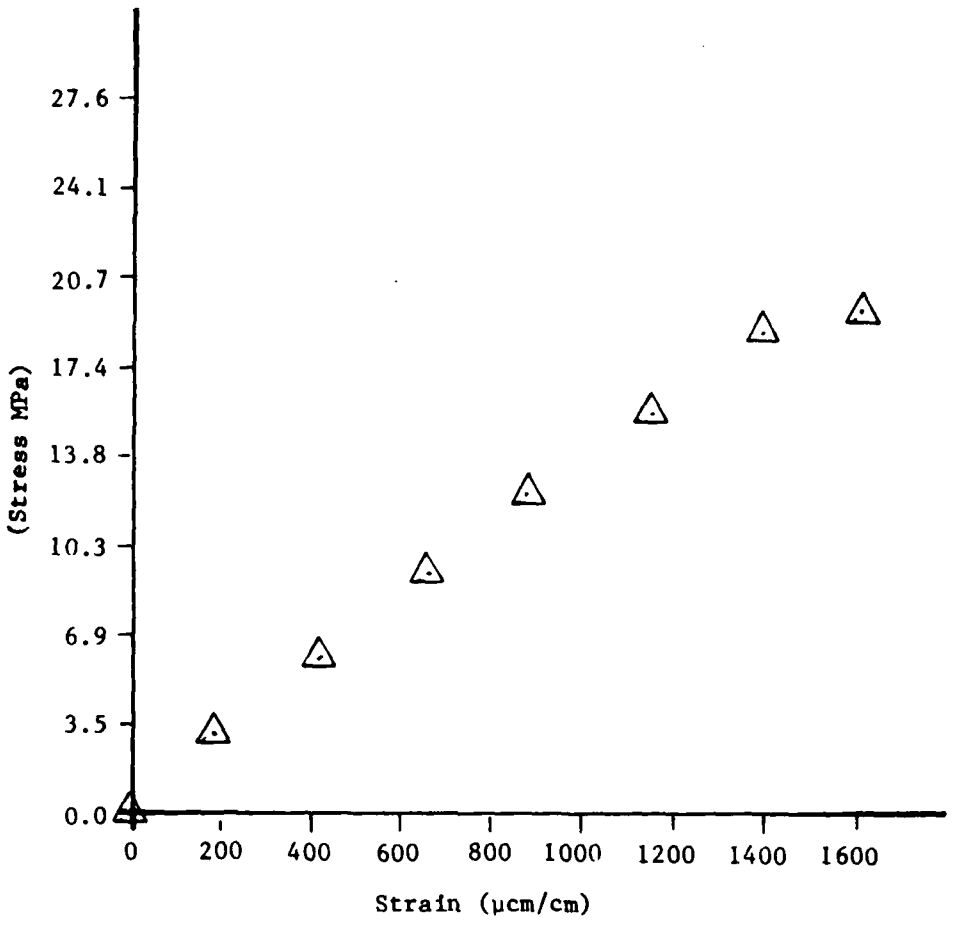

Figure A-22. Stress versus strain (T-90°-5).

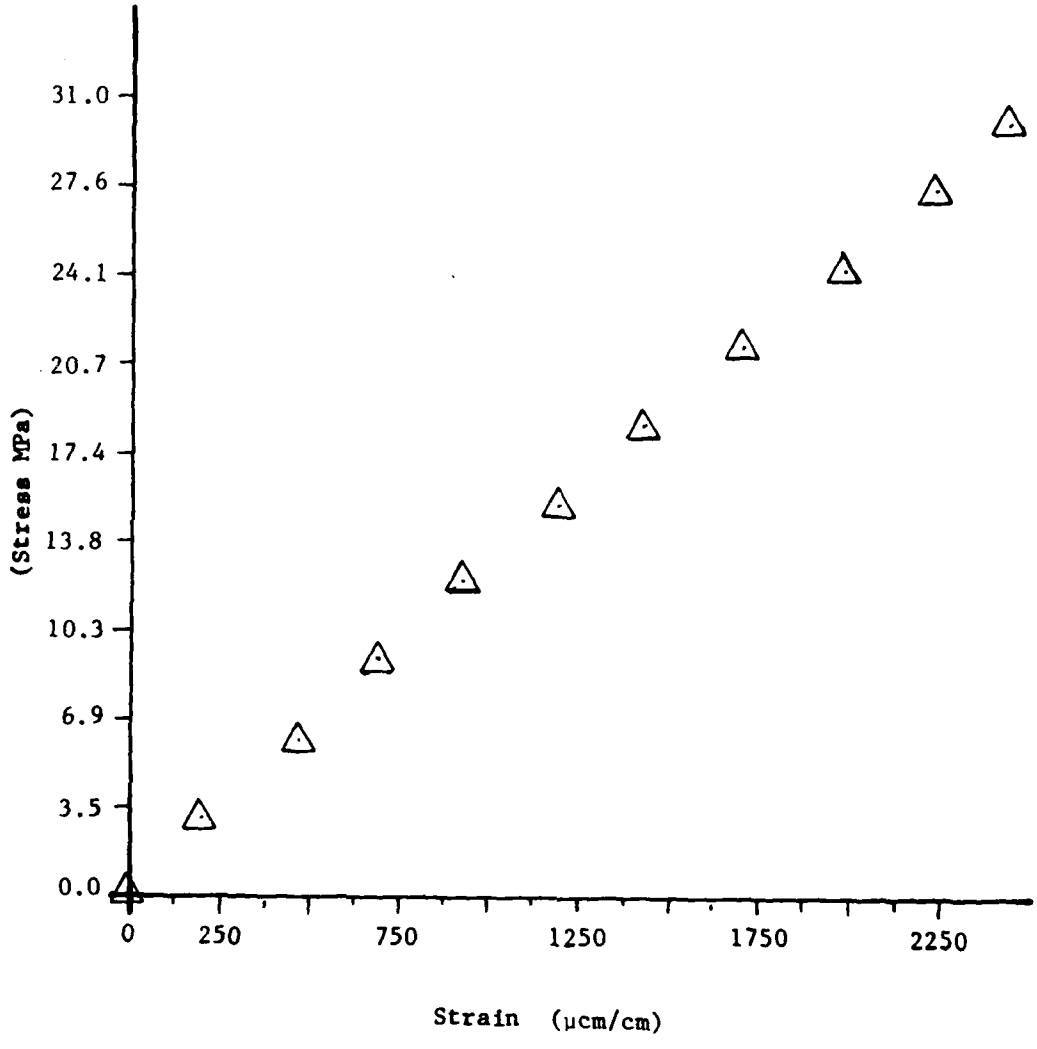

Figure A-23. Stress versus strain (T-90°-6).

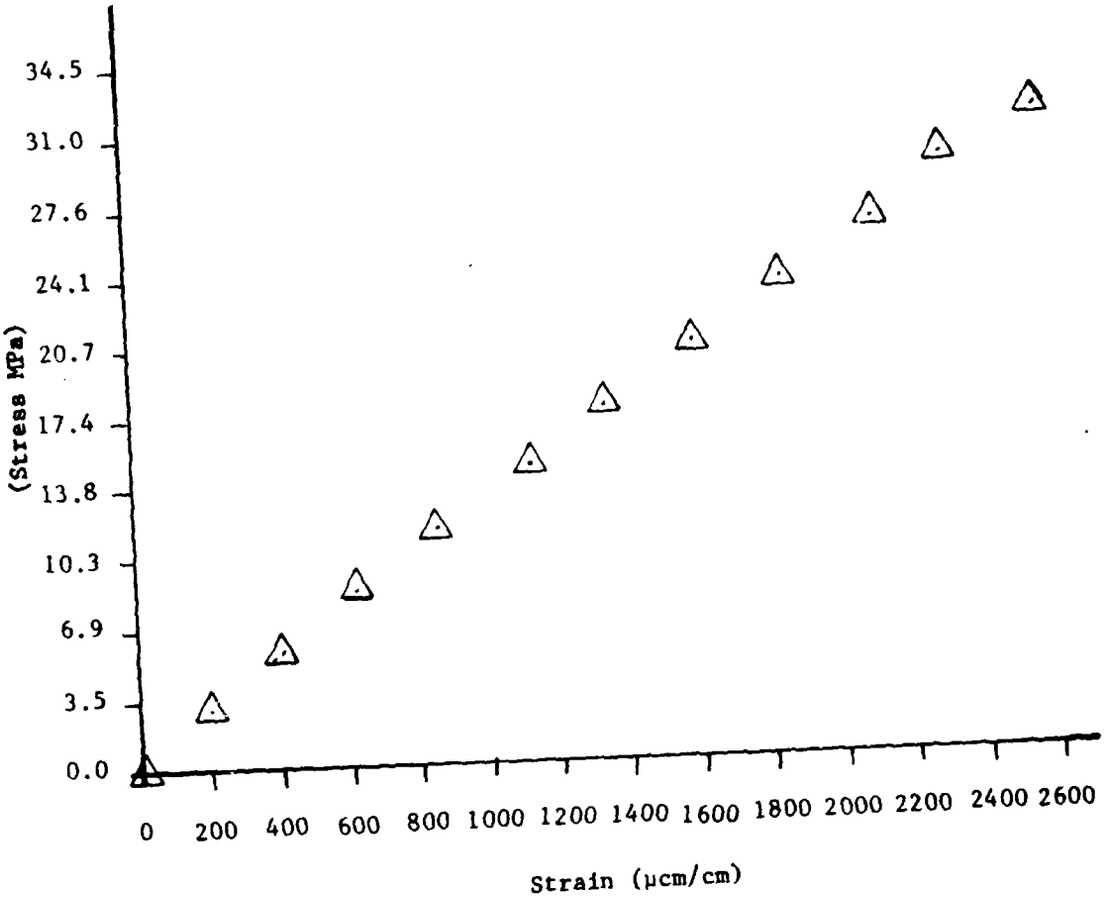

Figure A-24. Stress versus strain (T-90°-7).

PROGRAM FUNCTION: To analyze interferograms on a point-by-point basis, computing horizontal and vertical displacements, translation of X-Y translation stage.

INPUT:

1) Stage to be advanced - either X-Direction or Y-Direction.
2) Stage increment - distance translation table moves between points.
3) Film scale factor - ratio of real object to image on interferogram.
4) Displacement - distance between fringes.
5) Angle - Angle of orientation of fringes.

OUTPUT: Data are printed on a decwriter.

```
      COMMON DD(2,200)
      WRITE(5,1)
    1 FORMAT(' MANUAL YOUNG FRINGE ANALYZER')
      WRITE(5,2)
    2 FORMAT(' STAGE TO BE ADVANCED? (0=X,1=Y)')
      READ(5,3) IA
    3 FORMAT(I1)
      WRITE(5,4)
    4 FORMAT(' STAGE INCREMENT?')
      READ(5,5) IC
    5 FORMAT(I4)
      WRITE(5,6)
    6 FORMAT(' FILM SCALE FACTOR?')
      READ(5,7) SF
    7 FORMAT(F10.0)
      ICC=0
    8 ICC=ICC+1
      ICP=ICC-1
      WRITE(5,9)
    9 FORMAT(' DISPLACEMENT?')
      READ(5,7) D
      WRITE(5,10)
   10 FORMAT(' ANGLE?')
      READ(5,7) A
      A=A*3.14159/180.
      IF(D.EQ.0) GOTO 13
      IF(D.LT.0) GOTO 15
      U=SF/D
      U1=U*COS(A)
      U2=U*SIN(A)
      H=FLOAT((ICC-1)*IC)*.001
```

Figure A-25. Computer code.

```
      WRITE(5,11) H,U,U1,U2
   11 FORMAT(3H H=,F10.3,5X,2HU=,F12.6,
     13HU1=,F12.6,5X,3HU2=,F12.6)
   12 DD(1,ICC)=U1
      DD(2,ICC)=U2
      GOTO 14
   13 DD(1,ICC)=0.
      DD(2,ICC)=0.
   14 IF(IA.EQ.1) CALL YADV(IC,5)
      IF(IA.EQ.0) CALL XADV(IC,5)
      GOTO 8
   15 ICC=(1-ICC)*IC
      IF(IA.EQ.1) CALL YADV(ICC,5)
      IF(IA.EQ.0) CALL XADV(ICC,5)
      WRITE(5,16)
   16 FORMAT(' ANALYSIS ENDED')
      STOP
      END
      SUBROUTINE YADV(IS,IR)
C     IS=NO. STEPS (+=FWD,-=REV)
C     IR=ADVANCE RATE OF STAGE
      X=0.
      IF(IS.GT.0) GOTO 3
      IP=IABS(IS)
      DO 2 I=1,IP,1
      CALL IPOKE('167772,'020000)
      DO 7 K=1,IR,1
    7 Y=SIN(X)
      CALL IPOKE('167772,'000000)
      DO 1 J=1,IR,1
    1 Y=SIN(X)
    2 CONTINUE
      GOTO 6
    3 CONTINUE
      DO 5 II=1,IS,1
      CALL IPOKE('167772,'010000)
      DO 8 KK=1,IR,1
    8 Y=SIN(X)
      CALL IPOKE('167772,'000000)
      DO 4 JJ=1,IR,1
    4 Y=SIN(X)
    5 CONTINUE
    6 CONTINUE
      RETURN
      END
```

Figure A-25. (Continued).

```
      SUBROUTINE XADV(IS,IR)
C     IS=NO. STEPS (+=FWD,-=REV)
C     IR=ADVANCE RATE OF STAGE
      X=0.
      IF(IS.GT.0) GOTO 3
      IP=IABS(IS)
      DO 2 I=1,IP,1
      CALL IPOKE('167772,'100000)
      DO 7 K=1,IR,1
    7 Y=SIN(X)
      CALL IPOKE('167772,'000000)
      DO 1 J=1,IR,1
    1 Y=SIN(X)
    2 CONTINUE
      GOTO 6
    3 CONTINUE
      DO 5 II=1,IS,1
      CALL IPOKE('167772,'040000)
      DO 8 KK=1,IR,1
    8 Y=SIN(X)
      CALL IPOKE('167772,'000000)
      DO 4 JJ=1,IR,1
    4 Y=SIN(X)
    5 CONTINUE
    6 CONTINUE
      RETURN
      END
```

Figure A-25. (Concluded).

APPENDIX B

SHEAR SPECIMEN DATA

APPENDIX B

LIST OF TABLES

APPENDIX B

LIST OF FIGURES

Table B-1. Displacement Data (μcm) from Laser Speckle Interferometry

SHEAR SPECIMEN				
S-0°7-L		Load Range: 2359-4139 Newtons		
		Free Edge Scan		
		A	B	C
Row 1	U_V	4156	5500	5846
	U_H	-73	-144	-51
		D	E	F
Row 2	U_V	4154	4796	5053
	U_H	-145	-84	-177
		G	H	I
Row 3	U_V	3724	4548	5180
	U_H	-359	-358	-408
		Center Scan		
		A	B	C
Row 1	U_V	3856	4557	4895
	U_H	-1290	-1052	-1266
		D	E	F
Row 2	U_V	3821	4043	4806
	U_H	-1391	-1314	-1066
		G	H	I
Row 3	U_V	4066	4644	5263
	U_H	-1243	-1201	-928

Table B-2. Displacement Data (μcm) from Laser Speckle Interferometry

SHEAR SPECIMEN				
S-0°-7-L		Load Range: 9345-11,125 Newtons		
		Free Edge Scan		
		A	B	C
Row 1	U_V	3379	4134	5028
	U_H	385	435	529
		D	E	F
Row 2	U_V	3282	3975	5053
	U_H	229	208	177
		G	H	I
Row 3	U_V	3114	3978	5055
	U_H	166	139	88
		Center Scan		
		A	B	C
Row 1	U_V	3349	3713	5157
	U_H	-591	-456	-633
		D	E	F
Row 2	U_V	3038	3797	5012
	U_H	-701	-399	-660
		G	H	I
Row 3	U_V	3101	5033	5494
	U_H	-659	-485	-288

Table B-3. Displacement Data (μcm) from Laser Speckle Interferometry

SHEAR SPECIMEN				
S-0°-7-L		Load Range: 16,243-18,023 Newtons		
		Free Edge Scan		
		A	B	C
Row 1	U_V	3011	3968	4744
	U_H	807	312	709
		D	E	F
Row 2	U_V	3020	3771	5324
	U_H	533	597	466
		G	H	I
Row 3	U_V	2953	3727	5160
	U_H	310	326	408
		Center Scan		
		A	B	C
Row 1	U_V	3315	4134	6020
	U_H	-407	-435	-421
		D	E	F
Row 2	U_V	2894	4437	5814
	U_H	-407	-388	-611
		G	H	I
Row 3	U_V	3216	4443	5492
	U_H	-654	-311	-336

Table B-4. Displacement Data (μcm) from Laser Speckle Interferometry

SHEAR SPECIMEN				
S-0°-8-L		Load Range: 2359-4116 Newtons		
		Free Edge Scan		
		A	B	C
Row 1	U_V	4126	4134	5461
	U_H	-506	-435	-671
		D	E	F
Row 2	U_V	4566	4708	4493
	U_H	-1012	-915	-792
		G	H	I
Row 3	U_V	4463	4574	5382
	U_H	-949	-972	-1144
		Center Scan		
		A	B	C
Row 1	U_V	4587	5339	5684
	U_H	-1402	-1331	-1365
		D	E	F
Row 2	U_V	4611	5534	6088
	U_H	-1322	-1227	-1350
		G	H	I
Row 3	U_V	4969	5488	6310
	U_H	-1519	-1419	-1341

Table B-5. Displacement Data (μcm) from Laser Speckle Interferometry

SHEAR SPECIMEN				
S-0°-8-L		Load Range: 7654-9345 Newtons		
		Free Edge Scan		
		A	B	C
Row 1	U_V	3147	3442	4440
	U_H	386	392	350
		D	E	F
Row 2	U_V	3396	3739	4676
	U_H	178	131	82
		G	H	I
Row 3	U_V	3400	3739	4676
	U_H	89	131	41
		Center Scan		
		A	B	C
Row 1	U_V	3741	3815	4793
	U_H	65	133	167
		D	E	F
Row 2	U_V	3116	3739	4674
	U_H	-109	-131	-163
		G	H	I
Row 3	U_V	3398	3897	4672
	U_H	-148	-68	-204

Table B-6. Displacement Data (μcm) from Laser Speckle Interferometry

SHEAR SPECIMEN				
S-0°-8-L		Load Range: 12,905-14,685 Newtons		
		Free Edge Scan		
		A	B	C
Row 1	U_V	3261	4015	4724
	U_H	966	1076	833
		D	E	F
Row 2	U_V	3375	3720	4518
	U_H	779	859	635
		G	H	I
Row 3	U_V	3122	3776	4537
	U_H	551	564	477
		Center Scan		
		A	B	C
Row 1	U_V	2878	3401	4796
	U_H	-50	-30	-42
		D	E	F
Row 2	U_V	3170	3741	4797
	U_H	-28	-33	0
		G	H	I
Row 3	U_V	3401	4249	4562
	U_H	-30	148	80

Table B-7. Displacement Data (μcm) from Laser Speckle Interferometry

SHEAR SPECIMEN				
S-0°-8-R		Load Range: 2359-4116 Newtons		
Center Scan				
		A	B	C
Row 1	U_V	4249	4770	6034
	U_H	-148	-501	-105
		D	E	F
Row 2	U_V	3975	5332	5668
	U_H	-208	-373	-99
		G	H	I
Row 3	U_V	3808	5337	5845
	U_H	-266	-280	-102

Table B-8. Displacement Data (μcm) from Laser Speckle Interferometry

SHEAR SPECIMEN				
S-0°-8-R		Load Range: 7654-9345 Newtons		
		Free Edge Scan		
		A	B	C
Row 1	U_V	3591	4440	4785
	U_H	220	350	335
		D	E	F
Row 2	U_V	3654	4066	5789
	U_H	320	71	357
		G	H	I
Row 3	U_V	3594	4448	4556
	U_H	157	232	239
		Center Scan		
		A	B	C
Row 1	U_V	3116	3803	4238
	U_H	109	333	334
		D	E	F
Row 2	U_V	3114	3398	4249
	U_H	163	148	148
		G	H	I
Row 3	U_V	3114	3882	4793
	U_H	163	340	167

Table B-9. Displacement Data (μcm) from Laser Speckle Interferometry

SHEAR SPECIMEN				
S-0°-8-R		Load Range: 12,905-14,685 Newtons		
		Free Edge Scan		
		A	B	C
Row 1	U_V	3641	3803	3958
	U_H	447	333	416
		D	E	F
Row 2	U_V	3396	4065	5051
	U_H	178	106	220
		G	H	I
Row 3	U_V	3217	3817	4672
	U_H	225	-33	204
		Center Scan		
		A	B	C
Row 1	U_V	3061	3740	5344
	U_H	-187	-65	-93
		D	E	F
Row 2	U_V	3168	3897	5499
	U_H	-138	-34	-192
		G	H	I
Row 3	U_V	3169	3897	5500
	U_H	-83	-34	-144

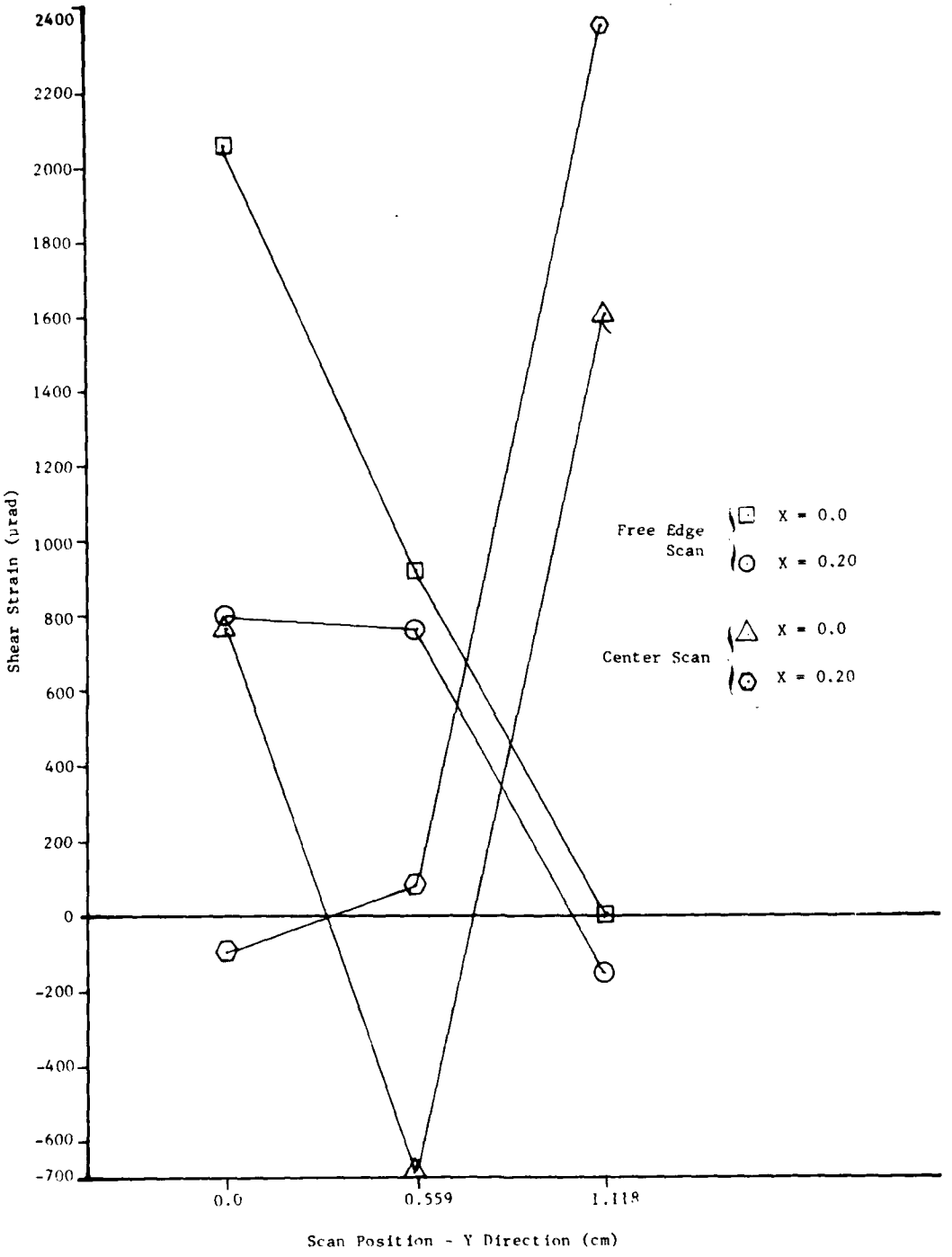

Figure B-1. Shear strain versus scan position (S-0°-7-L). Load Range: (2359-4139) Newtons

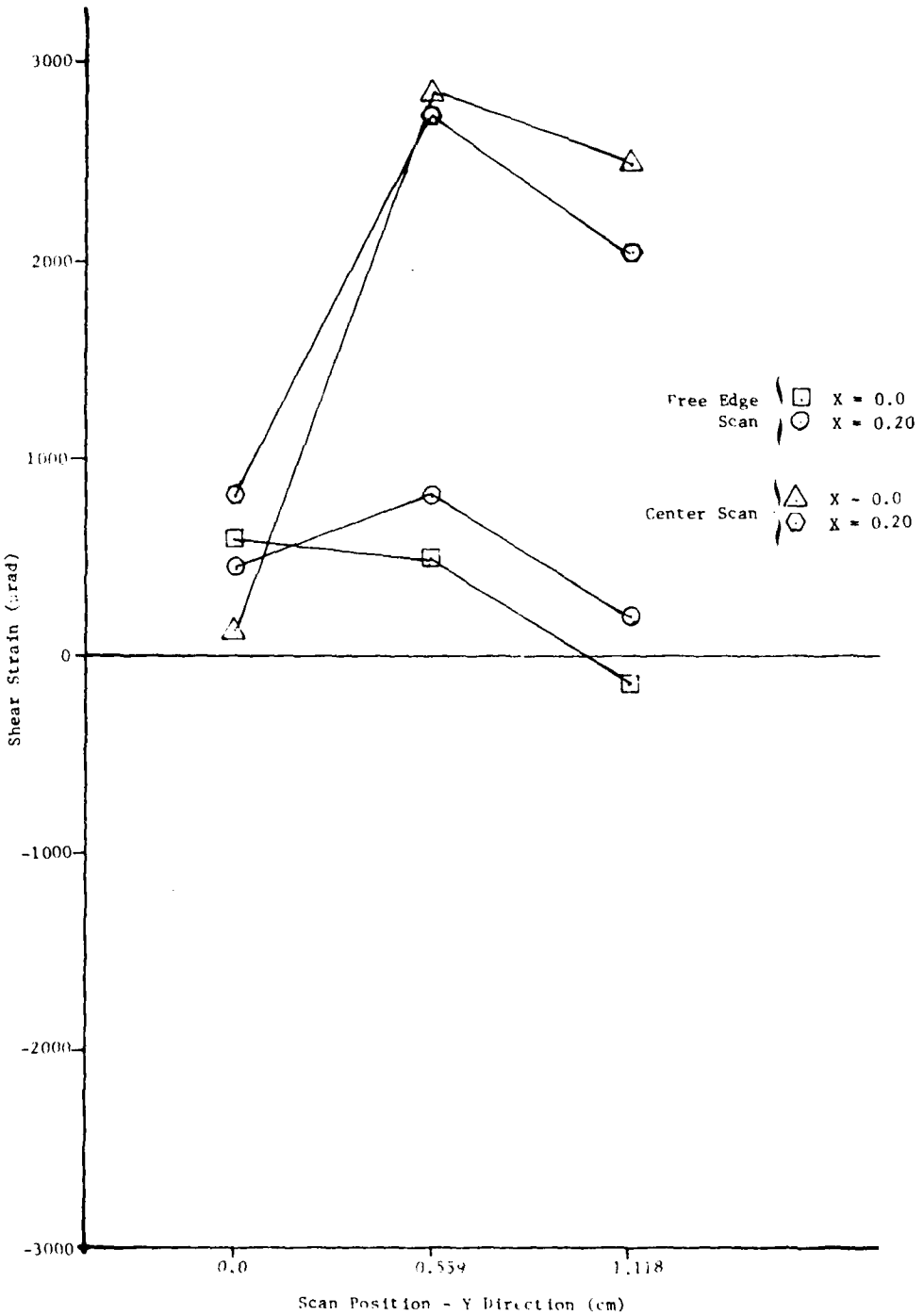

Figure B-2. Shear strain versus scan position (S-0°-7-L). Load Range: (9345-11,125) Newtons

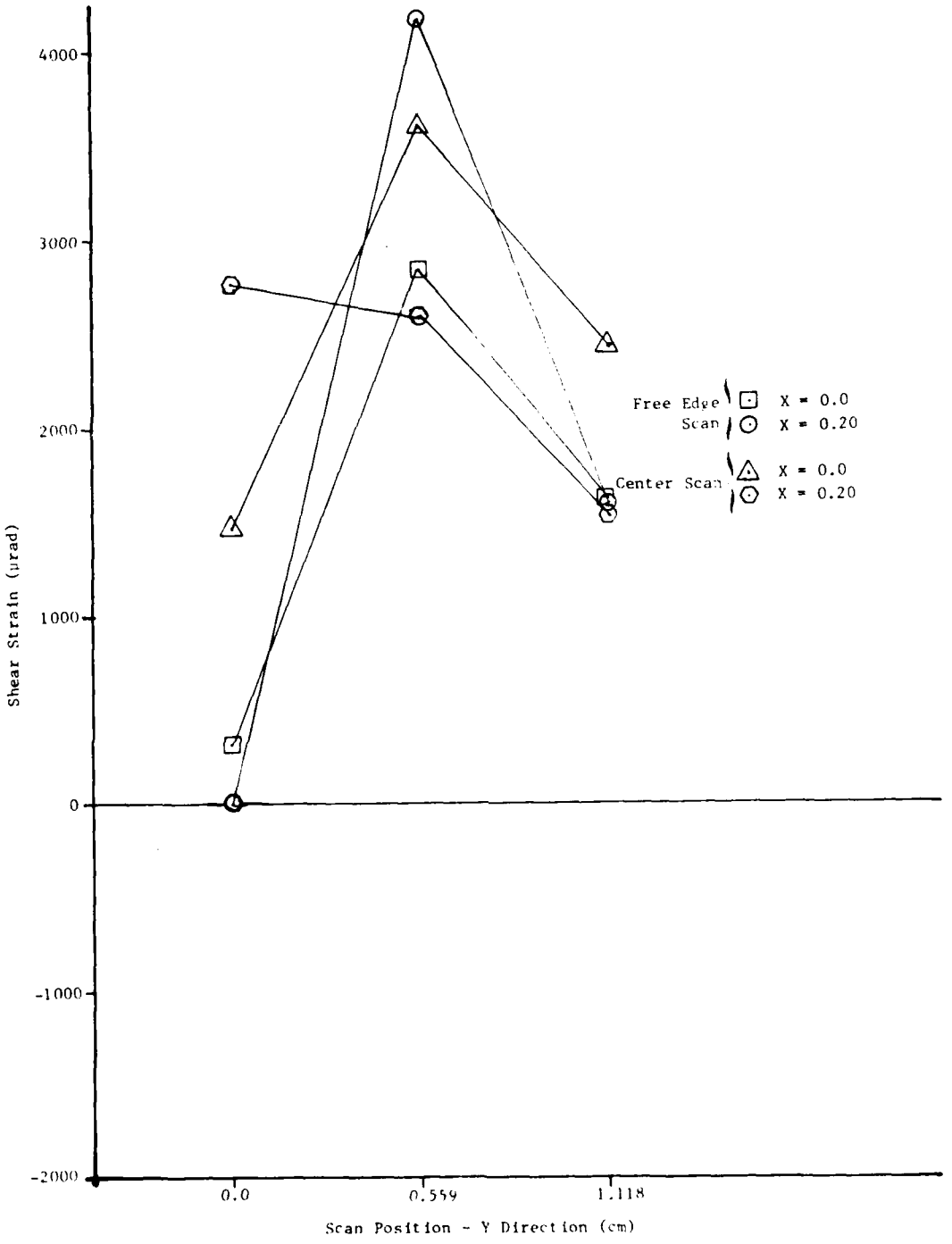

Figure B-3. Shear strain versus scan position (S-0°-7-L). Load Range: (16,243-18,023) Newtons

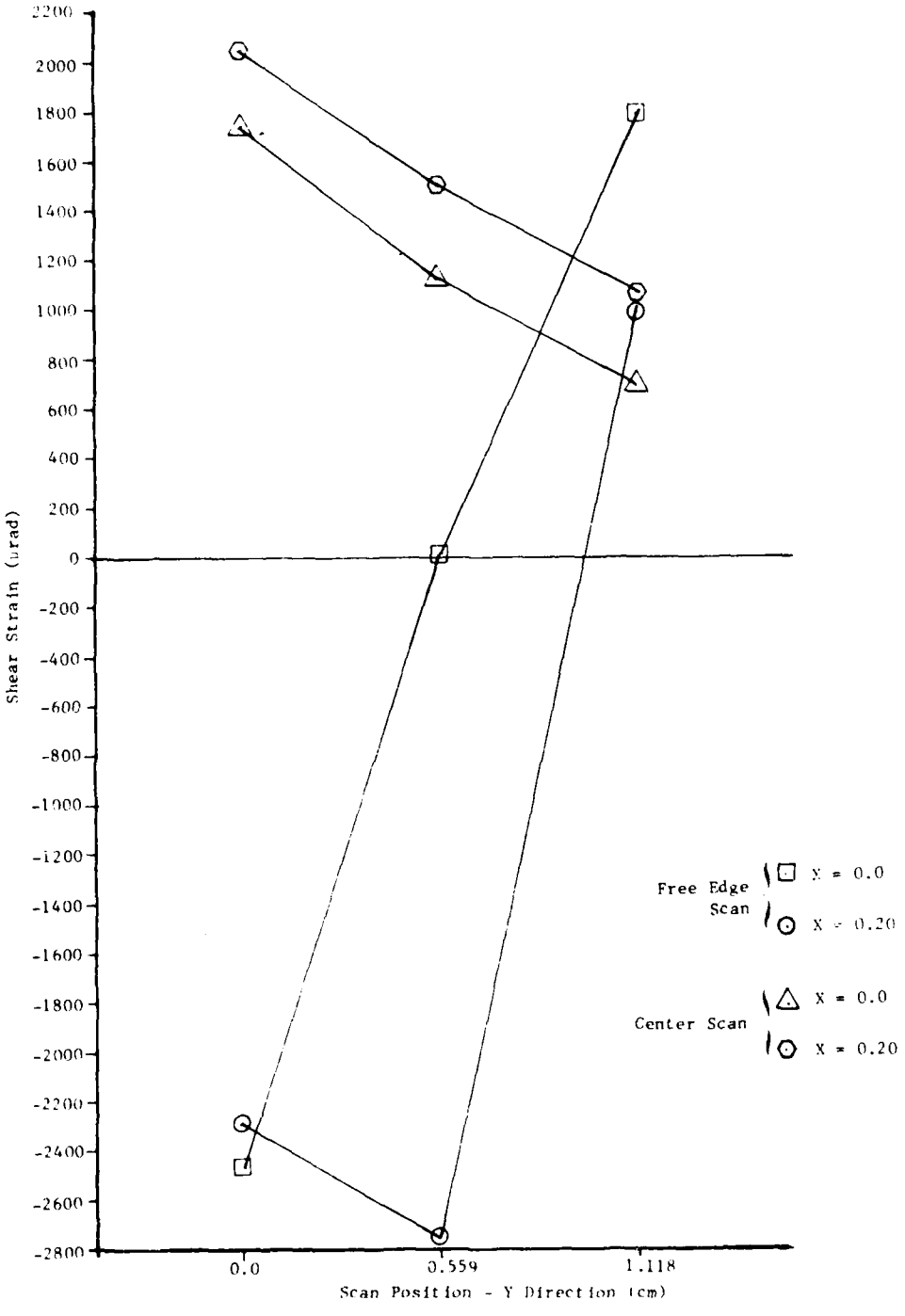

Figure B-4. Shear strain versus scan position (S-0°-8-L). Load Range: (2359-4116) Newtons

AD-A105 805 ARMY MISSILE COMMAND REDSTONE ARSENAL AL GROUND EQU--ETC F/G 11/4
WHOLE-FIELD EXPERIMENTAL STRESS ANALYSIS USING LASER SPECKLE IN--ETC(U)
FEB 81 T L VANDIVER
UNCLASSIFIED DRSMI/RL-81-10-TR SBIE-AD-E950 170 NL

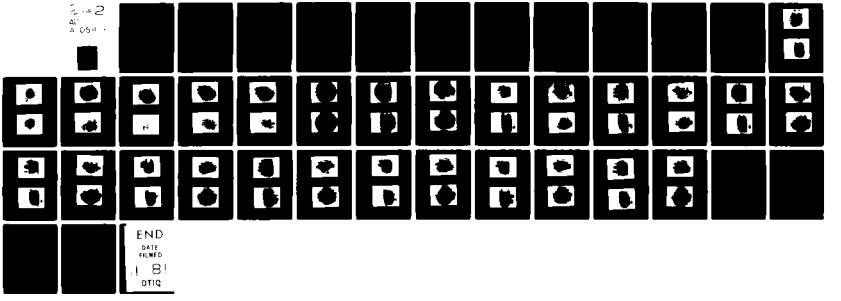

END
DATE FILMED
1 81
DTIC

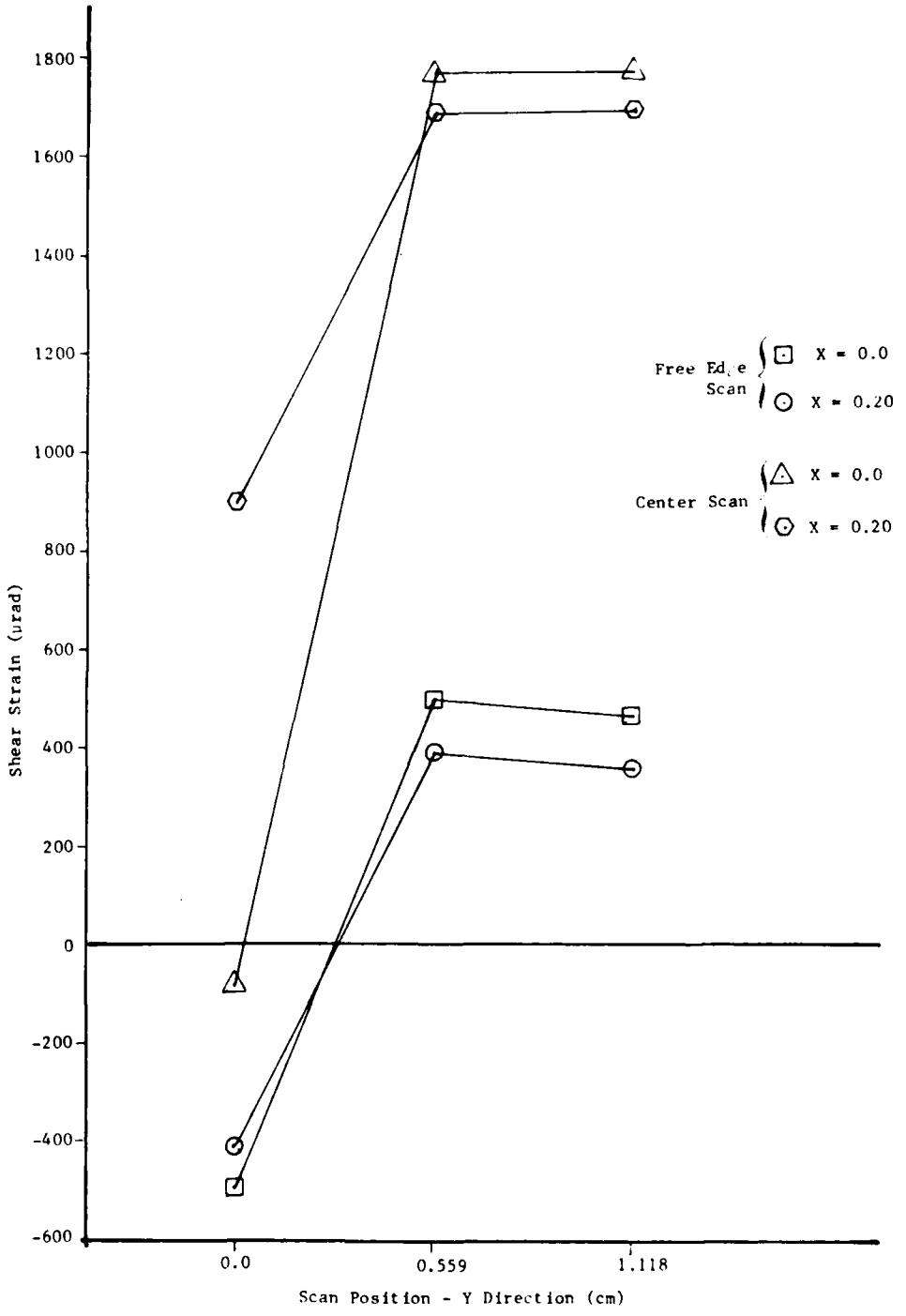

Figure B-5. Shear strain versus scan position (S-0°-8-L). Load Range: (7654-9345) Newtons

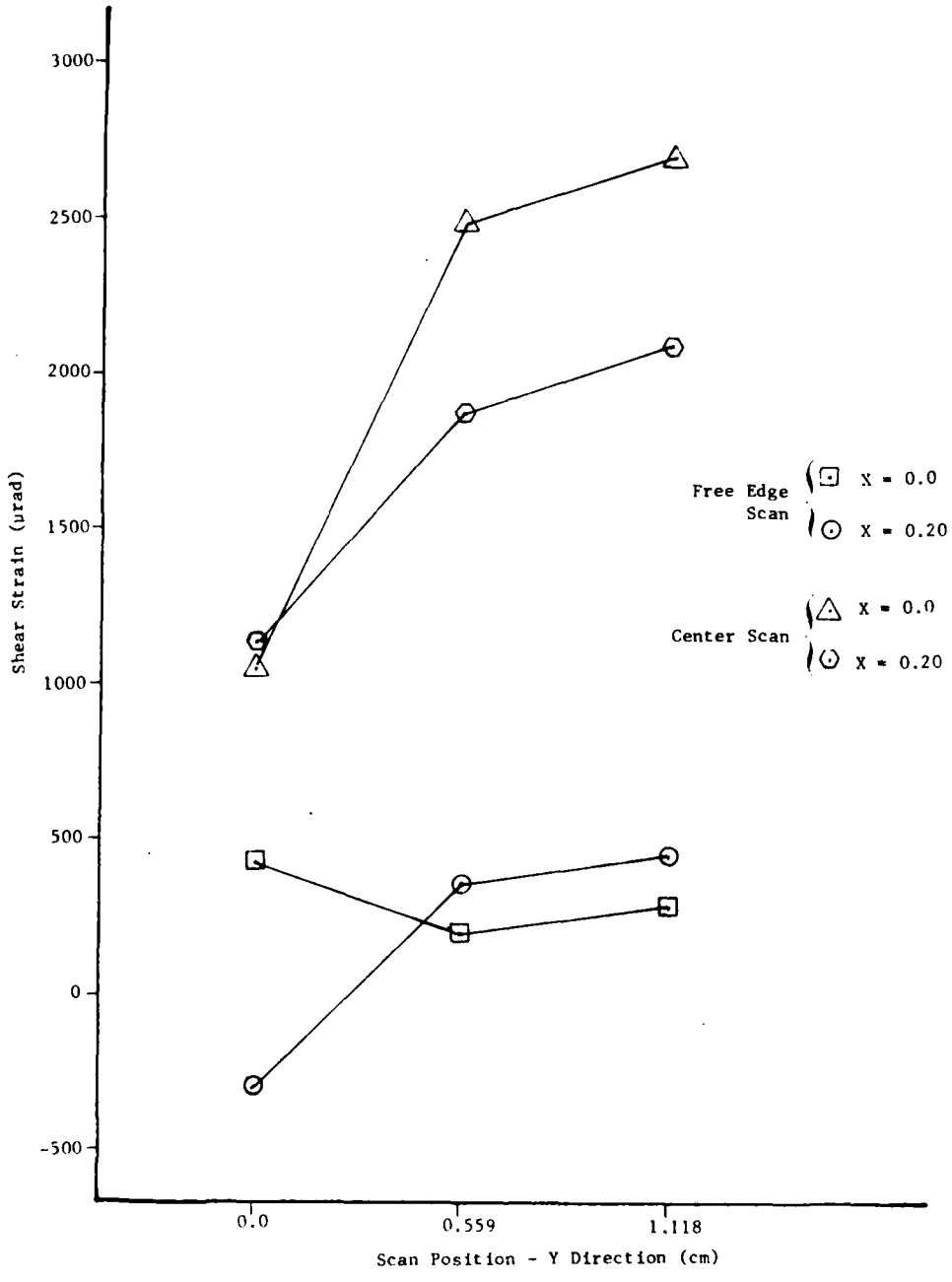

Figure B-6. Shear strain versus scan position (S-0°-8-L)
Load Range: (12,905-14,685) Newtons

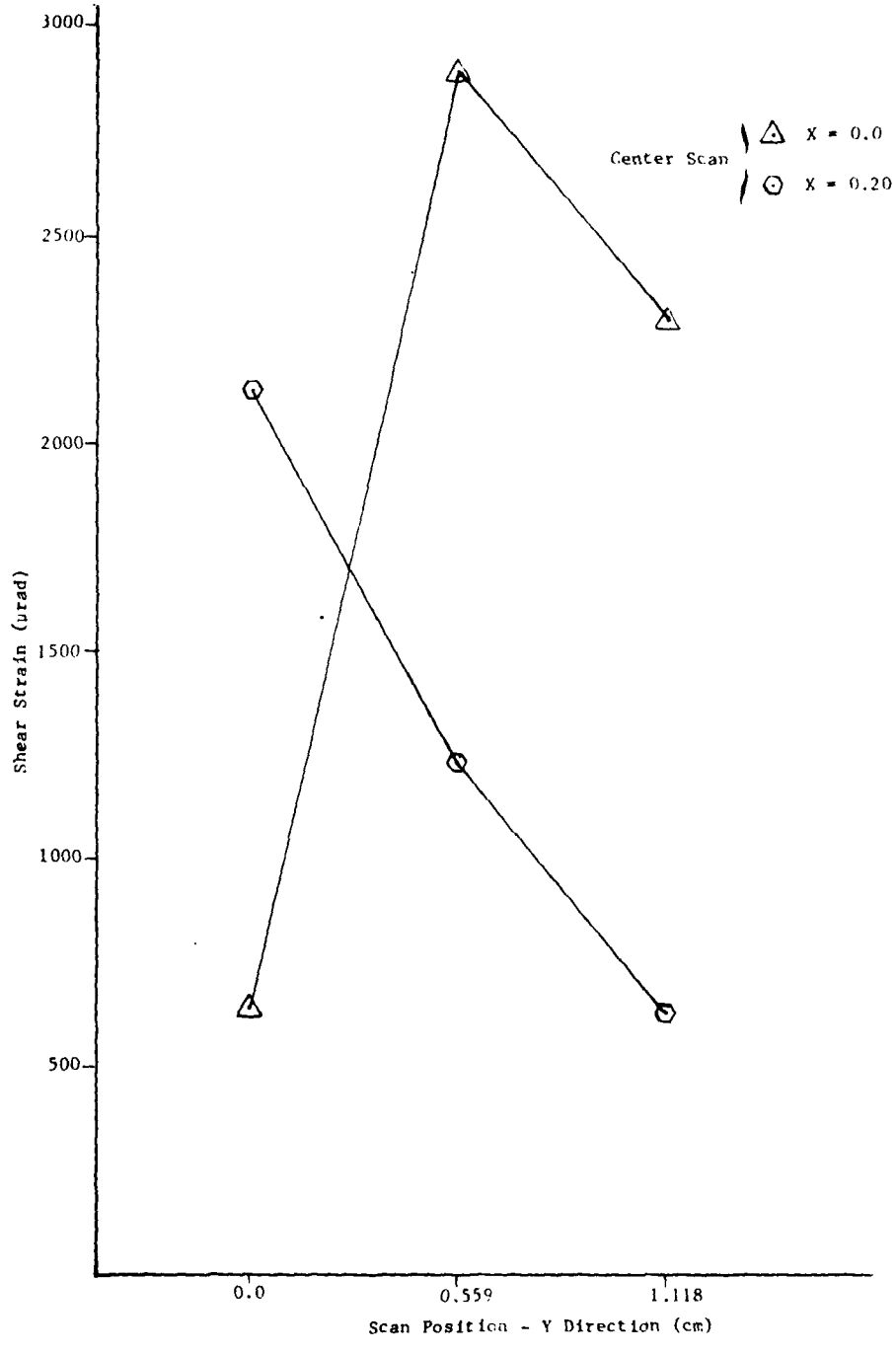

Figure B-7. Shear strain versus scan position (S-0°-8-R).
Load Range: (2359-4116) Newtons

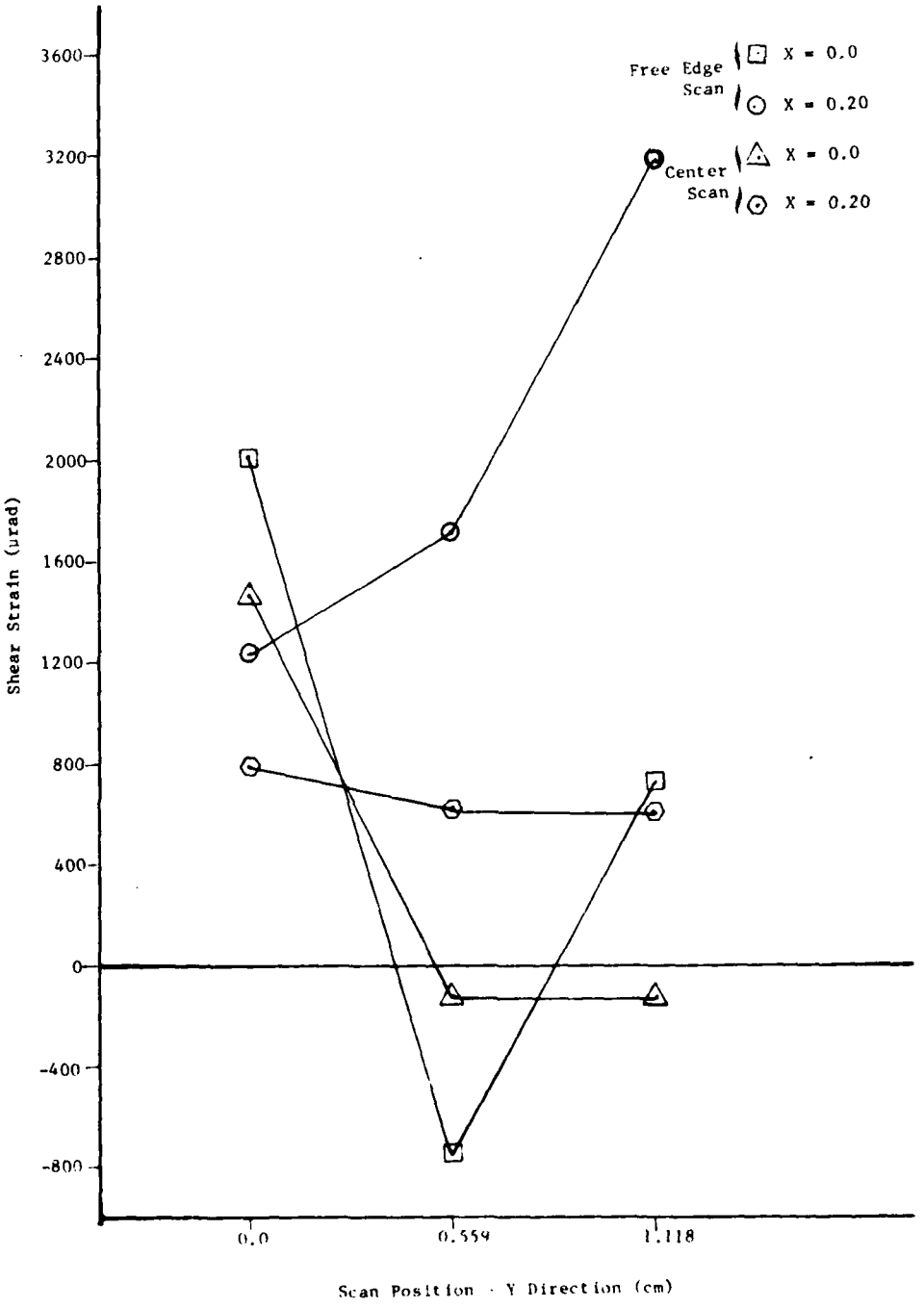

Figure B-8. Shear strain versus scan position (S-0°-8-R). Load Range: (7654-9345) Newtons

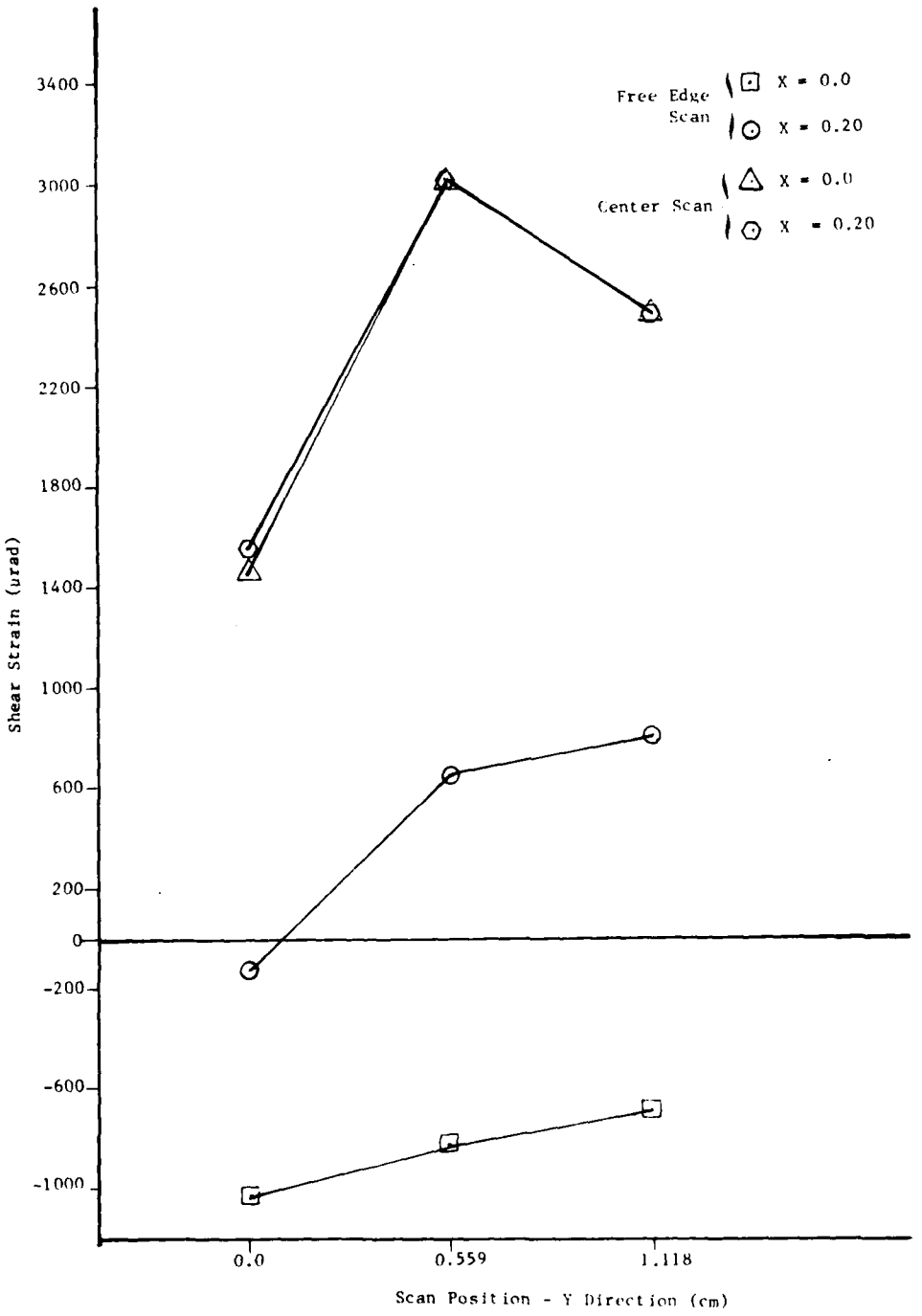

Figure B-9. Shear strain versus scan position (S-0°-8-R). Load Range: (12,905-14,685) Newtons

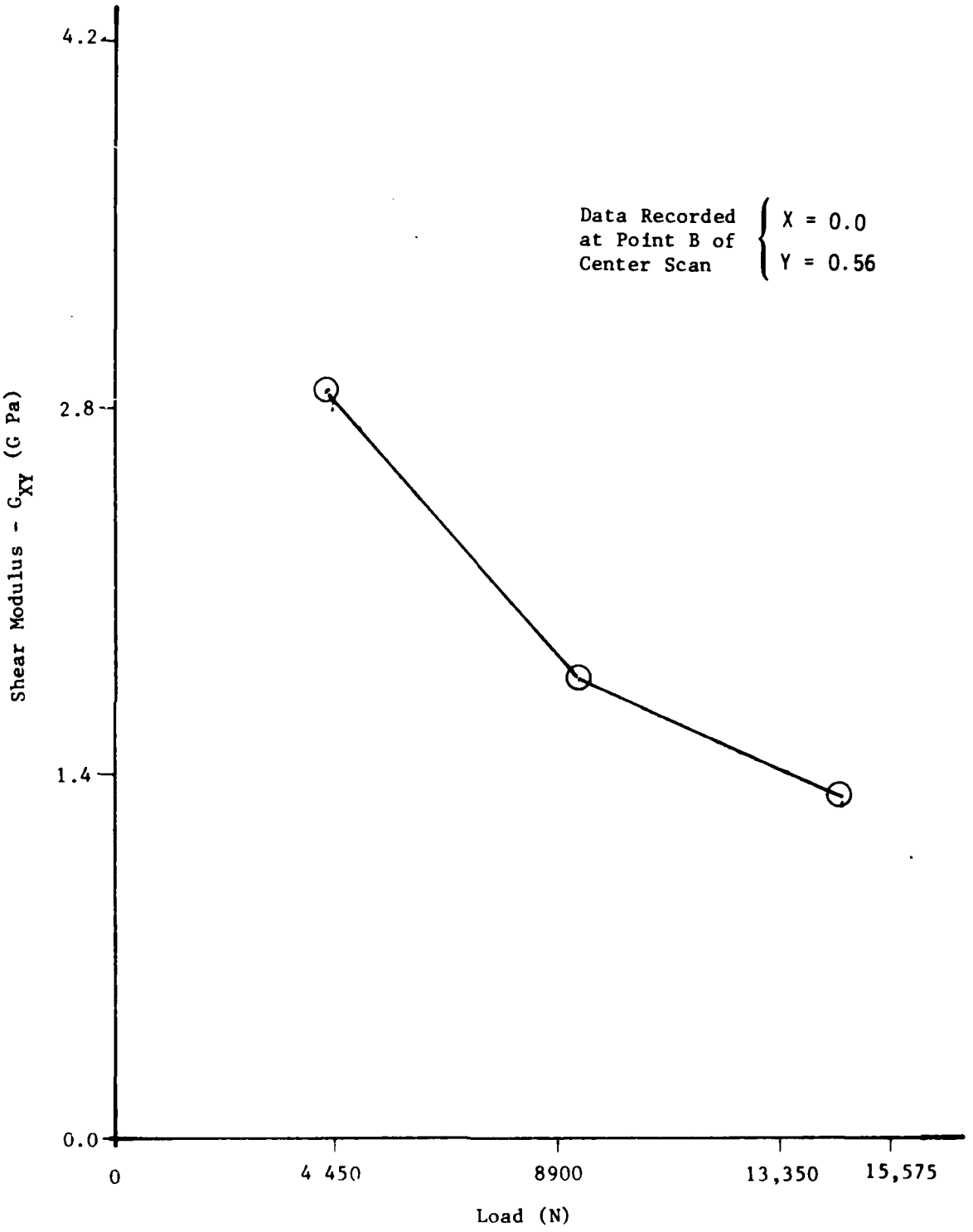

Figure B-10. Shear Modulus versus load (S-0°-8-L) center scan.

APPENDIX C

APERTURE RECONSTRUCTION

APPENDIX C

LIST OF FIGURES

APPENDIX C

LIST OF FIGURES (Continued)

APPENDIX C

LIST OF FIGURES (Continued)

APPENDIX C

LIST OF FIGURES (Concluded)

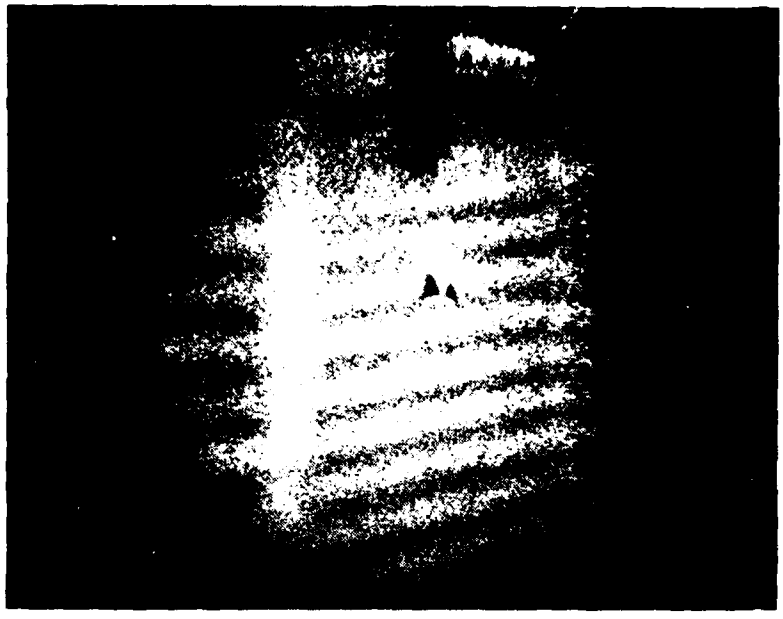

Figure C-1. Shear test specimen (S-O°-5-L-F).
Load Range: (1914-4228) Newtons

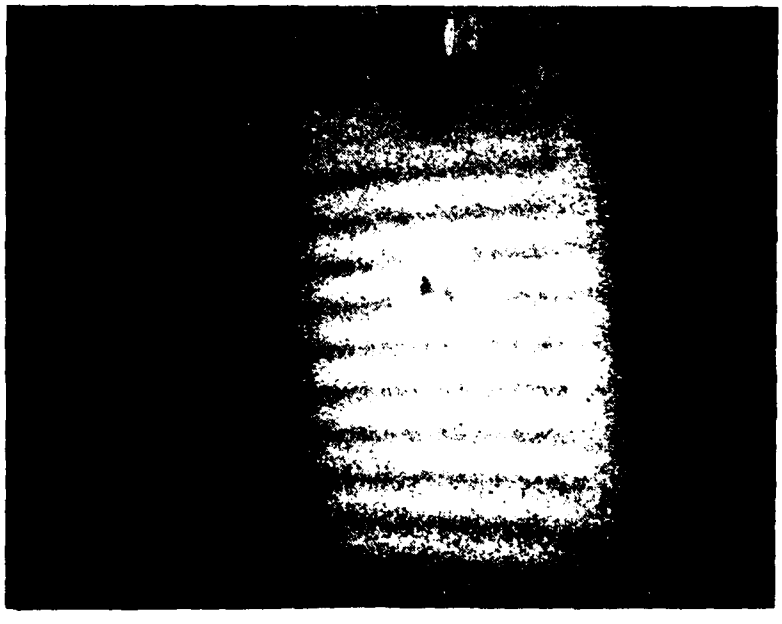

Figure C-2. Shear test specimen (S-O°-5-R-F).
Load Range: (1914-4228) Newtons

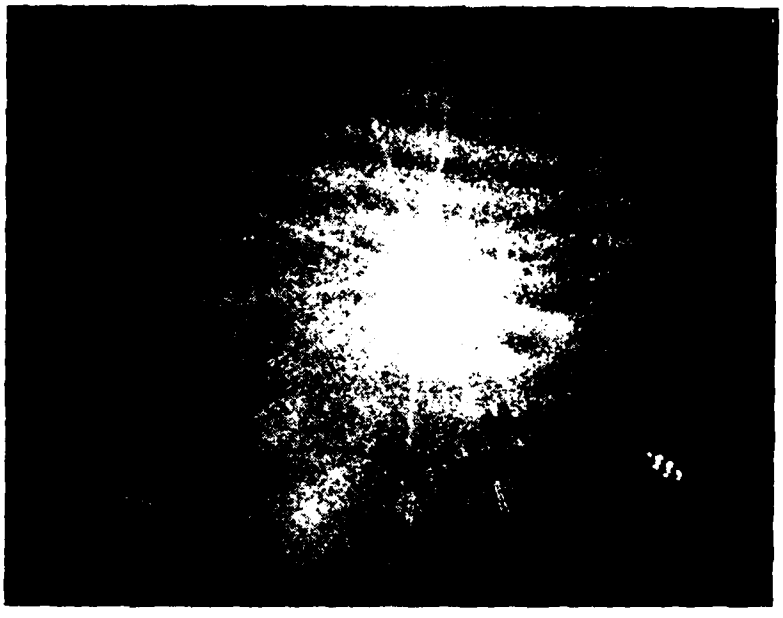

Figure C-3. Shear test specimen (S-0°-5-L-C).
Load Range: (1914-4228) Newtons

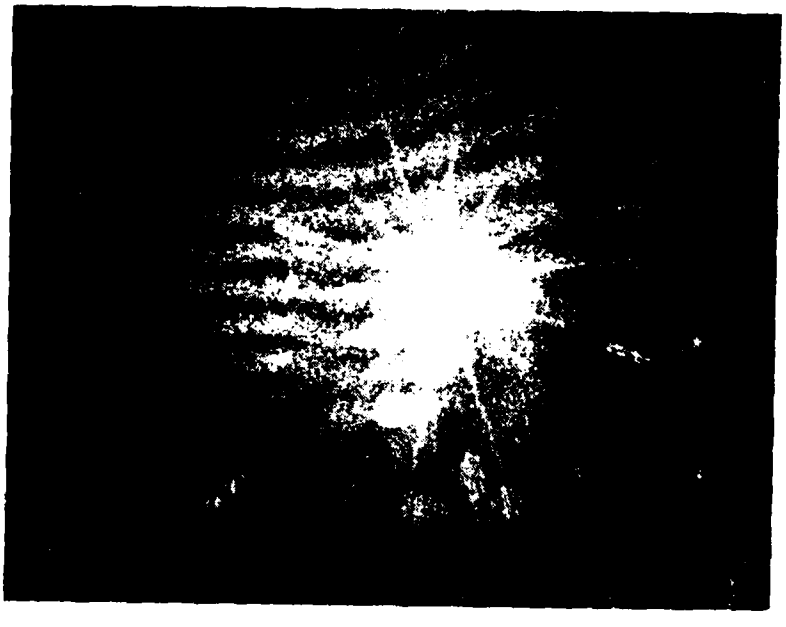

Figure C-4. Shear test specimen (S-0°-5-R-C).
Load Range: (1914-4228) Newtons

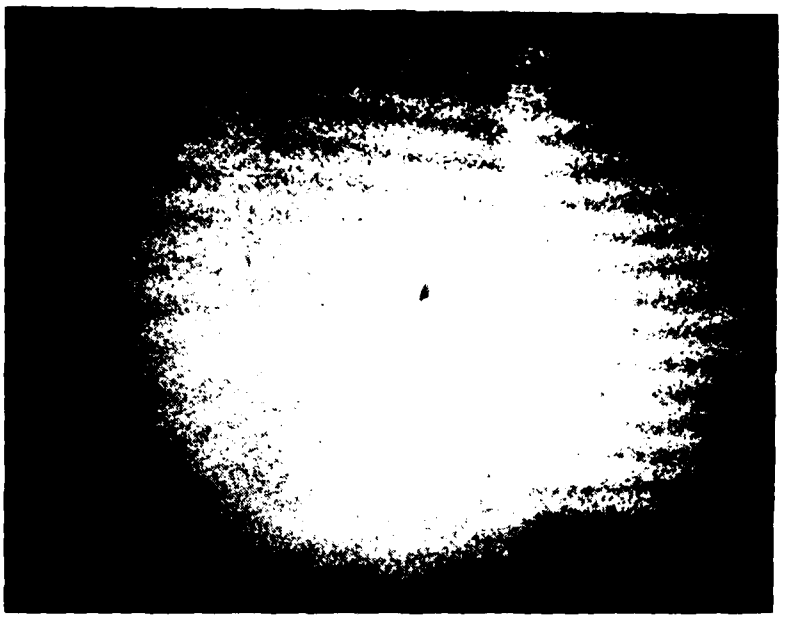

Figure C-5. Shear test specimen (S-0°-6-L-C).
Load Range: (623-2537) Newtons

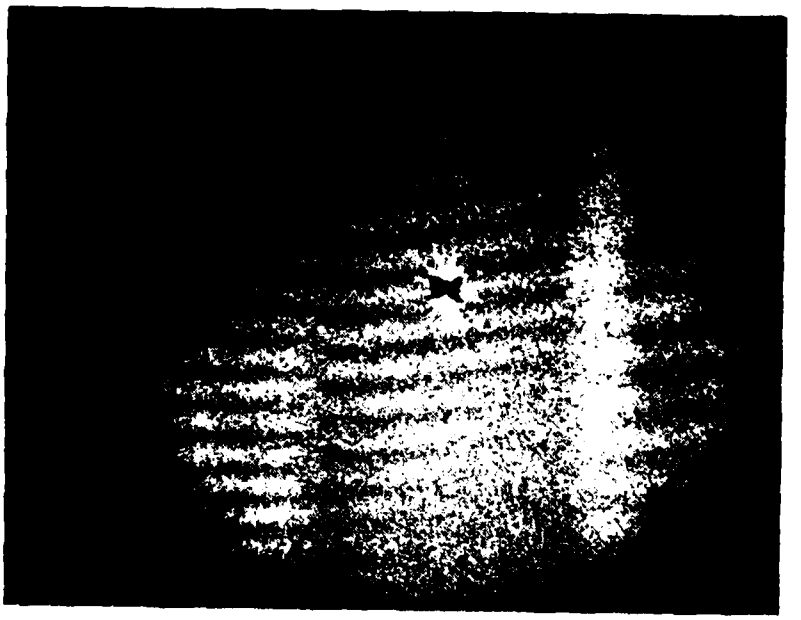

Figure C-6. Shear test specimen (S-0°-6-R-C).
Load Range: (623-2537) Newtons

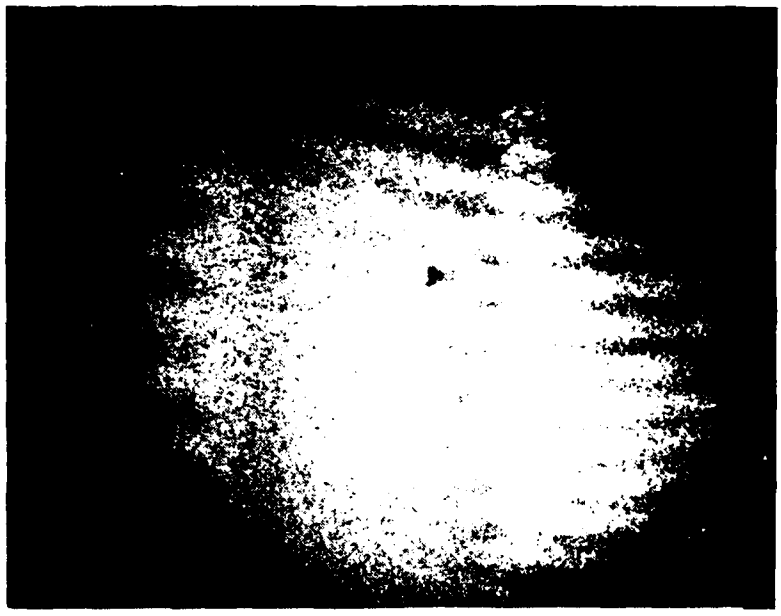

Figure C-7. Shear test specimen (S-O°-6-L-C).
Load Range: (2537-4228) Newtons

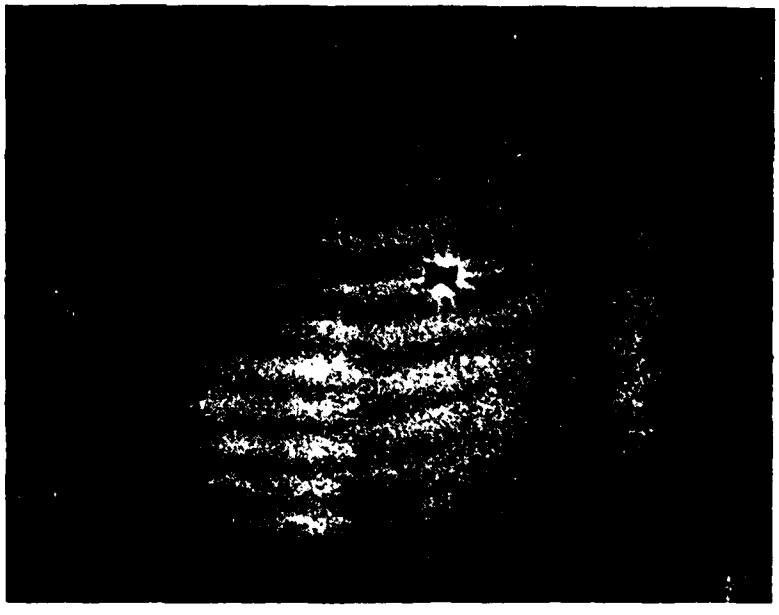

Figure C-8. Shear test specimen (S-O°-6-R-C).
Load Range: (2537-4228) Newtons

Figure C-9. Shear test specimen (S-O°-6-L-C).
Load Range: (4228-5874) Newtons

Figure C-10. Shear test specimen (S-O°-6-R-C).
Load Range: (4228-5874) Newtons

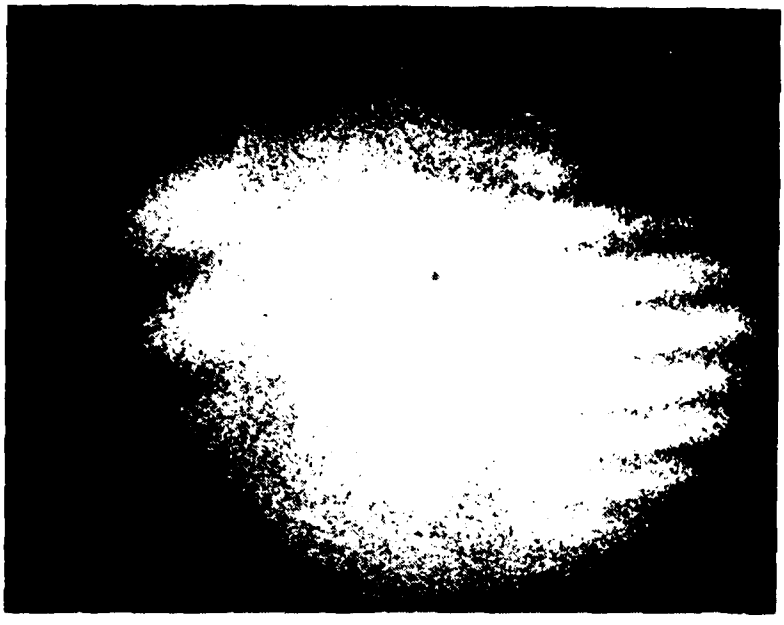

Figure C-11. Shear test specimen (S-0°-6-L-C).
Load Range: (5874-7743) Newtons

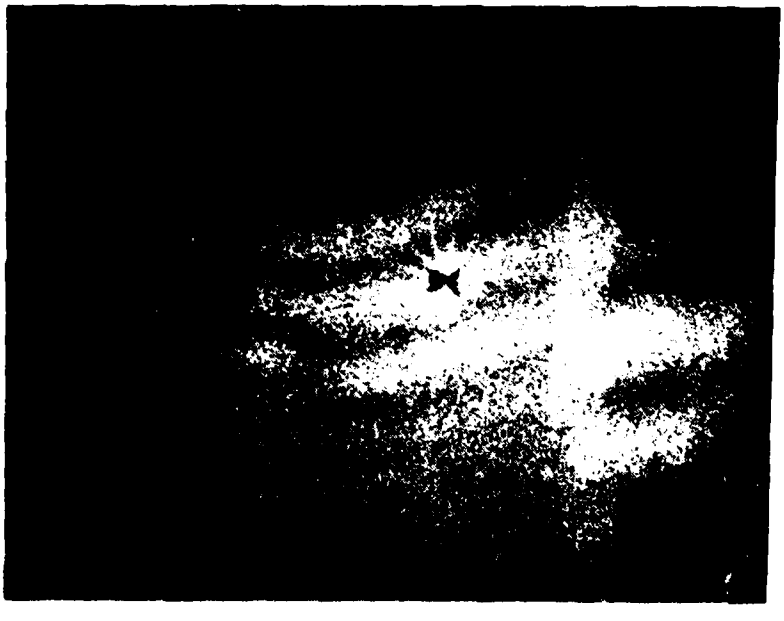

Figure C-12. Shear test specimen (S-0°-6-R-C).
Load Range: (5874-7743) Newtons

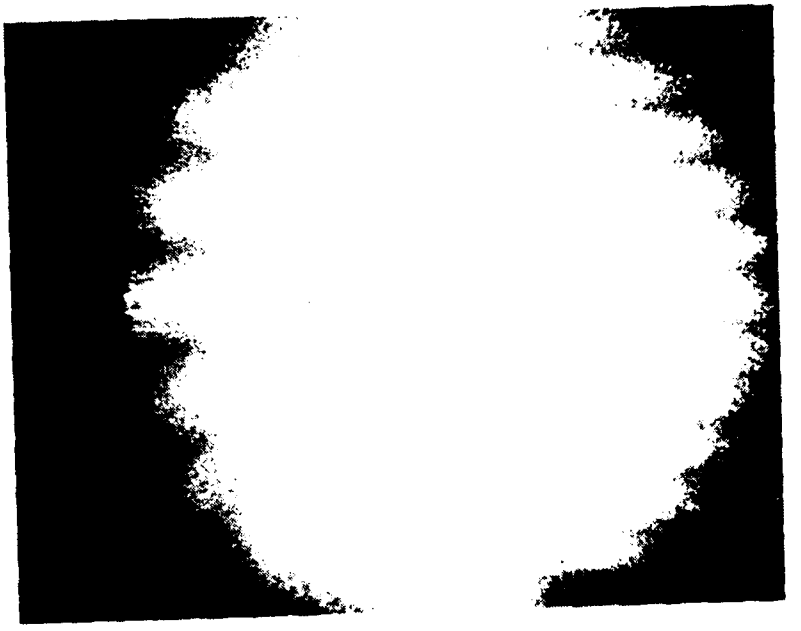

Figure C-13. Shear test specimen (S-0°-6-L-C).
Load Range: (7743-9301) Newtons

Figure C-14. Shear test specimen (S-0°-6-R-C).
Load Range: (7743-9301) Newtons

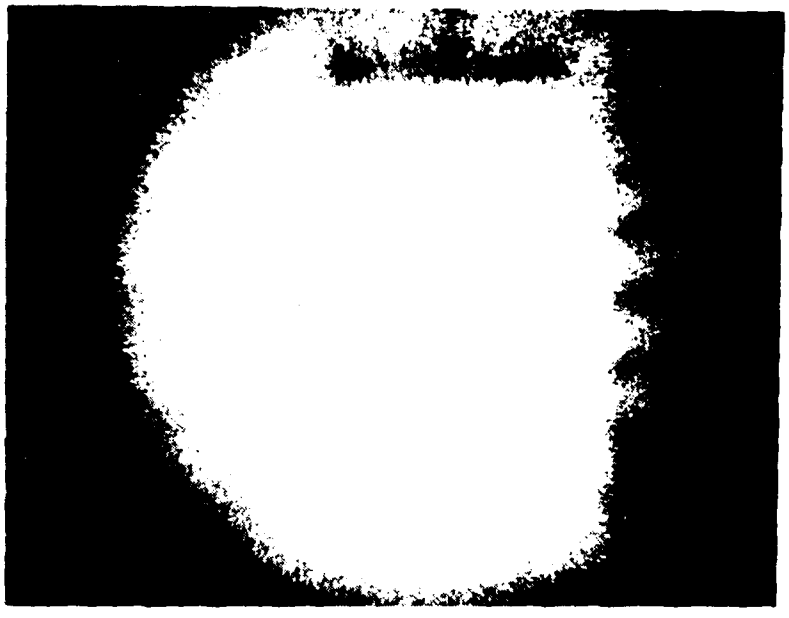

Figure C-15. Shear test specimen (S-0°-7-L-F).
Load Range: (2359-4139) Newtons

Figure C-16. Shear test specimen (S-0°-7-R-F).
Load Range: (2359-4139) Newtons

Figure C-17. Shear test specimen (S-0°-7-L-C).
Load Range: (2359-4139) Newtons

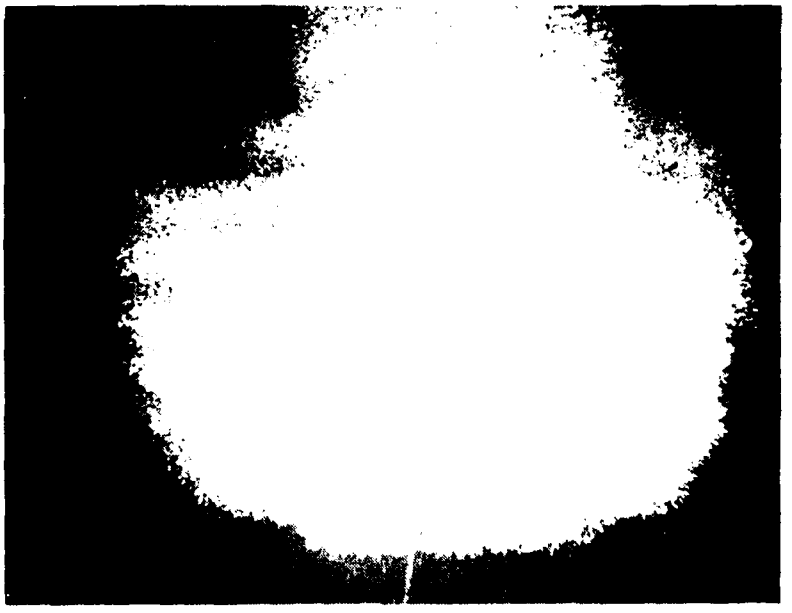

Figure C-18. Shear test specimen (S-0°-7-R-C).
Load Range: (2359-4139) Newtons

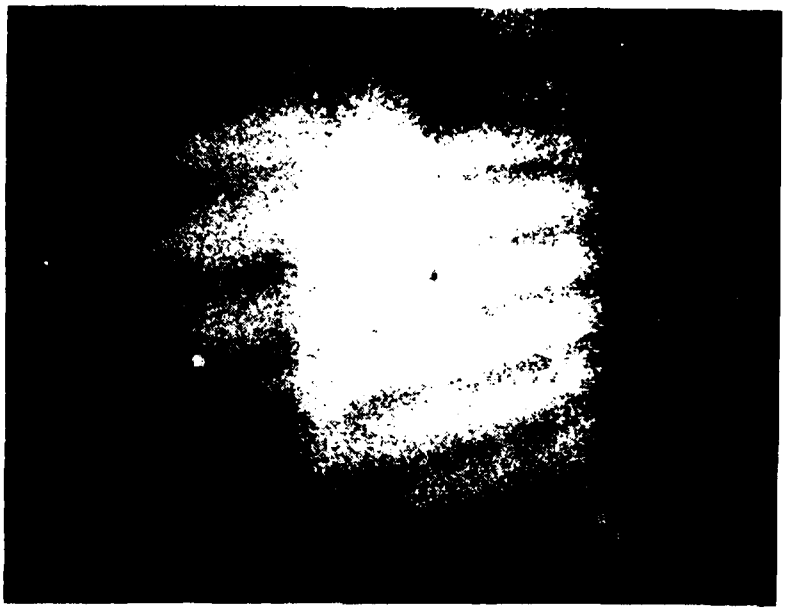

Figure C-19. Shear test specimen (S-0°-7-L-F).
Load Range: (5874-7565) Newtons

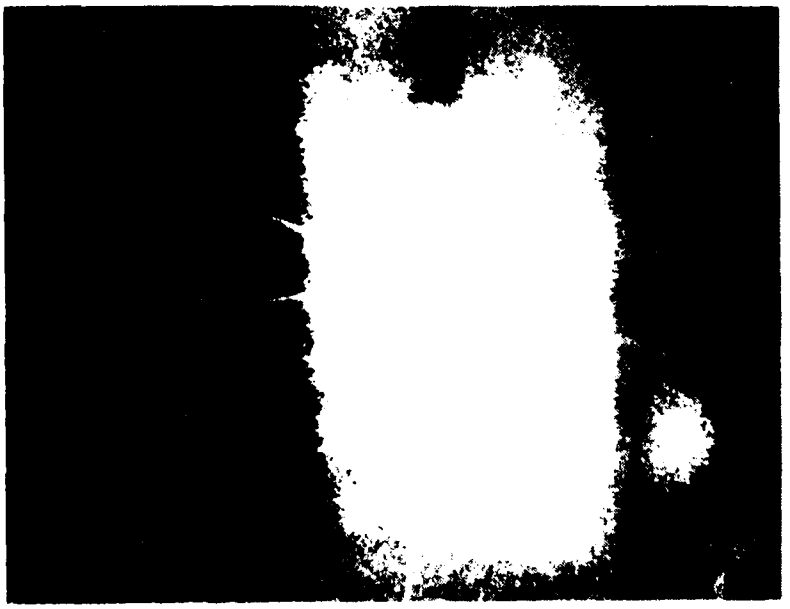

Figure C-20. Shear test specimen (S-0°-7-R-F).
Load Range: (5874-7565) Newtons

Figure C-21. Shear test specimen (S-0°-7-L-C).
Load Range: (5874-7565) Newtons

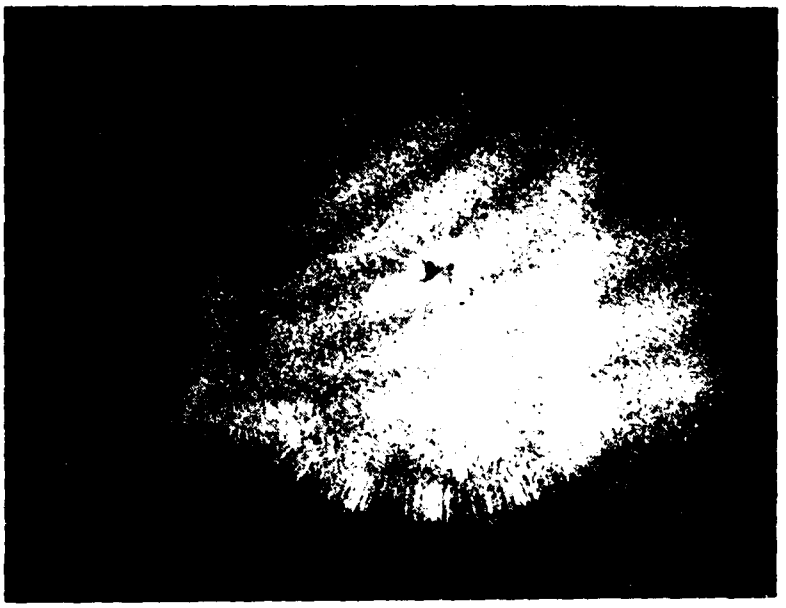

Figure C-22. Shear test specimen (S-0°-7-R-C).
Load Range: (5874-7565) Newtons

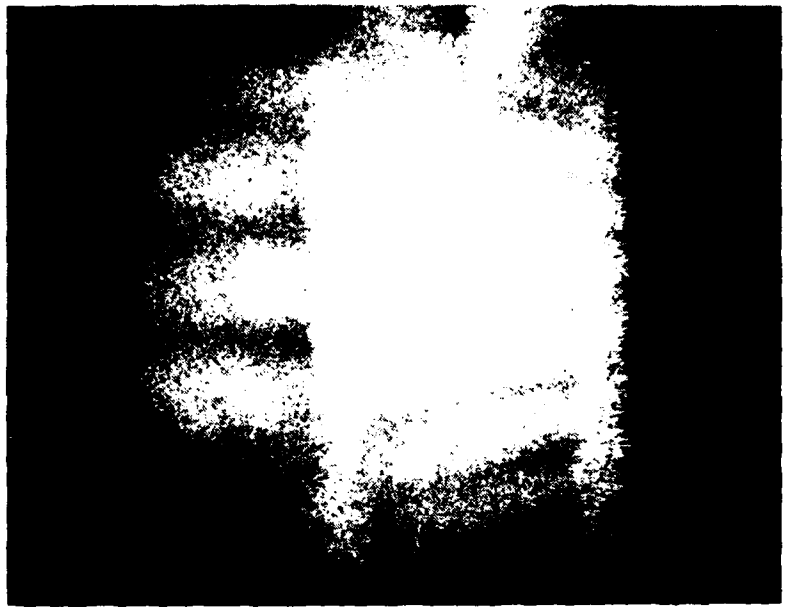

Figure C-23. Shear test specimen (S-O°-7-L-F).
Load Range: (9345-11,125) Newtons

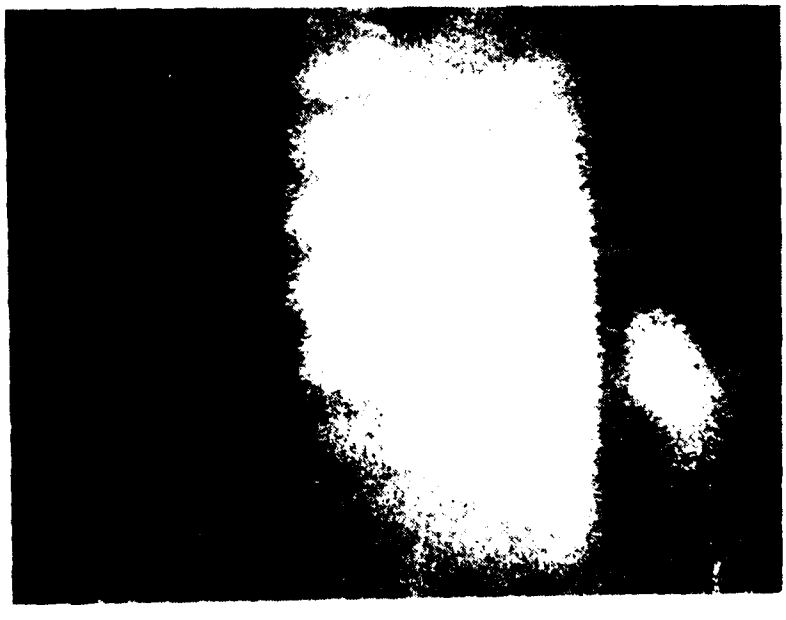

Figure C-24. Shear test specimen (S-O°-7-R-F).
Load Range: (9345-11,125) Newtons

Figure C-25. Shear test specimen (S-O°-7-L-C).
Load Range: (9345-11,125) Newtons

Figure C-26. Shear test specimen (S-O°-7-R-C).
Load Range: (9345-11,125) Newtons

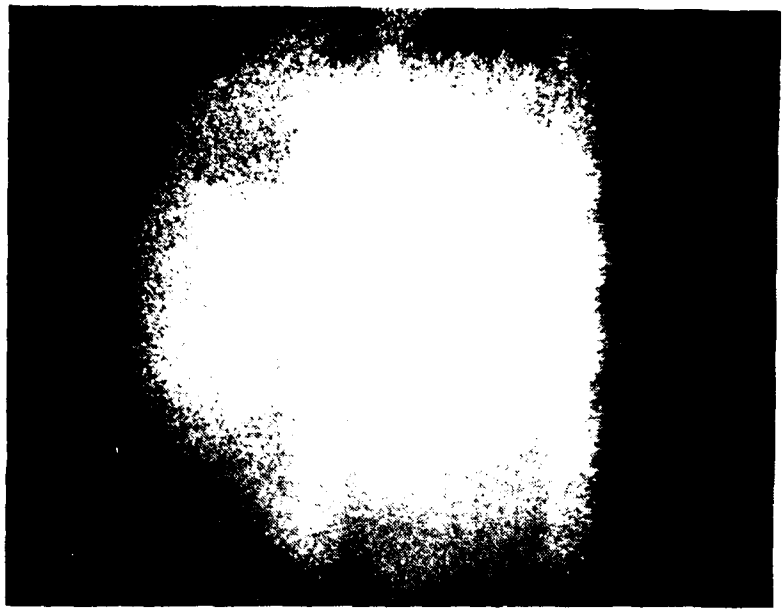

Figure C-27. Shear test specimen (S-0°-7-L-F).
Load Range: (12,683-14,552) Newtons

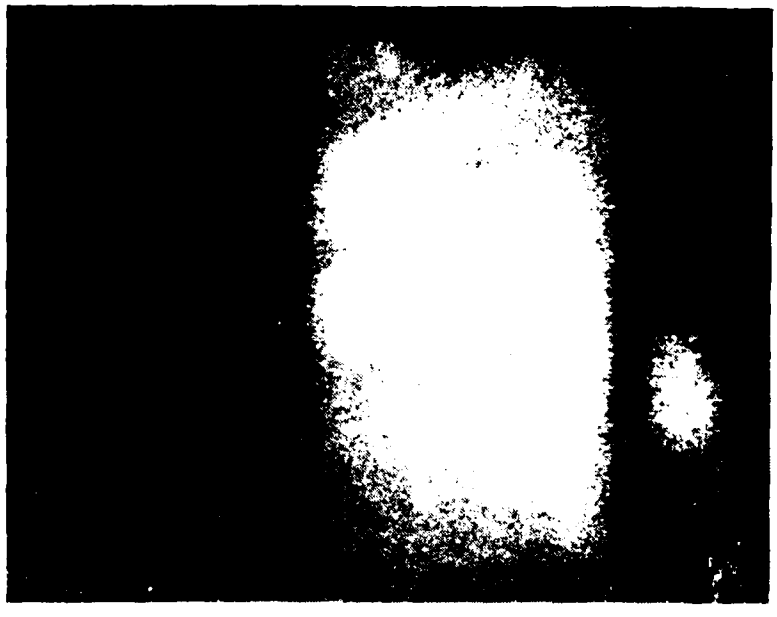

Figure C-28. Shear test specimen (S-0°-7-R-F).
Load Range: (12,683-14,552) Newtons

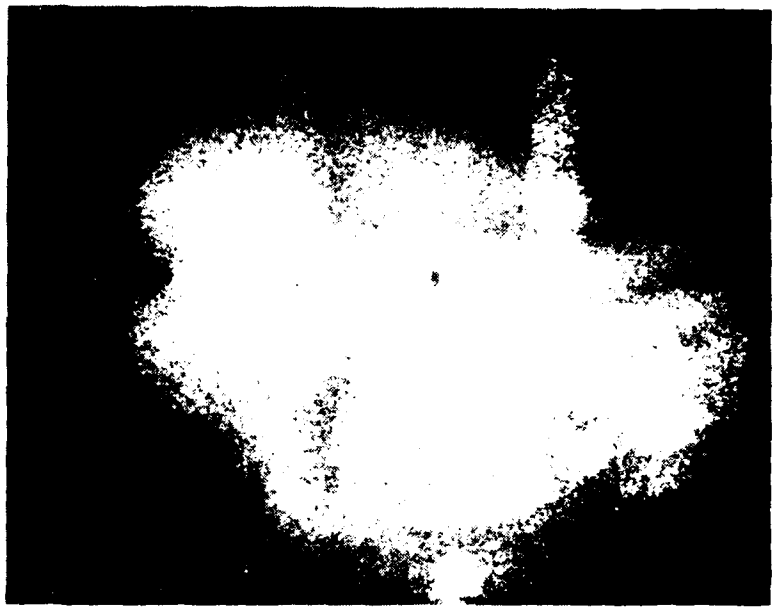

Figure C-29. Shear test specimen (S-0°-7-L-C).
Load Range: (12,683-14,552) Newtons

Figure C-30. Shear test specimen (S-0°-7-R-C).
Load Range: (12,683-14,552) Newtons

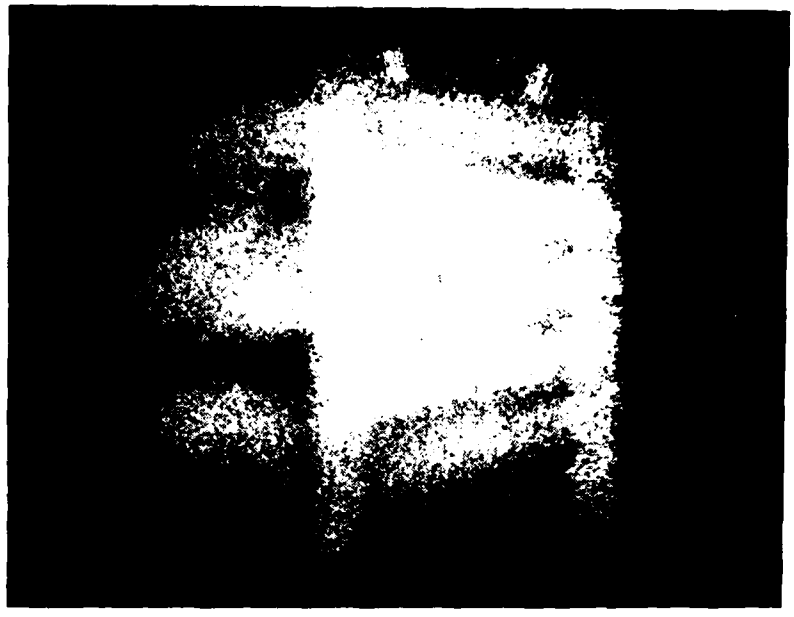

Figure C-31. Shear test specimen (S-O°-7-L-F).
Load Range: (16,243-18,023) Newtons

Figure C-32. Shear test specimen (S-O°-7-R-F).
Load Range: (16,243-18,023) Newtons

Figure C-33. Shear test specimen (S-O°-7-L-C).
Load Range: (16,243-18,023) Newtons

Figure C-34. Shear test specimen (S-O°-7-R-C).
Load Range: (16,243-18,023) Newtons

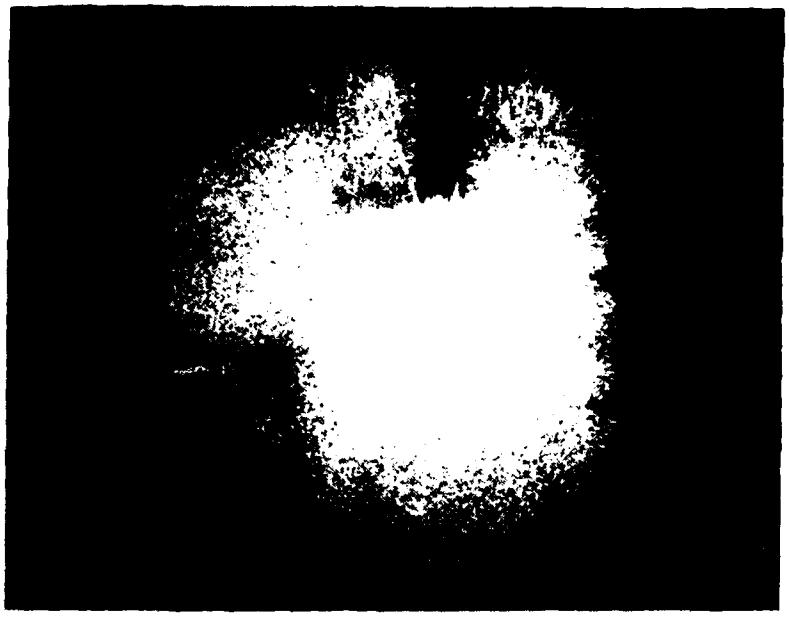

Figure C-35. Shear test specimen (S-O°-8-L-F).
Load Range: (2359-4116) Newtons

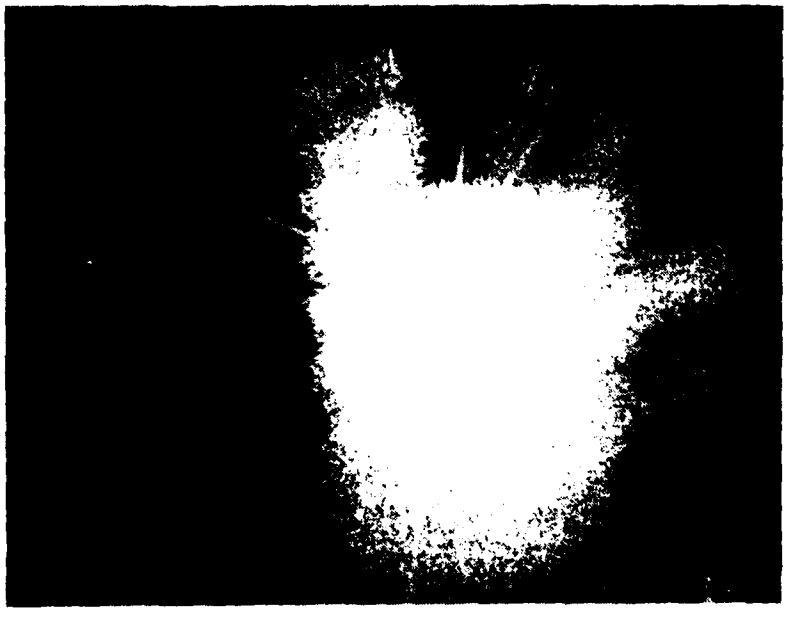

Figure C-36. Shear test specimen (S-O°-8-R-F).
Load Range: (2359-4116) Newtons

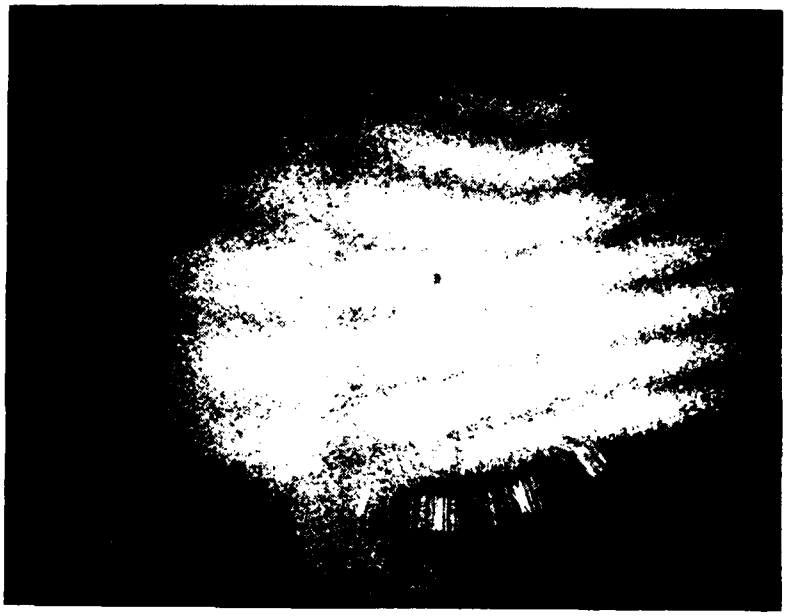

Figure C-37. Shear test specimen (S-O°-8-L-C).
Load Range: (2359-4116) Newtons

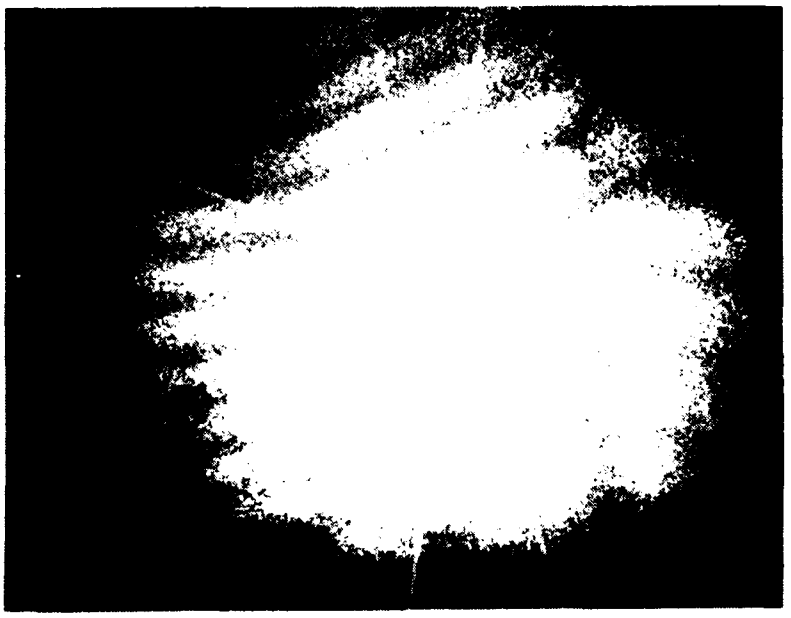

Figure C-38. Shear test specimen (S-O°-8-R-C).
Load Range: (2359-4116) Newtons

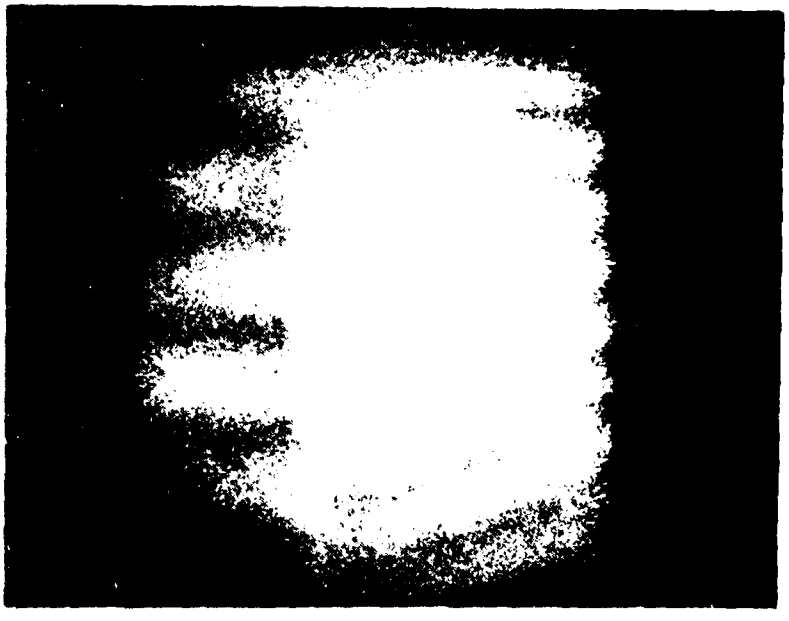

Figure C-39. Shear test specimen (S-C°-8-L-F).
Load Range: (5896-7654) Newtons

Figure C-40. Shear test specimen (S-O°-8-R-F).
Load Range: (5896-7654) Newtons

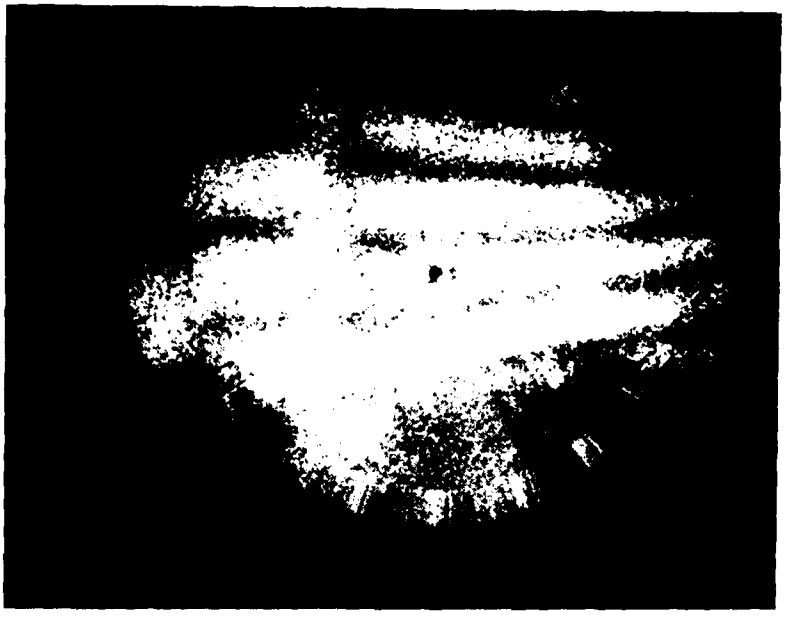

Figure C-41. Shear test specimen (S-0°-8-L-C).
Load Range: (5896-7654) Newtons

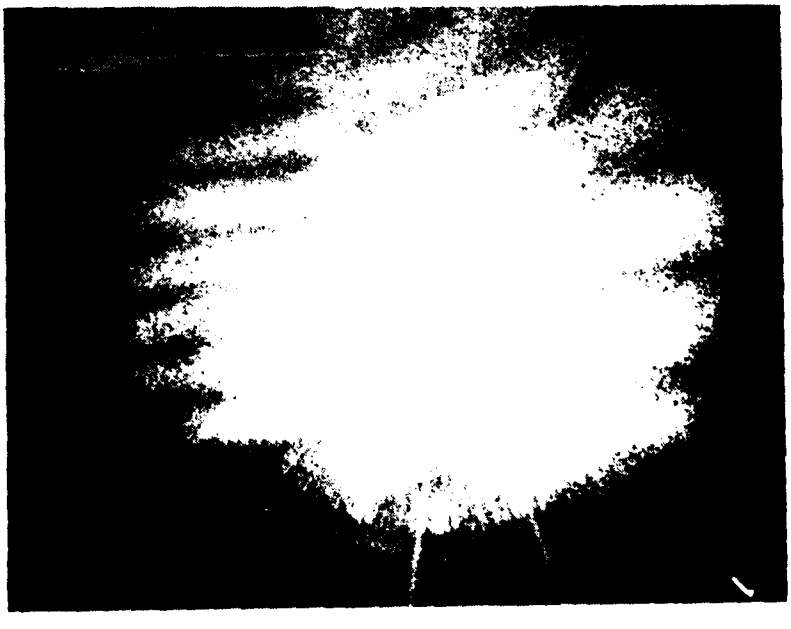

Figure C-42. Shear test specimen (S-0°-8-R-C).
Load Range: (5896-7654) Newtons

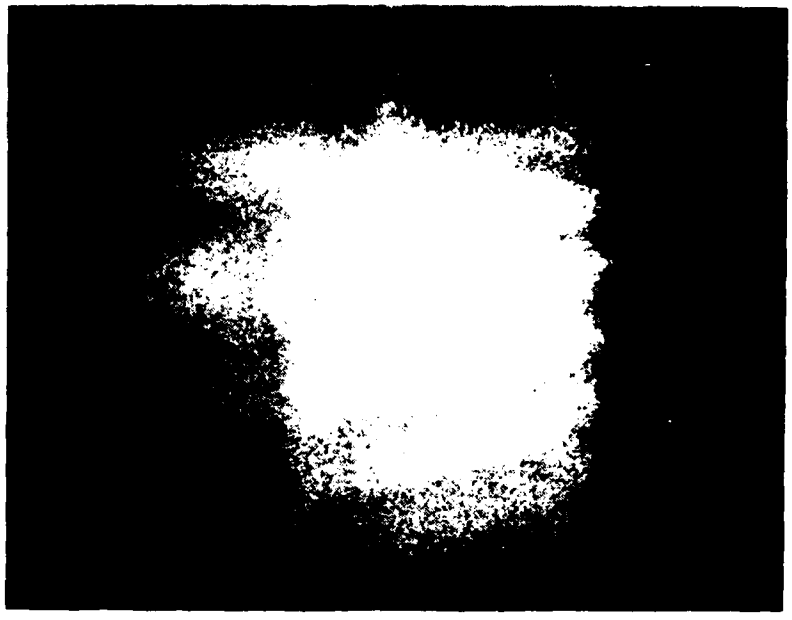

Figure C-43. Shear test specimen (S-0°-8-L-F).
Load Range: (7654-9345) Newtons

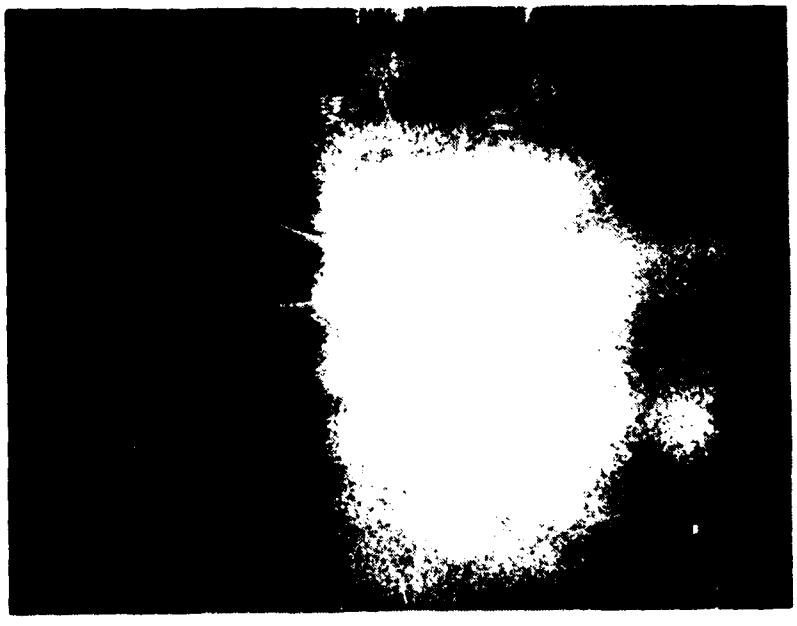

Figure C-44. Shear test specimen (S-0°-8-R-F).
Load Range: (7654-9345) Newtons

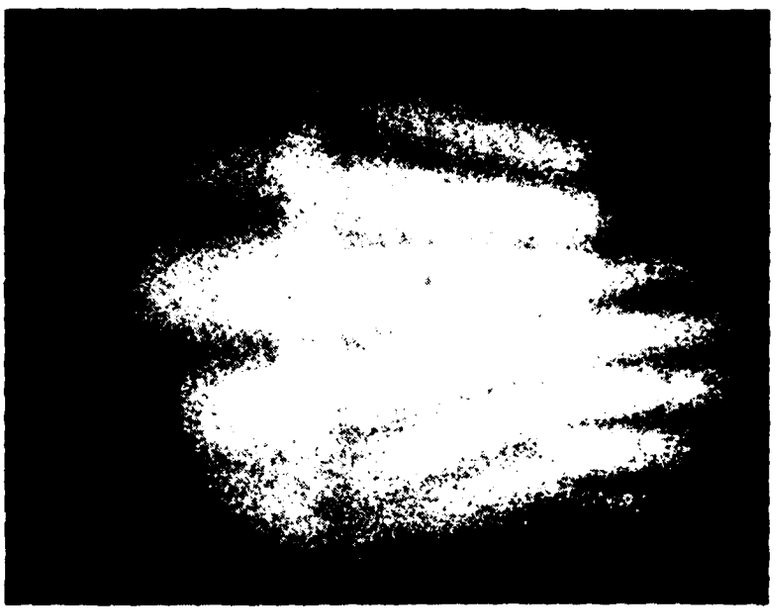

Figure C-45. Shear test specimen (S-0°-8-L-C).
Load Range: (7654-9345) Newtons

Figure C-46. Shear test specimen (S-0°-8-R-C).
Load Range: (7654-9345) Newtons

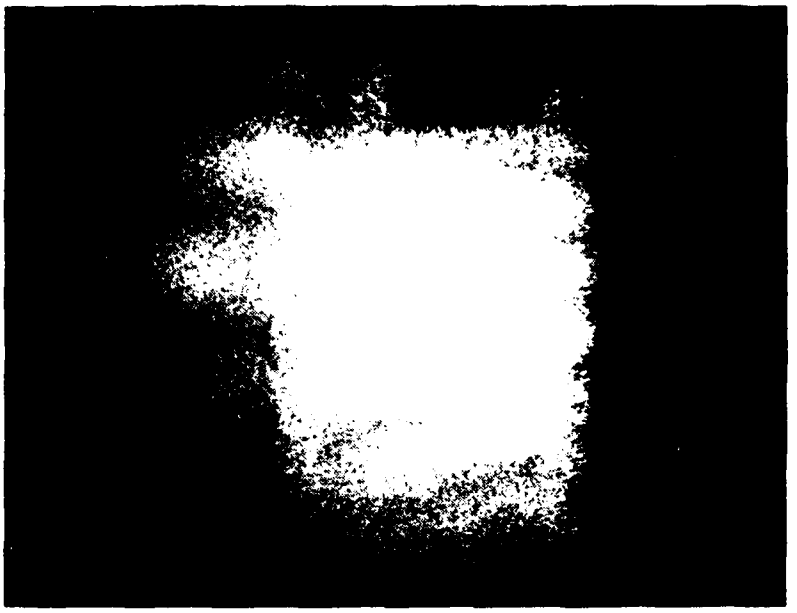

Figure C-47. Shear test specimen (S-0°-8-L-F).
Load Range: (11,125-12,905) Newtons

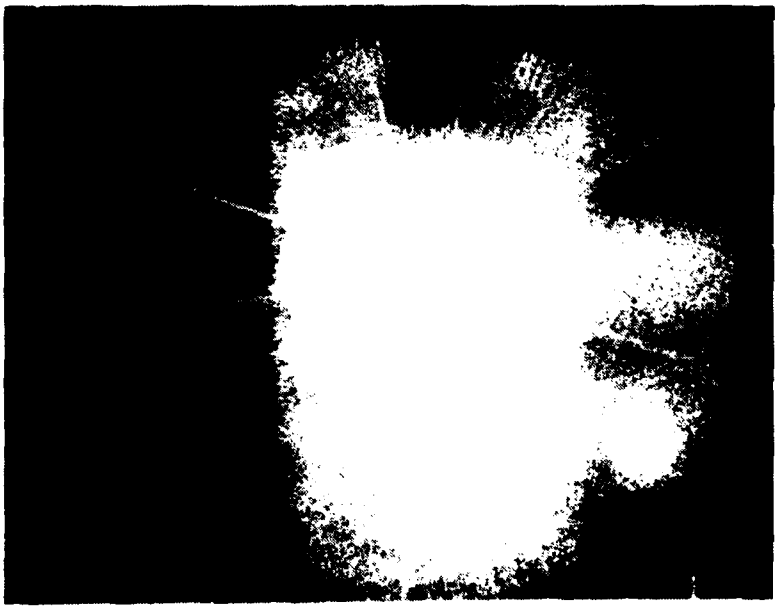

Figure C-48. Shear test specimen (S-0°-8-R-F).
Load Range: (11,125-12,905) Newtons

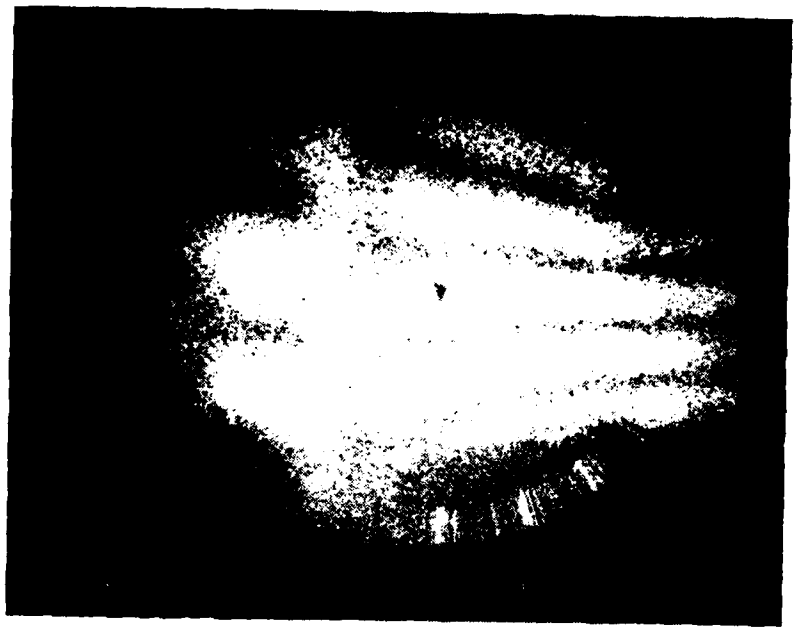

Figure C-49. Shear test specimen (S-0°-8-L-C).
Load Range: (11,125-12,905) Newtons

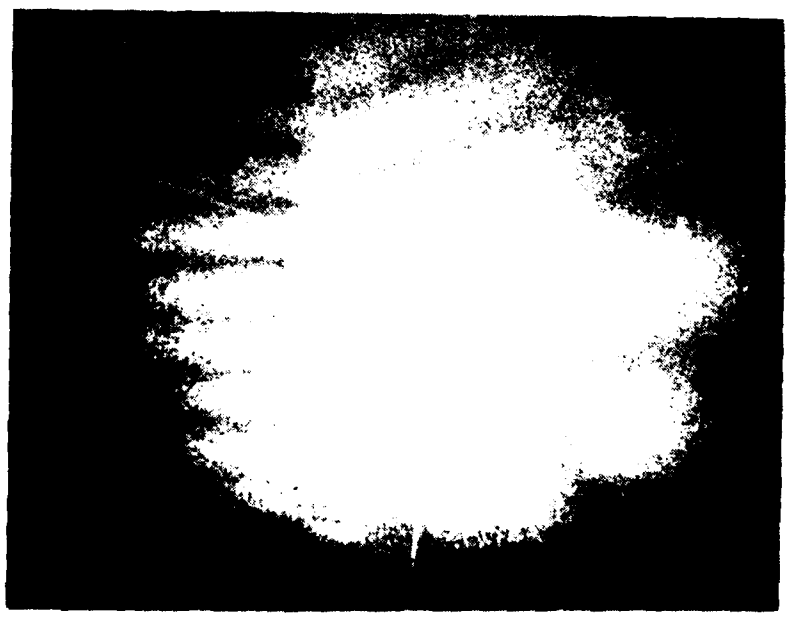

Figure C-50. Shear test specimen (S-0°-8-R-C).
Load Range: (11,125-12,905) Newtons

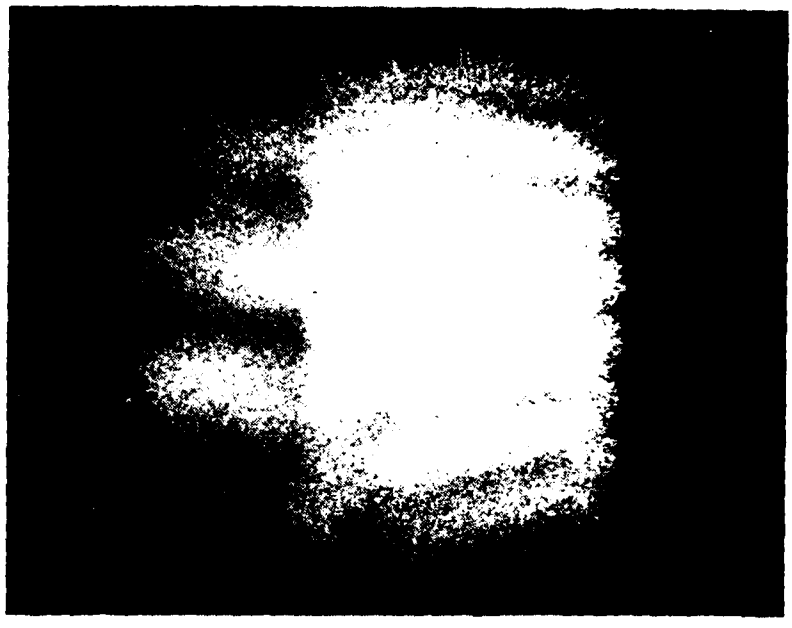

Figure C-51. Shear test specimen (S-0°-8-L-F).
Load Range: (12,905-14,685) Newtons

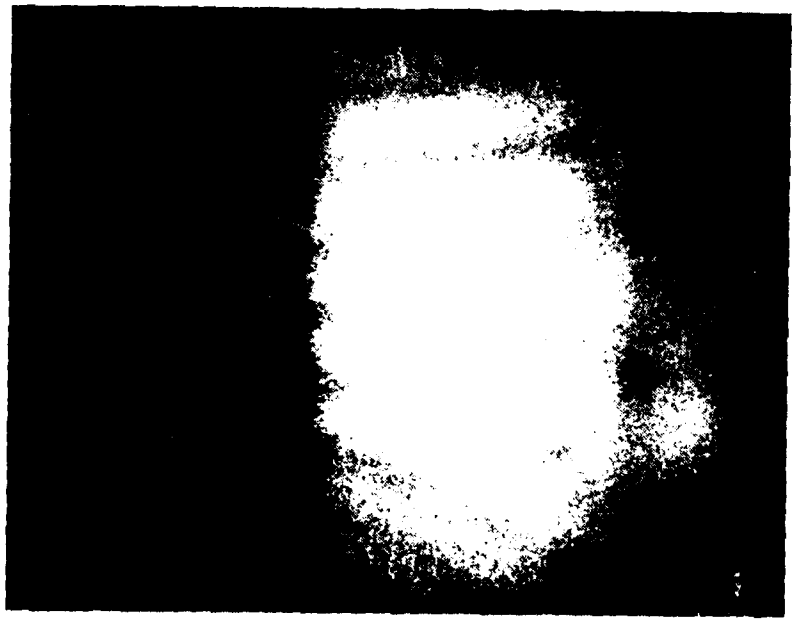

Figure C-52. Shear test specimen (S-0°-8-R-F).
Load Range: (12,905-14,685) Newtons

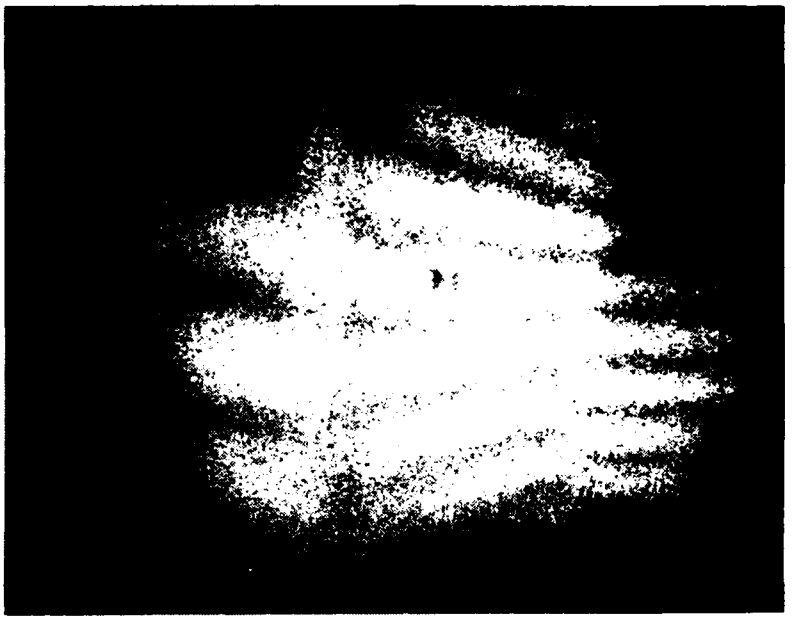

Figure C-53. Shear test specimen (S-0°-8-L-C).
Load Range: (12,905-14,685) Newtons

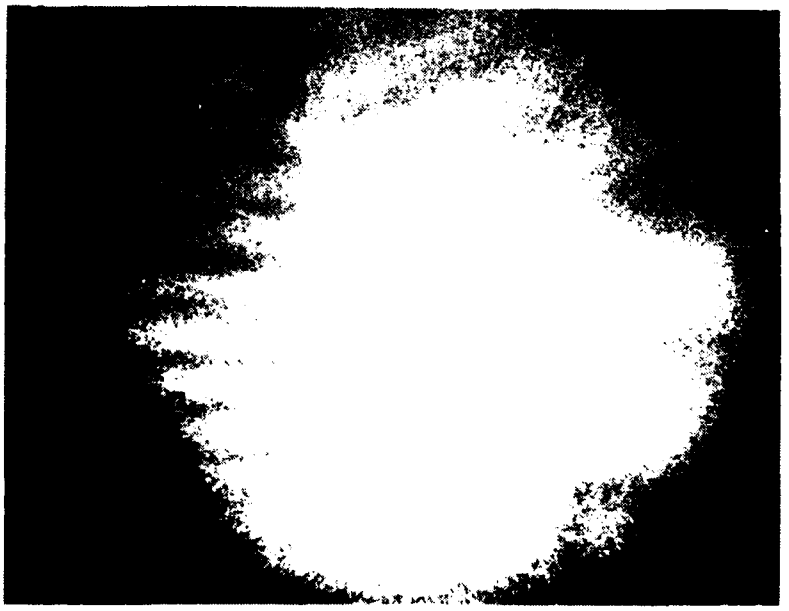

Figure C-54. Shear test specimen (S-0°-8-R-C).
Load Range: (12,905-14,685) Newtons

DISTRIBUTION

	No. of Copies
Director USA Mobility Equipment Research and Development Center Coating and Chemical Laboratory ATTN: STSFB-CL Aberdeen Proving Ground, Maryland 21005	1
Commander Edgewood Arsenal ATTN: SAREA-TS-A Aberdeen Proving Ground, Maryland 21010	1
Commander Picatinny Arsenal ATTN: SARPA-TS-S, Mr. M. Costello Dover, New Jersey 07801	1
Commander Rock Island Arsenal Research and Development ATTN: 9320 Rock Island, Illinois 61201	1
Commander Watervliet Arsenal Watervliet, New York 12189	1
Commander US Army Aviation Systems Command ATTN: DRSAV-EE DRSAV-MT, Mr. Vollmer St. Louis, Missouri 63166	1 1
Commander US Army Test and Evaluation Command ATTN: DRSTE-RA Aberdeen Proving Ground, Maryland 21005	1
Commander ATTN: STEAP-MT Aberdeen Proving Ground, Maryland 21005	1
Chief Bureau of Naval Weapons Department of the Navy Washington, DC 20390	1

DISTRIBUTION (CONTINUED)

	No. of Copies
Chief Bureau of Ships Department of the Navy Washington, DC 20315	1
Naval Research Laboratory ATTN: Dr. M. M. Krafft Code 8430 Washington, DC 20375	1
Commander Wright Air Development Division ATTN: ASRC Wright-Patterson AFB, Ohio 45433	1
Director Army Materials and Mechanics Research Center ATTN: DRXMR-PL DRXMR-MT, Mr. Farrow Watertown, Massachusetts 02172	1 1
Commander White Sands Missile Range ATTN: STEWS-AD-L White Sands Missile Range, New Mexico 88002	1
Jet Propulsion Laboratory California Institute of Technology ATTN: Library/Acquisitions 111-113 4800 Oak Grove Drive Pasadena, California 91103	1
Sandia Laboratories ATTN: Library P. O. Box 969 Livermore, California 94550	1
Commander US Army Air Defense School ATTN: ATSA-CD-MM Fort Bliss, Texas 79916	1
Commander US Army Materiel Development and Readiness Command ATTN: DRCMT Washington, DC 20315	1

DISTRIBUTION (CONTINUED)

	No. of Copies
Commander Rock Island Arsenal ATTN: SARRI-KLPL-Technical Library Rock Island, Illinois 61201	1
Commander (Code 233) Naval Weapons Center ATTN: Library Division China Lake, California 93555	1
Department of the Army US Army Research Office ATTN: Information Processing Office P. O. Box 12211 Research Triangle Park, North Carolina 27709	1
Headquarters Department of the Army Office of the DCS for Research Development and Acquisition ATTN: DAMA-ARZ Washington, DC 20310	2
Director Air Force Materiel Laboratory ATTN: AFML-DO-Library Wright-Patterson AFB, Ohio 45433	1
US Army Materiel Systems Analysis Activity ATTN: DRXSY-MP Aberdeen Proving Ground, Maryland 21005	1
IIT Research Institute ATTN: GACIAC 10 West 35th Street Chicago, Illinois 60616	1
ADTC (DLDSL) Eglin Air Force Base, Florida 32542	
Commander US Army Materiel Development and Readiness Command ATTN: DRCRD DRCDL 5001 Eisenhower Avenue Alexandria, Virginia 22333	1
Director Defense Advanced Research Projects Agency 1400 Wilson Boulevard Arlington, Virginia 22209	1

DISTRIBUTION (CONCLUDED)

		No. of Copies
DRSMI-LP,	Mr. Voigt	1
-R,	Dr. McCorkle	1
-RL,	Mr. Cobb	1
-RLA,	Dr. Richardson	1
-RLA,	Mr. Vandiver	50
-RPR		15
-RPT	(Record Set)	1
-RPT	(Reference Set)	1


DAT
FILM